ANL-6435

Argonne National Laboratory

THE U-Pu-C TERNARY PHASE DIAGRAM BELOW 50 ATOMIC PERCENT CARBON

by

S. Rosen, M. V. Nevitt,
and A. W. Mitchell

DISCLAIMER

Price $2.25 . *Available from the Office of Technical Services, Department of Commerce, Washington 25, D.C.*

ANL-6435
Chemistry
(TID-4500, 32nd Ed.)
AEC Research and
Development Report

ARGONNE NATIONAL LABORATORY
9700 South Cass Avenue
Argonne, Illinois 60440

THE U-Pu-C TERNARY PHASE DIAGRAM BELOW 50 ATOMIC PERCENT CARBON

by

S. Rosen, M. V. Nevitt,
and A. W. Mitchell

Metallurgy Division

Final Report - Metallurgy Program 9.3.8

Portions of the material in this report have appeared in the following Metallurgy Division Annual Reports:

Report No.	Pages	Date
ANL-6330	151	1960
ANL-6516	230-237	1961
ANL-6677	265-267	1962

March 1964

Operated by The University of Chicago
under
Contract W-31-109-eng-38
with the
U. S. Atomic Energy Commission

TABLE OF CONTENTS

TABLE OF CONTENTS

LIST OF FIGURES

LIST OF FIGURES

LIST OF FIGURES

LIST OF FIGURES

LIST OF TABLES

NOMENCLATURE

Symbol	Explanation
a/o	atomic percent
w/o	weight percent
v/o	volume percent
α	alpha
β	beta
γ	gamma
δ	delta
δ'	delta prime
ϵ	epsilon
ζ	zeta
η	eta
C	as cast
Q	quenched
FC	furnace cooled
R	as received
W	Widmanstatten precipitate
ATM	atmospheric
b	black
g	gray
w	white
m	martensitic
tr	transformed
den	dendritic
eut	eutectic
c	corroded intergranularly
v	difference between computed $\sin^2\theta$ and observed $\sin^2\theta$

Figure captions for photomicrographs give information in following order:

Annealing Temperature (°C), Annealing Time (days), Quenched or Furnace Cooled; Etchant,* Magnification, Illumination (BF = bright field, PL = polarized light); Identification of Phases Present.

*For etchants A, B, C, D, E, F, and G, see pp. 24 and 25.

THE U-Pu-C TERNARY PHASE DIAGRAM BELOW 50 ATOMIC PERCENT CARBON

by

S. Rosen, M. V. Nevitt,
and A. W. Mitchell

ABSTRACT

The U-Pu-C ternary phase diagram for the composition range from 0 to 50 a/o carbon and for temperatures below 635°C has been constructed from metallographic, X-ray diffraction, and melting-range data. Isothermal sections at 400°C, 570°C, and 635°C are presented, and certain four-phase reactions are outlined.

Uranium monocarbide forms a complete series of solid solutions with plutonium monocarbide. All phase boundaries other than those of the monocarbide phase represent the sides of three-phase tie-triangles which have one side coincident with either the U-Pu or the Pu-C side and have the opposite apex touching the phase boundary of the monocarbide solid solution, (U,Pu)C.

The metal:carbon stoichiometry of the monocarbide is influenced by the uranium:plutonium ratio. The monocarbide phase is stoichiometric as regards its carbon content in a composition range from 0 to 35 a/o plutonium. With a further increase in plutonium content it deviates from ideal stoichiometry toward greater metal-to-carbon ratios, forming the defect (U,Pu)C phase. Plutonium expands the unit cell of the monocarbide over the composition range in which it retains its stoichiometric character. In the region of the defect structure the lattice parameter decreases with increasing plutonium content, the extent of the decrease being dependent upon the carbon content.

The variation of lattice parameter with composition for binary plutonium-carbon alloys has been determined and has been used to define portions of the low-carbon boundary of the PuC phase field.

Metallographic observations of cast alloys show that a transition in the microstructures occurs between uranium-rich alloys, which show a homogeneous carbide phase, and plutonium-rich alloys, which show a cored carbide phase. Compositional variations in these alloys have been considered.

Unique microstructural characteristics are associated with the preference of the Pu_3C_2 phase to grow as platelets in its peritectoidal formation, rather than as an interfacial envelope surrounding the PuC reactant.

I. INTRODUCTION

Uranium-plutonium-carbon alloys containing around 50 a/o carbon are of interest as potential fuel-bearing materials for reactors. For this reason, an investigation of the U-Pu-C phase diagram was undertaken. The determination of the phase diagram was also recognized as an important preliminary step in a study of the electronic structure of the alloys of the actinide metals with carbon.

In past work, carbon additions to uranium and plutonium were studied only in connection with the binary systems. More recent investigations of ternary alloys have been limited to carbon concentrations around 50 a/o, the compositions which have potential as reactor fuel alloys. Information concerning low-carbon ternary alloys has not been available. The present study, limited to the metal-rich portion of the U-Pu-C diagram, the portion below 50 a/o carbon, has determined the essential features of the 400 and 570°C isothermal sections, which are below the solidus, and the 635°C section, which intersects the liquidus and solidus surfaces. Portions of the U-Pu and Pu-C binary diagrams were also investigated.

II. REVIEW OF PRIOR WORK

The U-Pu diagram determined by Ellinger et al[12] (see Figure 1), contains the three allotropic forms of uranium, the six allotropic modifications of plutonium, and two intermediate phases, (η) eta and (ζ) zeta, having wide homogeneity ranges. The eta phase is stable only at elevated temperatures. The body-centered cubic epsilon phase of plutonium, the only plutonium allotrope in which uranium is appreciably soluble, forms a complete series of solid solutions with gamma uranium. A minimum exists in the liquidus at about 10 a/o uranium.

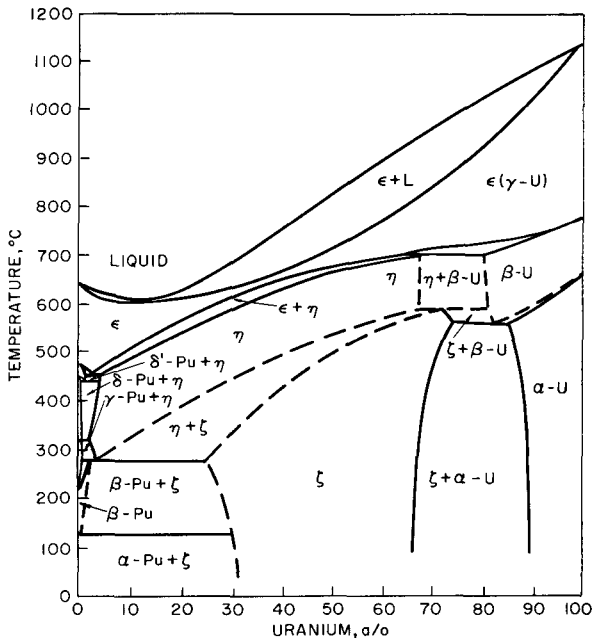

106-6428

Figure 1. Pu-U Phase Diagram (Los Alamos)

Crystallographic data for the uranium and plutonium allotropes are presented in Table I. Zeta has been indexed on the basis of a primitive cubic unit cell.[12] The lattice constant decreases from 10.692 Å at 35 a/o uranium to 10.651 Å at 70 a/o uranium. The approximate number of atoms in the unit cell was found to be 58, as calculated from the observed densities of 18.5 to 18.8 gm/cm^3. Although massive regions of eta phase could not be retained upon quenching, a capillary quenching method enabled Ellinger to index the complex pattern on the basis of a tetragonal unit cell. For a 25 a/o uranium alloy quenched from 500°C, a_0 = 10.57 Å and c_0 = 10.76 Å. The density of the eta phase deduced from dilatometric data, 17.3 gm/cm^3, indicates that the unit cell contains approximately 52 atoms per cell.

The U-Pu phase diagram has also been determined at Harwell[9] and by Bochvar et al.[4] The Los Alamos and British versions agree in their essential features; the Russian version differs considerably from these in phase-boundary details. The results of this investigation corroborate the Los Alamos version and, hence, this diagram is referred to in the present work.

The U-C phase diagram, given in Figure 2,[30] shows only the monocarbide up to 50 a/o carbon; there is no appreciable carbon solubility in the terminal uranium phases.[3] The Pu-C diagram, Figure 3, has been established by Mulford et al.[26] In the region that is pertinent to the present work there is a monocarbide, which exists as a phase deficient in

carbon, and another intermediate phase, ζ, having the formula Pu_3C_2. Carbon is not appreciably soluble in any of the plutonium allotropic modifications. The UC and PuC phases have the NaCl-type structure.

Table I

CRYSTAL STRUCTURES OF THE PLUTONIUM AND URANIUM ALLOTROPES

Allotrope	Temp Range, °C	Space Lattice	Unit Cell Dimensions, Å	X-ray Density, g/cm³
Plutonium:				
Alpha	Below 122	Monoclinic	(21°C) a = 6.1835 ± 0.0005 b = 4.8244 ± 0.0005 c = 10.973 ± 0.001 (α = 101.80 ± 0.02°)	19.82
Beta	122-206	Monoclinic	(190°C) a = 9.284 ± 0.003 b = 10.463 ± 0.004 c = 7.859 ± 0.003 (α = 92.13 ± 0.03°)	17.70
Gamma	206-319	Orthorhombic	(235°C) a = 3.1587 ± 0.0004 b = 3.7682 ± 0.0004 c = 10.162 ± 0.002	17.4
Delta	319-452	Cubic face-centered	(320°C) a = 4.6371 ± 0.0004	15.92
Delta-Prime	452-480	Tetragonal body-centered	(465°C) a = 3.327 ± 0.003 c = 4.482 ± 0.007	16.00
Epsilon	480-640	Cubic body-centered	(490°C) a = 3.6361 ± 0.004	16.51
Uranium:				
Alpha	Below 668	Orthorhombic	a = 2.852 (25°C) b = 5.865 c = 4.952	19.07
Beta	668-775	Tetragonal	a = 10.744 (668°C) c = 5.652	18.17
Gamma	775-1132	Cubic body-centered	a = 3.532 (775°C)	17.94

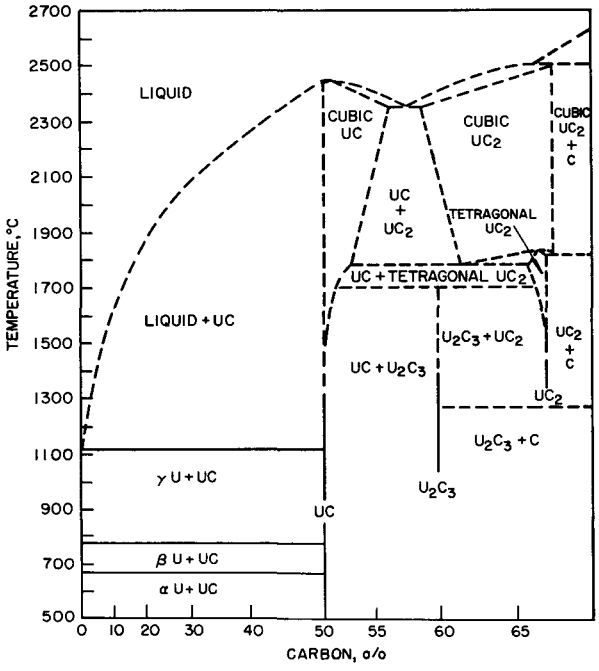

106-6438

Figure 2. U-C Phase Diagram (BMI)

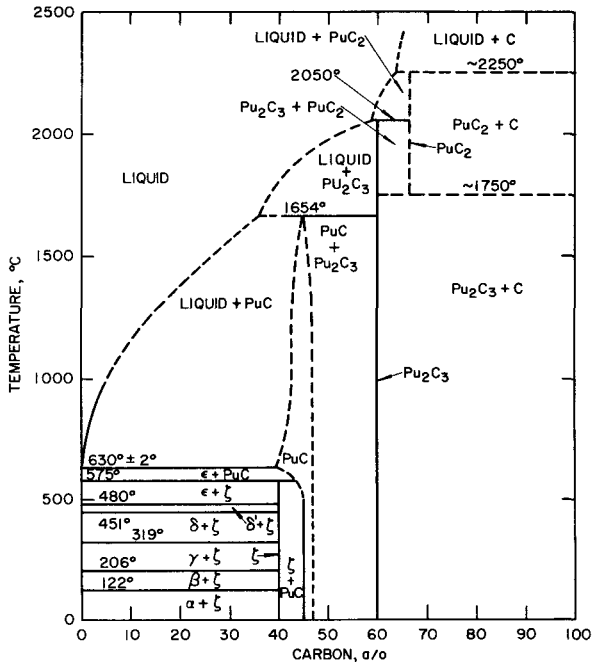

106-6424

Figure 3. Pu-C Diagram (Los Alamos)

The lattice parameter of UC prepared by reacting carbon with uranium or uranium oxide has been reported to be 4.961 ± 0.001 Å by Rundle et al.,[31] and 4.955 Å by Litz et al.[21] For the fused carbide the parameter has been given as 4.951 Å,[23] and 4.962 Å.[6] Boettcher[5] quoted a value of 4.961 ± 0.004 Å for monocarbide prepared by carbon reduction of the oxide and sintered at 1800°C. The solid-state reaction of uranium and graphite yielded a carbide with the parameter 4.963 ± 0.001 Å,[39] and more recently Austin[1] has given 4.9598 ± 0.0003 Å for a preparation made by arc melting under helium. Finally, Williams et al.,[41] reported that the cell edge in arc-melted uranium-carbon alloys varied between 4.9600 ± 0.0005 Å and 4.9520 ± 0.0002 Å in a systematic manner with carbon content. Annealing at 1300°C in vacuo caused all cell edges to approach the former value slowly.

The values for the edge of the unit cell of PuC available at present are those reported by Mulford et al.,[26] Chikalla,[7] and Kruger.[20] Using arc-melted and cast alloys Mulford obtained a variation of the unit cell dimension from 4.9582 ± 0.0003 Å for the carbon-poor phase to 4.9737 ± 0.0003 Å for the carbon-rich phase. Chikalla found 4.960 Å for a Pu-43 a/o C alloy, and 4.972 Å for a Pu-48 a/o C alloy. Kruger has reported 4.954 Å for the carbon-poor phase and 4.9730 Å for the carbon-rich monocarbide.

III. DESCRIPTION OF APPARATUS AND EXPERIMENTAL METHOD

The principal method used to determine the phase diagram was metallographic examination of isothermally annealed and quenched specimens. X-ray diffraction analysis was used in conjunction with metallography as an aid in phase identification. Observations of incipient and complete melting were also employed in establishing the liquid-solid reactions. Thermal analysis was not considered practicable because of the high melting range and the reactivity of the uranium-plutonium-carbon alloys. Dilatometric methods were contemplated for studying the solid-state reactions, but the equipment on hand lacked automatic features and could not be readily adapted for the precision measurements that would have been necessary for studying the sluggish plutonium-rich alloys.

A. Glovebox Facilities

Except for the X-ray diffraction apparatus, all equipment was contained and all work was performed within glovebox enclosures. This was necessitated by the very high toxicity of plutonium, the permissible total body-burden being approximately 0.6 μg.[38] An inert helium atmosphere was provided in the glovebox train used for alloy preparation; a nitrogen atmosphere was maintained in the metallographic train and in the glovebox containing most of the heat-treating furnaces. Oxygen, which was by far the largest impurity in either atmosphere, usually was present in concentrations between 100 and 300 ppm (as measured by a Beckman Model G2 oxygen analyzer). Torch sealing of glass capsules and capillaries was performed in an air box by methods which are described later. The glovebox trains and the procedures used in handling plutonium at the Argonne National Laboratory have been discussed in detail by L. R. Kelman.[19]

B. Alloy Preparation

1. Materials

The present study was performed with plutonium obtained in the form of rods having a diameter of about 3.2 mm and a length of about 5.1 cm from Los Alamos Scientific Laboratory; the concentration of analyzed impurities was less than 550 ppm. Uranium of 99.96 w/o purity, prepared at Argonne National Laboratory, and spectroscopic carbon rod were the other starting materials. The analyses of the uranium and plutonium are presented in Table II.

Figure 4 shows a micrograph of a section of one of the plutonium rods. The major impurity is carbon, so the spheroidal inclusions may be PuC. Inclusions similar to the acicular phase have been identified

as Pu_2O_3 at Los Alamos.[18] The high-purity uranium ingot was received as a cylindrical casting, 27.94 cm long x 2.54 cm in diameter. Metallographic examination showed no inclusions in either the as-polished or etched condition.

Table II

IMPURITIES IN STARTING MATERIALS

Element	Concentration, ppm		
	Pu (Ingot No. 1)	Pu (Ingot No. 2)	U
Ag	<1		<1
Al	10	25	<5
As			<10
B	<0.5	<0.5	0.2
Be	<0.2	<0.2	<0.5
Bi	<1	<1	<1
C	35	215	25
Ca	5	<5	<50
Co	<5	<5	<5
Cr	<20	20	1
Cu	2	5	1
F	<2	<2	
Fe	70	60	<2
K			<50
La	<10	<10	
Li	<0.2	<0.2	<1
Mg	30	<5	1
Mn	60	5	<1
Mo			<20
N	164		13
Na	<10	<10	<10
Ni	<20	40	<5
O	35	30	19
P		<10	<50
Pb	<1	1	<1
Sb			1
Si	<10	25	10
Sn	<1	<1	<5
Ta		<60	
Ti			<50
Zn	<10	10	<50
Total	<503	<546	<389

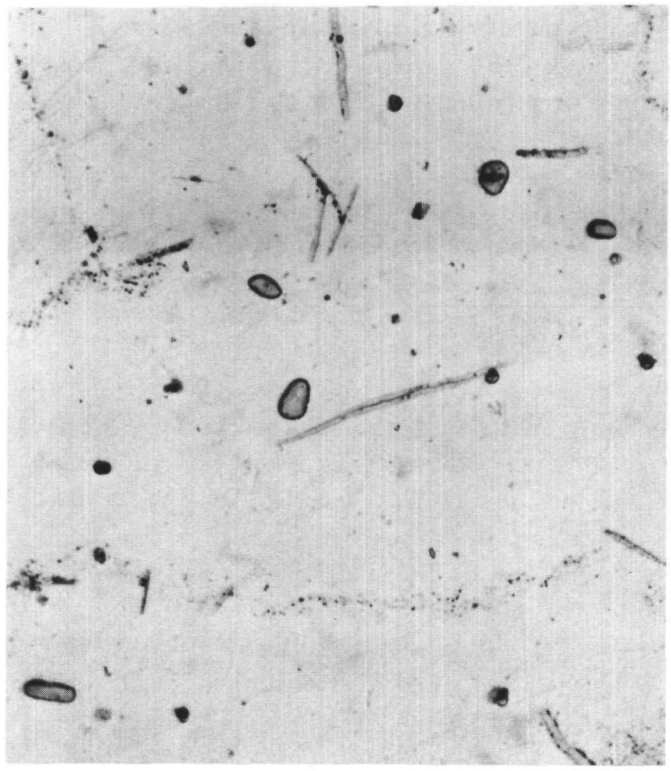

Micro 30624

Figure 4

Photomicrograph of As-received Plutonium Ingot No. 2; D, 500, BF; Pu + Inclusions

2. Charge Preparation

Preparatory to melting, the plutonium rod was cleaned with a wire brush to produce a bright metallic luster and cut to the correct size by grinding on a lathe with a silicon carbide wheel. The pieces were then repolished and stored under vacuum prior to melting.

A portion of the uranium ingot was rolled to sheet 0.38 mm thick, which could easily be cut with a pair of scissors. It was cleaned by electropolishing at about 100 mA/cm^2 for one minute in Etchant A, described on page 24.

3. Arc-melting

Alloys were prepared by arc-melting in an argon-helium atmosphere the plutonium, uranium, and graphite on a water-cooled copper hearth in a furnace with a tungsten electrode. In order to minimize the volatilization of plutonium and the sublimation of carbon, the charge was placed in the hearth with the uranium sheet uppermost. Ten 30-g charges were prepared initially, but metallographic examination indicated gross inhomogeneities, especially for uranium-rich, high-carbon alloys. Charges weighing approximately 5 g were prepared for the remaining 106 alloys. Although inhomogeneities were occasionally found in the 5-g alloys, they were estimated to represent compositional variations amounting to a few a/o carbon at most.

A copper hearth containing three depressions was used. One depression contained a zirconium button which was used as a getter for the furnace atmosphere prior to the melting of the charges in the other two depressions. Each ingot was melted for at least three 60-sec periods, being inverted between meltings. Alloying was rapid, occurring in less than 5 sec. A water-cooled tungsten electrode was used in all but a few initial experiments. A series of alloys, which were cast to determine the suitability of a graphite electrode, showed that this type of electrode could also be used, but vaporization of carbon quickly covered the viewing window with a layer of soot.

Alloys containing less than 30 a/o carbon were always homogeneous after three one-minute melts when power was supplied at about 200 Amp and 40 V. For compositions above 30 a/o carbon, the buttons showed a small degree of inhomogeneity after three melts; it was necessary to melt these alloys at 300 Amp (the capacity of the equipment) for periods of 6 min to ensure homogeneity. Some spattering and vaporization occurred under these conditions, resulting in weight losses. It was observed, however, that losses could be eliminated in most cases if sufficient care was taken to control the initial melting rate. Weight losses were usually of the order of 0.1 to 1.0 w/o.

Contamination resulting from alloying was considered negligible on the basis of spectroscopic and chemical analyses. Table III shows representative analytical results. The tungsten contamination found in the uranium-33 a/o plutonium-45 a/o carbon alloy occurred when the electrode came in contact with the melt. Contact could be observed quite easily either during melting or by observing the bright appearance of the tungsten tip after melting. The relatively high oxygen values shown in Table III are probably the result of surface contamination, as discussed in Appendix I.

Because a high-temperature annealing furnace was not available for long heat treatments, it was difficult to remove the inhomogeneous remnants of the cast structure in high-carbon alloys. In an attempt to improve the situation, the melting arc was maintained at about 60 Amp for approximately 60 sec after the last remelting operation. In most cases, this procedure kept the alloy below its melting point, as indicated by the solid appearance of the button. Although alloys cast in this manner still contained microscopic inhomogeneities, the procedure was not abandoned; for it helped to reduce shattering in cast alloys containing about 50 a/o carbon. These high-carbon alloys were sensitive to thermal shock and often shattered into many pieces upon cooling, making it difficult to prepare desired compositions. Maintaining a low-current arc for a period of one minute and then evacuating the arc-melt chamber at the instant the arc was discontinued successfully eliminated cracking, presumably because of the reduced cooling rate.

Table III

CONCENTRATIONS OF CONTAMINANTS IN THE CAST ALLOYS

Alloy Composition, a/o			Impurities Analyzed, ppm*			
U	Pu	C	O_2	N_2	Cu	W
95	5	0	360			
82	18	0	151			
50	50	0	590			
45	55	0			<5	350
16	84	0				10
12	88	0				<5
10	90	0	290			
8	92	0	243			5
19	80	1				15
4	95	1				30
0	98	2	488			70
1	79	20		24	<5	
34.5	30.5	35				30
17	48	35				60
6	52	42				30
0	56	44				50
28	27	45				50
22	33	45				1000
41	13	46				100
25	28	47		15	<5	
8	44	48		39		
32.5	19	48.5		203	<10	
6.5	45	48.5		8	8	
20	31	49		5	<2	
43.5	6	50.5		156	<5	

*By weight.

C. Heat Treatment

Specimens for homogenization and isothermal annealing treatments were prepared from the arc-melted buttons. Suitable specimens of about 0.25 to 1 g (approximately a 3-mm cube) were obtained by cracking the cast ingot with a hammer. Although a cold-working treatment would have been desirable to accelerate the diffusion process during annealing, all the alloys except uranium-rich and plutonium-rich low-carbon alloys were too brittle to be worked.

Before encapsulating, an alloy sample was wrapped in tantalum foil, having a thickness of 0.025 mm, to prevent contact with the capsule material or other specimens. The tantalum also served as a getter for oxygen that was not removed in the evacuating process. The wrapped specimens were placed in a 9-mm-OD Vycor tube, sealed at one end. The other end was attached by a rubber tube to a mechanical vacuum pump, and the tube was evacuated. A thermocouple gage indicated an equilibrium pressure of about 25 μ. After about $\frac{1}{2}$ hr, the rubber tube was closed with a pinch clamp and the Vycor tube containing the samples disconnected from the vacuum system by cutting the rubber tubing on the vacuum pump side of the pinch clamp. The Vycor tube containing the specimens was transferred through an air lock into an interconnected air box, where the portion of the tube containing the specimens was sealed with a natural gas-oxygen torch about 5 to 7.6 cm from the closed end.

In most cases the specimens retained their bright surface appearance after heat treatment. The appearance of the tantalum wrapping was always consistent with the appearance of the heat-treated specimens. A poor encapsulation always resulted in partial oxidation of the tantalum surface, and this oxidized appearance served as a basis for rejection of the specimens. Only about 2 percent of the specimens encapsulated were rejected. Usually six to ten specimens were contained in each Vycor capsule.

The specimens were annealed by suspending the capsule in one of six Kanthal-wound vertical tube furnaces. They contained nickel heat sinks, 7.6 cm long, which provided a zone of the same length in which the temperature was constant to within 1°C between 400 and 635°C. At 1100°C, the maximum temperature at which the furnace was operated, the temperature variation along the zone was less than 2°C. Temperatures were measured by means of Pt/Pt-10% Rh thermocouples and were maintained constant to within 3°C or better by controllers equipped with saturable core reactors. At about one month intervals a Pt/Pt-10% Rh thermocouple calibrated by the National Bureau of Standards was used to check the accuracy of the temperature measurements.

A quench was obtained by allowing the capsule to fall into a can, where it was crushed under Octoil high vacuum pump oil. This operation required about one second. No appreciable surface contamination resulted from reaction of the samples with the quenching bath. Initially a NaK quench was used, but it was believed that the more rapid quench available with the NaK bath did not justify the danger inherent in its use. Water quenching resulted in extensive surface contamination and decarburization of a series of alloys, and was rejected for this reason.

A horizontal tantalum-tube resistance furnace was occasionally available for annealing treatments at 1400 or 1500°C for periods of time up to one day. The furnace was connected to a vacuum system, equipped

with a diffusion pump, which allowed a dynamic vacuum of about 10^{-6} mm Hg to be maintained. Specimens required no encapsulation, and were simply wrapped in tantalum foil, placed in a tantalum boat, and inserted into the center of the furnace. The furnace had a small heat capacity; a moderately rapid quench was obtained by turning off the power.

A summary of the typical preliminary homogenizations and the equilibrating heat treatments at 400, 570, and 635°C is given in Table IV.

Table IV

TYPICAL HEAT TREATMENTS FOR TERNARY ALLOYS

	Homogenization Treatment[1]	Annealing Time at 400, 570, or 635°C (days)
U-rich		
Low-carbon (0-40 a/o C)	600°C - 3 days	4-10
High-carbon (40-50 a/o C)	1050°C - 3 days	7-20
Intermediate		
Low-carbon (0-45 a/o C)	None	4-10
High-carbon (45-50 a/o C)	1050°C - 3 days	7-15
Pu-rich		
Low-carbon (0-45 a/o C)	None	4-10
High-carbon (45-50 a/o C)	1050°C - 3 days	7-15

[1] A preliminary three-day homogenization heat treatment at 600°C was given all alloys annealed at temperatures below 400°C.

D. Incipient Melting Technique

The data for determining the plutonium-rich boundaries of the 635°C isotherm (see Figure 7 on p. 50) were obtained by both an incipient-melting technique and a metallographic examination of isothermally annealed and quenched alloys.

The incipient-melting technique consisted of looking for visual signs of melting on rod-shaped specimens that had been isothermally annealed for periods of time not less than one-half hour. The specimens were individually sealed in evacuated Vycor capsules and held in an upright position in a tantalum cup. Incipient melting was associated with rounding of corners; total melting was assumed when the specimen collapsed completely.

The furnace temperature was regulated by a Wheelco Model 407 controller. Fine temperature control and adjustment was provided for by

a Wheelco Model 404-S241 adjustable external resistor attached to the controller. For the short periods of time required for these anneals, no difficulty was encountered in keeping the temperature constant to within ±1°C. Temperature measurements were made at 10-min intervals, by means of a Pt-Pt 10% Rh thermocouple placed adjacent to the Vycor capsule. The accuracy of the temperature measurements was investigated by observing the melting point of cylinders of pure cadmium and pure aluminum. Melting points usually agreed with the literature values to within 1°C.

In some cases, when poor vacuums were obtained in the encapsulating process, the formation of an oxide shell prevented the specimen from collapsing although it was known that the melting point had been exceeded. This was especially true for some of the pure aluminum cylinders used in the temperature calibration.

Alloys which showed excessive darkening were rejected. The ternary alloys were usually too brittle to be formed into rods, so that in most cases chips of suitable shape were taken from the cast buttons. Observations were usually made over temperature intervals of several degrees.

E. X-ray Diffraction

X-ray diffraction patterns were used in the identification of phases and in determining the lattice parameters of the carbide phases. The patterns were obtained with filtered Cu-Kα radiation by the use of a Debye-Scherrer powder camera, 114.6 mm in diameter, which was located outside the glovebox system. Exposures were usually for 4 hr at 50 kV and 16 mA on a Norelco X-ray diffraction unit. Ambient temperature during exposure ranged from 21 to 26°C.

Needle-shaped specimens, which were abraded with a file, were prepared from the ductile low-carbon alloys in the composition region near pure plutonium and that near pure uranium. The other alloys were sufficiently brittle for the preparation of powder specimens by crushing with a mortar and pestle until the material passed through a fine silk screen. The powder was then loaded into a 0.3-mm quartz capillary, which had previously been introduced into the system inside a 13-mm-OD x 100-mm test tube with only the open end extending through a rubber stopper inserted into the top of the tube. In this way, the outside of the capillary remained uncontaminated during the loading operation. The test tube was then brought to the air box where the rubber stopper holding the capillary was gently removed. The loaded end of the capillary was grasped firmly but gently with uncontaminated rubber-tipped tweezers, which were brought into the system for this purpose, and the capillary was manually held over a natural gas-oxygen flame and sealed.

It was necessary to set up procedures for removing the X-ray specimens from within the glovebox system and transferring them to the X-ray

machine, which was outside the box system. The sealed capillary or needle specimen was placed into an uncontaminated vial, which was immediately closed and placed into a vinyl pouch for removal from the glovebox system according to the procedure described by Kelman.[19]

The remaining operations of loading the camera with the specimen and film were performed in exhaust hoods. The vinyl pouch was slit and the capillary removed. The capillary was picked up with the rubber-tipped tweezers again, coated with collodion, and placed into a brass insert for loading into the Debye-Scherrer powder diffraction camera. The collodion was used to fix any loose radioactive material that may have accidentally adhered to the outside of the capillary during the sealing operation within the air box. Needle specimens were coated both before and after removal from the protective atmosphere; the initial coat serving as a barrier against surface contamination.

Suitable diffraction patterns for phase identification were obtained by this procedure. The pattern of the brittle carbide phase that was present in high-carbon alloys always contained sharp lines that could be used for parameter measurements. In the case of the low-carbon alloys, reannealing of the X-ray specimens was required to sharpen the broad and diffuse lines typical of plutonium-alloy powder patterns. The diffraction data shown in Tables X (see p. 55) and XI (see p. 74), for the zeta and Pu_3C_2 phases, respectively, were obtained from powders that were annealed after preparation but prior to loading into the X-ray capillaries. Although a noticeable improvement in the resolution of high-angle doublets was obtained, the patterns still contained many diffuse lines, as indicated in Table XI.

Lattice parameters were obtained with the aid of an IBM-704 computer in accordance with a program devised by Mueller and Heaton (see Appendix III).

F. Metallography

The metallographic preparation and examination of the alloys was performed in a glovebox train containing a nitrogen atmosphere. The specimens were mounted in a catalyzed liquid casting resin (Polylite No. 8173 proprietary resin supplied by Reichhold Chemical Inc., Argo, Illinois). The mounts were usually cast late in the day and were cured by standing overnight at room temperature. This method produced a hard mount, and the temperature rise on curing was insufficient to alter the structures. Rough polishing was performed with an Automet polisher, which allowed six specimens to be polished at one time. The specimens were ground on a sequence of 320-, 400-, and 600-grit silicon carbide papers for periods of about

one minute. Hyprez (Buehler Ltd., Chicago, Illinois) was used as a lubricant through the grinding and polishing operations. Absolute alcohol was used as the washing agent. Polishing was performed for periods of 2 min with diamond paste on Buehler Metcloth.

An Americal Optical Company Model 2400P research metallograph was employed for microscopic examination and for photographing the specimen surfaces.

The following etching reagents and procedures were found to be satisfactory:

Uranium-rich Alloys

Electropolish: Etchant "A"

Orthophosphoric acid, 85 w/o, C.P.	5 parts by volume
Ethylene glycol	5 parts by volume
Ethyl alcohol, 95 w/o	8 parts by volume

Electroetch: Etchant "B"

Citric acid, C.P.	10.0 gm
Nitric acid, 70 w/o, C.P.	2.5 ml
Distilled water	490.0 ml

Electropolish for polarized light at about 40 mA/cm^2 for 2 min. Etch for bright field at about 15 mA/cm^2 for one minute.

Plutonium-rich Alloys

Electroetch and electropolish: Etchant "C"

Orthophosphoric acid, 85 w/o, C.P.	32 parts by volume
2-Ethoxyethanol	59 parts by volume
Distilled water	9 parts by volume

Chemical etch: Etchant "D"

(same as Etchant "C")

When electrolysis was performed at low current density (10 to 15 mA/cm^2) etching occurred; when the current density was raised (30 to 40 mA/cm^2) polishing occurred. Electrolysis time was between 30 and 60 sec. For many alloys a 5-sec swab produced a suitably etched surface.

Carbon-rich Alloys

Chemical etch: Etchant "E"

Nitric acid, 70 w/o C.P.	1 part by volume
Acetic acid	1 part by volume
Distilled water	1 part by volume

Chemical etch: Etchant "F"

Silver nitrate	0.25 gm
Hydrogen fluoride	0.10 ml
Distilled water	99.70 ml

Etching time for reagent "E" was about 15 sec. Etchant "F" required much shorter periods of time, 1 to 3 sec.

The choice of etchant for many alloys, especially those of intermediate composition, was made by a process of elimination. In instances when none of the etchants described above was satisfactory, different mixtures of HF, HNO_3, HAc, and H_2O were prepared to produce a suitable surface. A mixture commonly employed is listed below:

Chemical etch: Etchant "G"

Nitric acid, 70 w/o, C.P.	1 part by volume
Distilled water	1 part by volume

Swabbing for 1 to 5 sec was usually sufficient.

Some revelation of microstructure could be achieved in high-carbon alloys by allowing the polished specimen to stand in the glovebox atmosphere for 3 to 5 min. Throughout the balance of the report this condition will be denoted as the "as polished" (AP) condition. Except for the Pu_3C_2 phase, this procedure did not usually disclose the microstructure as well as did the etching reagents, nor was it entirely reproducible.

G. Chemical Analysis

The analytical work was performed by the Chemistry Division of Argonne National Laboratory. The procedures used are outlined in Appendix I.

All of the 116 alloys were analyzed for carbon content; 12 alloys were also analyzed for uranium and plutonium contents, and the sum of the uranium, plutonium, and carbon analyses for a given alloy totaled 100 ± 1 a/o. An additional 70 alloys were analyzed for either uranium or plutonium. In most cases the chemical analyses agreed to within 1 a/o with the intended compositions, so the latter have been used in reporting the results.

IV. RESULTS AND CONCLUSIONS

One hundred and sixteen alloys were used in establishing the isothermal sections, and 439 metallographic specimens were prepared from these alloys in both the as-cast and annealed conditions. The annealing treatments and resulting microstructures are tabulated in Table V. Incipient melting observations are recorded in Table VI.

Table V

SUMMARY OF METALLOGRAPHIC OBSERVATIONS

Alloy Composition, a/o			Annealing Conditions*		
U	Pu	C	Temp (°C)	Time (days)	Structure**
100	0	0	R		alpha U
95	5	0	C		alpha U
			400	7	alpha U
			570	7	alpha U
82	18	0	C		beta U
			400	7	alpha U + zeta (c)
			545	9	alpha U + zeta
			553	10	alpha U + zeta (c)
			562	5	beta U + trace zeta
			570	7	beta U
75	25	0	704	5	tr eta (c)
			710	5	beta U + tr gamma U
			714	4	beta U + tr gamma U
			721	13	tr eta (c)
72	28	0	598	5	zeta (c)
			604	11	zeta (c)
			610	9	beta U + tr eta (c)
70	30	0	C		zeta (c)
			400	7	zeta (c)
			570	7	zeta (c)
50	50	0	C		zeta
			400	7	zeta
			570	7	tr eta
45	55	0	C		zeta + den inclusions
			737	1/8	zeta + den inclusions

Table V (Contd.)

Alloy Composition, a/o			Annealing Conditions*		
U	Pu	C	Temp (°C)	Time (days)	Structure**
23	77	0	278	29	zeta + tr eta
			400	22	zeta + tr eta
			570	7	tr eta + tr epsilon Pu
			620	13	tr epsilon Pu
16	84	0	C		tr epsilon Pu
			570	4	tr epsilon Pu
15	85	0	288	29	zeta + tr eta
			295	22	zeta + tr eta
			635	6	tr epsilon Pu (specimen melted)
12	88	0	628	3	tr epsilon Pu
			631	1/48	tr epsilon Pu (specimen melted)
10	90	0	C		tr epsilon Pu
			400	7	tr delta Pu
			570	7	tr epsilon Pu
8	92	0	C		tr epsilon Pu
0	100	0	R		Pu + den inclusions
			R-1†		Pu + acicular and spheroidal inclusions
			R-2†		Pu + acicular and spheroidal inclusions (see Figure 4, page 17)
			C-2†		Pu + spheroidal inclusions
82	17	1	545	9	alpha U + zeta
			553	10	alpha U + zeta
			562	5	beta U + trace zeta
74.5	24.5	1	704	5	tr eta (c)
			710	5	beta U + tr eta (c)
			714	4	beta U + tr gamma U
			721	13	beta U + tr gamma U
71	28	1	598	5	beta U + tr eta (c)
			604	11	beta U + tr eta (c)
			610	9	beta U + tr eta (c)
58	41	1	570	4	zeta + tr eta
			638	6	tr eta (c)
40	59	1	400	5	zeta + tr eta

Table V (Contd.)

Alloy Composition, a/o			Annealing Conditions*		
U	Pu	C	Temp (°C)	Time (days)	Structure**
40	80	1	C		tr epsilon Pu
			628	3	tr epsilon Pu
40	59	1	635	6	tr eta + tr epsilon Pu
19	80	1	635	7	tr epsilon Pu + tr liquid + eut (U,Pu)C
14.5	84.5	1	288	29	zeta + tr eta + eut (U,Pu)C
			295	22	zeta + tr eta + eut (U,Pu)C
			635	6	tr epsilon Pu (specimen melted)
4	95	1	C		tr epsilon Pu + eut (U,Pu)C
			628	3	tr epsilon Pu + eut (U,Pu)C
			635	7	tr epsilon Pu + tr liquid + eut (U,Pu)C
94	4	2	635	4	alpha U
			800	4	tr gamma U
92	6	2	635	4	alpha U + beta U
0	98	2	C		tr epsilon Pu
			629	1/48	tr epsilon Pu
81	16	3	545	9	alpha U + zeta
			553	10	beta U + trace zeta
			562	5	beta U + trace zeta
			570	4	beta U
			635	3	beta U
73	24	3	570	4	beta U + trace zeta
			635	3	beta U + tr eta (c)
			704	5	tr eta (c)
73	24	3	710	5	beta U + tr eta (c)
			714	4	beta U + tr gamma U
			721	13	beta U + tr gamma U
70	27	3	400	5	zeta (c)
			598	5	beta U + tr eta
			604	11	beta U + tr eta
			610	9	beta U + tr eta
			635	3	tr eta (c)
			800	4	tr gamma U + grain boundary phase

Table V (Contd.)

Alloy Composition, a/o			Annealing Conditions*		
U	Pu	C	Temp (°C)	Time (days)	Structure**
14	83	3	288	29	zeta + tr eta
			298	22	zeta + tr eta
			570	4	tr epsilon Pu
			635	6	tr epsilon Pu + tr liquid + eut (U,Pu)C
5	90	5	C		tr epsilon Pu + eut and den (U,Pu)C
			635	1/48	tr epsilon Pu + eut (U,Pu)C
			635	7	tr epsilon Pu + eut and den (U,Pu)C
82	11	7	400	5	alpha U + zeta
			570	5	alpha U + beta U
			635	5	beta U
79	14	7	400	5	alpha U + zeta
			570	5	beta U + alpha U
			635	5	beta U
75	18	7	400	5	alpha U + zeta
			560	4	beta U + zeta
			570	5	beta U + zeta
			620	11	beta U + tr eta
			635	5	beta U + tr eta
70	23	7	400	5	zeta (c) + alpha U
			570	4	zeta (c)
			590	11	zeta (c)
			635	5	tr eta (c) + beta U
			704	11	tr eta (c)
58	35	7	400	5	zeta (c)
			570	5	zeta (c)
			635	7	tr eta (c)
52	41	7	400	5	zeta
			570	4	tr eta (c)
36	57	7	400	4	tr eta + zeta
			570	4	tr eta
			620	11	tr eta (c) + tr epsilon Pu
			635	5	tr eta + tr epsilon Pu

Table V (Contd.)

Alloy Composition, a/o			Annealing Conditions*		
U	Pu	C	Temp (°C)	Time (days)	Structure**
26	67	7	400	4	tr eta + zeta
			570	5	tr eta + tr epsilon Pu
			620	11	tr epsilon Pu
23	70	7	400	4	tr eta (c)
			400	21	tr eta
			570	4	tr eta + tr epsilon Pu
			620	11	tr epsilon Pu
			635	7	tr epsilon Pu
15	78	7	C		tr epsilon Pu
			400	4	tr eta
			570	4	tr epsilon Pu + eut and den (U,Pu)C
			620	4	tr epsilon Pu + eut and den (U,Pu)C
			635	6	tr epsilon Pu + tr liquid + eut and den (U,Pu)C
			668	1/48	tr epsilon Pu + eut and den (U,Pu)C (specimen melted)
6	87	7	C		tr epsilon Pu + eut and den (U,Pu)C
			400	4	tr eta + tr delta Pu + eut and den (U,Pu)C
			400	21	tr eta + tr delta Pu + eut and den (U,Pu)C
			570	5	tr epsilon Pu + eut and den (U,Pu)C
			622	2	tr epsilon Pu + eut and den (U,Pu)C
			631	1/48	tr epsilon Pu + eut and den (U,Pu)C
			635	6	tr epsilon Pu + eut and den (U,Pu)C (specimen melted)
2	91	7	C		tr epsilon Pu + eut and den (U,Pu)C
			400	4	tr delta Pu + eut and den (U,Pu)C
			400	21	tr delta Pu + eut and den (U,Pu)C
			400	34	tr delta Pu + eut and den (U,Pu)C

Table V (Contd.)

Alloy Composition, a/o			Annealing Conditions*		
U	Pu	C	Temp (°C)	Time (days)	Structure**
2	91	7	570	4	tr epsilon Pu + eut and den (U,Pu)C
			620	11	tr epsilon Pu + eut and den (U,Pu)C
			635	6	tr epsilon Pu + eut and den (U,Pu)C
78	5	17	C		alpha U
			400	4	alpha U
			570	10	alpha U
55.5	27.5	17	C		zeta (c)
			400	4	zeta (c)
			570	10	zeta (c)
39	44	17	C		zeta (c)
			400	4	zeta + tr eta
			570	10	tr eta
10	73	17	C		tr epsilon Pu
			400	4	tr eta + tr delta Pu
			570	10	tr epsilon Pu
64	16	20	C		zeta (c)
			400	4	zeta (c) + alpha U
29.5	50.5	20	635	9	tr epsilon Pu + tr eta
23	57	20	570	6	tr eta + tr epsilon Pu
15	65	20	107	75	zeta
			225	75	zeta
			311	22	tr eta
			336	17	tr eta
			400	12	tr eta
			440	14	tr eta
			470	11	tr eta
			500	7	tr eta
			570	12	tr epsilon Pu
			635	7	tr epsilon Pu
10	70	20	107	75	zeta
			225	75	zeta
			311	22	tr gamma Pu
			336	17	tr eta + tr delta Pu
			400	12	tr delta Pu + tr eta
			440	14	tr delta Pu
			470	11	tr Pu

Table V (Contd.)

Alloy Composition, a/o			Annealing Conditions*		
U	Pu	C	Temp (°C)	Time (days)	Structure**
10	70	20	500	7	tr epsilon Pu
			570	12	tr epsilon Pu
			635	7	tr epsilon Pu (specimen melted)
5	75	20	C		tr epsilon Pu
			107	75	alpha Pu
			225	75	tr Pu
			311	22	tr gamma Pu + Pu_3C_2
			336	17	tr delta Pu + Pu_3C_2
			400	8	tr delta Pu + Pu_3C_2
			400	34	tr delta Pu + Pu_3C_2
			440	14	tr delta Pu + Pu_3C_2
			470	11	tr Pu + Pu_3C_2
			500	7	tr epsilon Pu + Pu_3C_2
			570	12	tr epsilon Pu
			628	3	tr epsilon Pu
			635	6	tr epsilon Pu + eut and den (U,Pu)C
1	79	20	107	75	alpha Pu + Pu_3C_2
			225	75	tr Pu + Pu_3C_2
			311	22	tr gamma Pu + Pu_3C_2
			336	17	tr delta Pu + Pu_3C_2
			400	12	tr delta Pu + Pu_3C_2
			440	14	tr delta Pu + Pu_3C_2
			470	11	tr Pu + Pu_3C_2 + trace (U,Pu)C
			500	7	tr epsilon Pu + Pu_3C_2
			570	4	tr epsilon Pu
			635	6	tr epsilon Pu
0	80	20	C		tr epsilon Pu
			195	34	tr beta Pu + Pu_3C_2
			300	21	tr gamma Pu + Pu_3C_2
			400	11	tr delta Pu + Pu_3C_2
			400	34	tr delta Pu + Pu_3C_2
			645	7	tr delta Prime Pu + Pu_3C_2
			545	28	tr epsilon Pu + Pu_3C_2
			554	21	tr epsilon Pu + Pu_3C_2
			560	11	tr epsilon Pu
			580	9	tr epsilon Pu
			500 then 600	33 then 21	tr epsilon Pu + spheroidal and den PuC
			622	2	tr epsilon Pu
			643	1/48	tr epsilon Pu (specimen melted)

Table V (Contd.)

Alloy Composition, a/o			Annealing Conditions*		
U	Pu	C	Temp (°C)	Time (days)	Structure**
9.5	62.5	28	400	6	tr delta Pu + Pu_3C_2
			570	4	tr epsilon Pu + tr eta
			750	1/12	tr epsilon Pu
64	6	30	400	6	alpha U
			570	4	alpha U
			1000	1/12	tr gamma U
53	17	30	400	6	zeta (c)
			570	4	zeta (c)
			1000	1/12	tr gamma U
43	27	30	400	6	zeta
			570	4	zeta (c)
			1000	1/12	tr gamma U
28	39	33	400	6	tr eta
			570	4	slightly cored (U,Pu)C + tr eta
			750	1/12	tr epsilon Pu
61	4	35	400	8	alpha U
			570	7	alpha U
			620	11	alpha U
			635	5	alpha U
59.5	5.5	35	400	8	alpha U + zeta
			570	7	alpha U + beta U
			635	5	beta U
58	7	35	400	8	alpha U + zeta (c)
			570	7	beta U
			635	5	beta U
56.5	8.5	35	400	8	alpha U + zeta (c)
			570	7	beta U + zeta
			635	5	beta U + tr eta
55	10	35	400	8	alpha U + zeta (c)
			570	12	zeta (c)
			635	3	beta U + tr eta
53.5	11.5	35	400	8	zeta (c)
			570	7	zeta (c)
			620	11	tr eta (c)
			635	3	tr eta (c)

Table V (Contd.)

Alloy Composition, a/o			Annealing Conditions*		
U	Pu	C	Temp (°C)	Time (days)	Structure**
42	23	35	400	11	zeta + tr eta
			570	7	zeta (c)
			675	7	tr eta (c)
40	25	35	400	11	zeta + tr eta
			570	7	zeta (c)
38	27	35	400	11	tr eta + zeta
			570	18	tr eta + zeta
36	39	35	400	11	tr eta + zeta + cored (U,Pu)C
			570	18	tr eta (c)
34.5	30.5	35	400	22	tr eta + cored (U,Pu)C
			570	17	tr eta + cored (U,Pu)C
33	32	35	400	11	tr eta
			570	17	tr eta + cored (U,Pu)C
			620	13	tr eta
			635	3	tr eta
17	48	35	107	78	zeta
			225	75	zeta
			311	22	tr eta
			336	17	tr eta
			400	22	tr delta Pu
			440	14	tr eta
			470	11	tr eta
			500	7	tr epsilon Pu
			570	12	tr eta + tr epsilon Pu + cored (U,Pu)C
			620	13	tr epsilon Pu
			635	6	tr epsilon Pu
14	51	35	107	75	zeta
			225	75	tr Pu
			311	22	tr gamma Pu
			336	7	tr delta Pu + tr eta
			400	12	tr delta Pu + Pu_3C_2
			440	14	tr delta Pu
			470	11	tr eta
			500	7	tr epsilon Pu + cored (U,Pu)C
			570	12	tr epsilon Pu + trace tr eta
			635	7	tr epsilon Pu + cored (U,Pu)C

Table V (Contd.)

Alloy Composition, a/o			Annealing Conditions*		
U	Pu	C	Temp (°C)	Time (days)	Structure**
11	54	35	107	75	zeta
			225	78	tr Pu + Pu_3C_2
			311	22	tr gamma Pu + Pu_3C_2
			336	17	tr delta Pu + Pu_3C_2
			400	22	tr delta Pu + Pu_3C_2
			440	14	tr delta Pu + Pu_3C_2
			470	11	tr Pu + Pu_3C_2
			500	7	tr epsilon Pu + Pu_3C_2
			570	17	tr epsilon Pu + cored (U,Pu)C
			620	13	tr epsilon Pu
			635	6	tr epsilon Pu (specimen melted)
9	56	35	107	75	alpha Pu + Pu_3C_2
			225	75	tr Pu + Pu_3C_2
			311	22	tr gamma Pu + Pu_3C_2
			336	17	tr delta Pu + Pu_3C_2
			400	22	tr delta Pu + Pu_3C_2
			440	14	tr delta Pu + Pu_3C_2
			470	11	tr Pu + Pu_3C_2
			500	7	tr epsilon Pu + Pu_3C_2
			570	17	tr epsilon Pu + cored (U,Pu)C
			620	13	tr epsilon Pu + cored (U,Pu)C
			635	6	tr epsilon Pu (specimen melted)
0	65	35	400	11	tr delta Pu + Pu_3C_2
			570	12	tr epsilon Pu
			595	10	tr epsilon Pu
			620	11	tr epsilon Pu
			635	7	tr epsilon Pu
0	62.5	37.5	400	11	tr delta Pu + Pu_3C_2
			500	14FC	tr epsilon Pu + Pu_3C_2 (no PuC)
			570	12	tr epsilon Pu
			595	10	tr epsilon Pu
			635	7	tr epsilon Pu
5	57	38	400	8	Pu_3C_2 + equiaxed (U,Pu)C
			400	34	Pu_3C_2 + tr delta Pu + equiaxed (U,Pu)C
			570	7	tr epsilon + cored (U,Pu)C
			620	11	tr epsilon + cored (U,Pu)C
			635	6	tr epsilon Pu + cored (U,Pu)C

Table V (Contd.)

Alloy Composition, a/o			Annealing Conditions*		
U	Pu	C	Temp (°C)	Time (days)	Structure**
0	61	39	400	11	Pu_3C_2
			500	14FC	Pu_3C_2 (no PuC)
			530	17	Pu_3C_2 (no PuC)
			570	4	tr epsilon Pu
			595	10	tr epsilon Pu
			625	4	tr epsilon Pu
			635	7	tr epsilon Pu
1	59	40	400	12	Pu_3C_2
			500	3	Pu_3C_2 [no (U,Pu)C]
			500	14FC	Pu_3C_2 [no (U,Pu)C]
			570	12	tr epsilon Pu
			635	6	tr epsilon Pu + cored (U,Pu)C
0	60	40	500	14FC	Pu_3C_2 (no PuC)
0	59	41	400	22	Pu_3C_2
			500	14FC	Pu_3C_2
			530	17	Pu_3C_2
			570	7	tr epsilon Pu
			595	10	tr epsilon Pu
			620	13	tr epsilon Pu
			625	4	tr epsilon Pu
6	52	42	400	22	Pu_3C_2 + equiaxed (U,Pu)C
			570	18	tr epsilon Pu
			620	13	tr epsilon Pu + cored (U,Pu)C
			635	6	tr epsilon Pu + cored (U,Pu)C
0	57.5	42.5	C		tr epsilon Pu + equiaxed PuC
			400	8	Pu_3C_2 + equiaxed PuC
			400	34	Pu_3C_2 + equiaxed PuC
			500	14FC	Pu_3C_2 + equiaxed PuC
			530	17	Pu_3C_2 + equiaxed PuC
			570	4	tr epsilon Pu + equiaxed PuC
			595	10	tr epsilon Pu + equiaxed PuC
			620	11	tr epsilon Pu + equiaxed PuC
			635	4	tr epsilon Pu + equiaxed PuC
3.7	52.3	44	400	11	Pu_3C_2 + equiaxed (U,Pu)C
			570	8	tr epsilon Pu + equiaxed (U,Pu)C
			635	7	tr epsilon Pu + equiaxed (U,Pu)C

Table V (Contd.)

Alloy Composition, a/o			Annealing Conditions*		
U	Pu	C	Temp (°C)	Time (days)	Structure**
0	56	44	400	11	cored equiaxed PuC
			570	18	cored equiaxed PuC
			635	7	cored equiaxed PuC
			1500	1/2	equiaxed PuC + tr liquid
28	27	45	400	11	tr eta
			570	18	tr eta
			635	7	tr eta
22	33	45	400	11	tr eta
			570	18	tr eta
			635	7	tr eta
10	45	45	400	11	Pu_3C_2 + equiaxed (U,Pu)C
			570	8	tr epsilon Pu + equiaxed (U,Pu)C
			635	7	tr epsilon Pu + tr liquid + equiaxed (U,Pu)C
41	13	46	400	11	zeta + tr eta
			570	18	zeta
			625	4	tr eta
			635	7	tr eta
0	54	46	400	22	cored equiaxed PuC
			570	17	cored equiaxed PuC
			620	13	cored equiaxed PuC
			1400	1/24	equiaxed PuC + tr liquid
			1500	1/2	equiaxed PuC + tr liquid
25	28	47	400	7	tr eta
			570	7	tr eta
			635	6	tr eta
20	33	47	400	7	tr delta Pu
			570	7	tr eta
			635	6	tr epsilon Pu
3.7	49.3	47	400	11	cored (U,Pu)C
			570	8	cored (U,Pu)C
			635	7	cored (U,Pu)C
			1500	1/2	equiaxed (U,Pu)C
0	52.5	47.5	C		cored equiaxed PuC
			570	7	cored equiaxed PuC
			1400	1/24	equiaxed PuC
			1500	1/2	equiaxed PuC or tr liquid

Table V (Contd.)

Alloy Composition, a/o			Annealing Conditions*		
U	Pu	C	Temp (°C)	Time (days)	Structure**
40.5	11.5	48	400	11	tr eta
			570	8	zeta
			635	7	tr eta
8	44	48	400	11	cored (U,Pu)C
			570	8	cored (U,Pu)C
			635	7	cored (U,Pu)C
45	6.5	48.5	400	7	zeta
			570	7	zeta
			635	6	tr eta
32.5	19	48.5	400	7	cored (U,Pu)C + tr eta
			570	7	zeta
			635	6	tr eta
6.5	45	48.5	400	7	cored (U,Pu)C
			570	7	cored (U,Pu)C
			635	6	cored (U,Pu)C
			1500	1/2	equiaxed (U,Pu)C + $(U,Pu)_2C_3$
51	0	49	C		tr gamma U
			570	21	alpha U
23	28	49	400	7	tr eta
			570	7	tr eta
			635	6	tr eta + cored (U,Pu)C
20	31	49	400	7	tr delta Pu + cored (U,Pu)C
			570	7	tr eta + cored (U,Pu)C
			635	6	tr epsilon Pu + cored (U,Pu)C
15	36	49	C		tr epsilon Pu + cored (U,Pu)C
			400	21	unidentified phase + cored (U,Pu)C
			570	21	tr eta + cored (U,Pu)C
			635	7	tr epsilon Pu + cored (U,Pu)C
			1500	1/2	tr liquid + cored (U,Pu)C
2	49	49	C		cored (U,Pu)C
			570	21	cored (U,Pu)C
			1500	1/2	equiaxed (U,Pu)C + $(U,Pu)_2C_3$
0	51	49	C		Pu_2C_3 + cored PuC
			570	7	Pu_2C_3 + cored PuC
			1400	1/24	equiaxed PuC + Pu_2C_3
			1500	1/8	equiaxed PuC + Pu_2C_3

Table V (Contd.)

Alloy Composition, a/o			Annealing Conditions*		
U	Pu	C	Temp (°C)	Time (days)	Structure**
6	44	50	400	7	cored (U,Pu)C
			570	7	cored (U,Pu)C
			635	6	cored (U,Pu)C
			1500	1/2	(U,Pu)C + $(U,Pu)_2C_3$
43.5	6	50.5	400	7	(U,Pu)C + $(U,Pu)_2C_3$ (W)
			570	7	(U,Pu)C + $(U,Pu)_2C_3$ (W)
			635	6	(U,Pu)C + $(U,Pu)_2C_3$ (W)
39.5	10	50.5	C		slightly cored (U,Pu)C + $(U,Pu)_2C_3$ (W)
			400	11	slightly cored (U,Pu)C + $(U,Pu)_2C_3$ (W)
			570	8	(U,Pu)C + $(U,Pu)_2C_3$ (W)
			635	7	cored (U,Pu)C + $(U,Pu)_2C_3$ (W)
			1500	1/2	cored (U,Pu)C + $(U,Pu)_2C_3$ (W)
49	0	51	C		UC + U_2C_3 (W)
			570	21	UC + U_2C_3 (W)
34	15	51	C		cored (U,Pu)C + $(U,Pu)_2C_3$ (W)
			570	21	cored (U,Pu)C + $(U,Pu)_2C_3$ (W)
29	20	51	C		cored (U,Pu)C
			570	21	cored (U,Pu)C
25	24	51	C		cored (U,Pu)C + eut $(U,Pu)_2C_3$
			570	21	cored (U,Pu)C + eut $(U,Pu)_2C_3$
			1500	1/2	cored (U,Pu)C + eut $(U,Pu)_2C_3$
20	29	51	400	7	cored (U,Pu)C + eut $(U,Pu)_2C_3$
			570	21	cored (U,Pu)C + eut $(U,Pu)_2C_3$
			635	6	cored (U,Pu)C + eut $(U,Pu)_2C_3$
15	34	51	C		cored (U,Pu)C + eut $(U,Pu)_2C_3$
			570	21	cored (U,Pu)C + eut $(U,Pu)_2C_3$
			1500	1/2	cored (U,Pu)C + eut $(U,Pu)_2C_3$
10	39	51	C		cored (U,Pu)C
			570	21	cored (U,Pu)C
			1500	1/2	cored (U,Pu)C + $(U,Pu)_2C_3$
0	48	52	C		cored PuC + Pu_2C_3
			570	7	cored PuC + Pu_2C_3
			1500	1/8	PuC + Pu_2C_3

*Alloys were homogenized as shown in Table IV.

**Dendritic (U,Pu)C appeared in all carbon alloys except where noted. See Nomenclature, page 10, for explanation of abbreviations.

†Number suffixes refer to plutonium ingots whose chemical analyses are given in Table II, page 16.

Table VI

MELTING DATA FOR THE PLUTONIUM-RICH CORNER OF THE 635°C ISOTHERMAL SECTION

Alloy Composition, a/o			Temp Range (°C)	Observation
U	Pu	C		
0	100	0[1]	639-641	Specimen collapsed
0	100	0[2]	641-643	Specimen collapsed
8	92	0	622-626	Specimen collapsed
12	88	0	626-631	Specimen collapsed
16	84	0	628-630	Specimen collapsed
23	77	0	634-642	Specimen collapsed
4	95	1	627-632	Specimen collapsed
19	80	1	630-636	Specimen collapsed
0	98	2	637-639	Specimen collapsed
14	83	3	626	Incipient melting
5	90	5	634-639	Incipient melting
6	87	7	636	Specimen collapsed
15	78	7	630	Specimen collapsed
23	70	7	635	Not melted
0	80	20	636-641	Specimen collapsed
1	79	20	635	Not melted
10	70	20	635	Specimen collapsed
15	65	20	626	Incipient melting
23	57	20	649	Specimen collapsed
0	65	35	635	Not melted
14	51	35	635	Not melted
17	48	35	635	Not melted
0	62.5	37.5	635	Not melted
5	57	38	635	Not melted
1	59	40	635	Not melted

[1]Ingot 1.
[2]Ingot 2.

One hundred and thirty X-ray diffraction patterns were also examined (see Tables VII and VIII). The room-temperature lattice parameters for the (U,Pu)C phase were determined from 70 of these patterns by the method outlined in Appendix III.

Table VII

IDENTIFICATION OF PHASES BY X-RAY DIFFRACTION

Alloy Composition, a/o			Annealing Temp (°C)	Phases Identified
U	Pu	C		
95	5	0	C	alpha U + zeta
			570	alpha U + zeta
82	18	0	C	beta U
			570	beta U
75	25	0	714	beta U + zeta + PuO
72	28	0	598	zeta
50	50	0	C	zeta
			570	zeta
23	77	0	278	zeta
10	90	0	C	zeta
			570	zeta
0	100	0	570	alpha Pu
74.5	24.5	1	714	zeta + alpha U
71	28	1	598	zeta + beta U + PuO
58	41	1	C	zeta
			275	zeta
			400	zeta
			400(1)	zeta
94	4	2	635	alpha U
			800	alpha U
92	6	2	635	alpha U + beta U
81	16	3	553	beta U + zeta
70	27	3	800	zeta
82	11	7	570	alpha U + zeta + (U,Pu)C
79	14	7	570	beta U + (U,Pu)C
75	17	7	570	beta U + (U,Pu)C
26	67	7	570	zeta + (U,Pu)C
15	78	7	400	zeta + (U,Pu)C
			278	alpha Pu + zeta + (U,Pu)C

Table VII (Contd.)

Alloy Composition, a/o			Annealing Temp (°C)	Phases Identified
U	Pu	C		
2	91	7	400	alpha Pu + (U,Pu)C
78	5	17	C	(U,Pu)C + PuO
			570	alpha U + (U,Pu)C
			300	(U,Pu)C + zeta
			400	alpha U + (U,Pu)C
55.5	27.5	17	C	zeta + (U,Pu)C
			400	zeta + (U,Pu)C
			300(1)	zeta + (U,Pu)C
			570	zeta + (U,Pu)C
39	44	17	400	zeta + (U,Pu)C
			300(1)	zeta + (U,Pu)C
			570	zeta + (U,Pu)C
64	16	20	300(1)	zeta + (U,Pu)C
10	70	20	336	alpha Pu + (U,Pu)C
1	79	20	225	alpha Pu + Pu_3C_2 + (U,Pu)C
0	80	20	C	alpha Pu + PuC
			400	alpha Pu + PuC
			465	alpha Pu + Pu_3C_2 + PuC
			570	alpha Pu + PuC
64	6	30	570	alpha U + (U,Pu)C
61	4	35	635	alpha U + (U,Pu)C
59.5	5.5	35	635	beta U + (U,Pu)C
58	7	35	570	beta U + (U,Pu)C
			635	alpha U + (U,Pu)C
56.5	8.5	35	400	alpha U + (U,Pu)C
17	48	35	570	zeta + (U,Pu)C
14	51	35	570	alpha Pu + (U,Pu)C
9	56	35	570	alpha Pu + (U,Pu)C
0	65	35	570	alpha Pu + PuC
			595	alpha Pu + PuC
0	62.5	37.5	570	alpha Pu + PuC
			595	alpha Pu + PuC
5	57	38	400	alpha Pu + Pu_3C_2 + (U,Pu)C

Table VII (Contd.)

Alloy Composition, a/o			Annealing Temp (°C)	Phases Identified
U	Pu	C		
0	61	39	400	alpha Pu + Pu_3C_2 + PuC
			530	alpha Pu + Pu_3C_2 + PuC
			595	alpha Pu + PuC
			635	alpha Pu + PuC
1	59	40	570	alpha Pu + (U,Pu)C
0	60	40	500	Pu_3C_2
0	59	41	400	Pu_3C_2
			570	Pu_3C_2
			595	PuC
			620	PuC
6	52	42	400	Pu_3C_2 + (U,Pu)C
			570	(U,Pu)C
			620	(U,Pu)C
0	57.5	42.5	C	PuC
			400	Pu_3C_2 + PuC
			595	PuC
			620	PuC
3.7	52.3	44	570	(U,Pu)C
0	56	44	400	PuC
			570	PuC
			1500	PuC
28	27	45	400	alpha Pu + (U,Pu)C
			570	alpha Pu + (U,Pu)C
22	33	45	400	zeta + (U,Pu)C
			570	zeta + (U,Pu)C
10	45	45	570	alpha Pu + (U,Pu)C
41	13	46	400	zeta + (U,Pu)C
			570	(U,Pu)C
0	54	46	400	PuC
			570	PuC
			620	PuC
			1500	PuC
25	28	47	570	(U,Pu)C
20	33	47	570	(U,Pu)C

Table VII (Contd.)

Alloy Composition, a/o			Annealing Temp (°C)	Phases Identified
U	Pu	C		
3.7	49.3	47	570	cored (U,Pu)C
			1500	cored (U,Pu)C
0	52.5	47.5	C	$PuC + Pu_2C_3$
			570	PuC
			1500	$PuC + Pu_2C_3$
40.5	11.5	48	570	(U,Pu)C
8	44	48	400	$(U,Pu)C + (U,Pu)_2C_3$
			570	cored (U,Pu)C
45	6.5	48.5	570	(U,Pu)C
32.5	19	48.5	570	(U,Pu)C
			635	zeta + (U,Pu)C
6.5	45	48.5	570	cored $(U,Pu)C + (U,Pu)_2C_3$
			1500	(U,Pu)C
51	0	49	570	UC
23	28	49	570	cored (U,Pu)C
20	31	49	570	cored (U,Pu)C
15	36	49	1500	(U,Pu)C
2	49	49	1500	(U,Pu)C
0	51	49	C	$PuC + Pu_2C_3$
			570	$PuC + Pu_2C_3$
			1500	PuC
6	44	50	C	$(U,Pu)C + (U,Pu)_2C_3$
			570	$(U,Pu)C + (U,Pu)_2C_3$
			1500	$(U,Pu)C + (U,Pu)_2C_3$
43.5	6	50.5	570	$(U,Pu)C + (U,Pu)_2C_3$
39.5	10	50.5	570	$(U,Pu)C + (U,Pu)_2C_3$
			1500	(U,Pu)C
49	0	51	570	UC
25	24	51	1500	$(U,Pu)C + (U,Pu)_2C_3$
15	34	51	C	$(U,Pu)C + (U,Pu)_2C_3$
			1500	$(U,Pu)C + (U,Pu)_2C_3$

Table VII (Contd.)

Alloy Composition, a/o			Annealing Temp (°C)	Phases Identified
U	Pu	C		
10	39	51	1500	$(U,Pu)C + (U,Pu)_2C_3$
0	48	52	C	$PuC + Pu_2C_3$
			570	$PuC + Pu_2C_3$
			1500	$PuC + Pu_2C_3$

(1)Powder annealed for 4 hr and furnace cooled.

Table VIII

LATTICE PARAMETER OF THE (U,Pu)C PHASE

Alloy Composition, a/o			Temp (°C)	Probable Error ($\times 10^{-4}$ Å)	Parameter, Å
U	Pu	C			
PuC					
0	80	20	C	2.0	4.9520
0	65	35	570	0.9	4.9549
			595	0.7	4.9545
0	62.5	37.5	570	0.8	4.9557
			595	0.9	4.9556
0	61	39	570	1.0	4.9530
			595	100	4.9535
			635	10.0	4.9487
0	59	41	570	3.0	4.9549
			595	1.0	4.9545
			620	0.7	4.9526
0	57.5	42.5	C	10.0	4.9549
			595	0.8	4.9572
			620	2.0	4.9538
0	56	44	400	2.0	4.9560
			570	3.0	4.9567
			1500	0.7	4.9672
0	54	46	400	1.0	4.9635
			570	1.0	4.9640
			620	3.0	4.9642
			1500	1.0	4.9681

Table VIII (Contd.)

Alloy Composition, a/o			Temp (°C)	Probable Error (x 10^{-4} Å)	Parameter, Å
U	Pu	C			
PuC					
0	52.5	47.5	570	2.0	4.9705
			1500	2.0	4.9721
0	51	49	C	20.0	4.9246(1)
0	51	49	570	3.0	4.9725
0	48	52	C	5.0	4.9630
			570	1.0	4.9729
(U,Pu)C					
55.5	27.5	17	570	2.0	4.9610
61	4	35	400	4.0	4.9546
56.5	8.5	35	400	3.0	4.9546
14	51	35	570	3.0	4.9717
5	57	38	400-8 day	10.0	4.9724
			400-34 day	2.0	4.9737
1	59	40	570	1.0	4.9537
6	52	42	400	5.0	4.9678
			570	1.0	4.9627
			620	0.9	4.9618
3.7	52.3	44	570	1.0	4.9589
28	27	45	400	1.0	4.9620
			570	4.0	4.9663
22	33	45	400	1.0	4.9621
			570	1.0	4.9675
10	45	45	570	1.0	4.9674
41	13	46	400	1.0	4.9545(1)
			570	1.0	4.9583
25	28	47	570	0.8	4.9711
20	33	47	570	0.7	4.9728
3.7	49.3	47	570	1.3	4.9695; 4.9792(2)
			1500	2.0	4.9707; 4.9711(2)
40.5	11.5	48	570	1.0	4.9603

Table VIII (Contd.)

Alloy Composition, a/o			Temp (°C)	Probable Error (x 10^{-4} Å)	Parameter, Å
U	Pu	C			
(U, Pu)C					
8	44	48	570	2.0	4.9671; 4.9786[2]
45	6.5	48.5	570	0.7	4.9597
32.5	19	48.5	570	0.5	4.9588
6.5	45	48.5	570	11.2	4.9800; 4.9820[2]
			1500	1.0	4.9760
51	0	49	570	1.0	4.9577
23	28	49	570	1.5	4.9715; 4.9825[2]
20	31	49	570	2.0	4.9710; 4.9825[2]
15	36	49	1500	1.0	4.9641
2	49	49	1500	3.0	4.9784
6	44	50	570	1.0	4.9756
			1500	1.5	4.9689; 4.9811[2]
43.5	6	50.5	570	2.0	4.9582
39.5	10	50.5	570	1.0	4.9462[1]
			1500	1.0	4.9438[1]
49	0	51	570	1.0	4.9580
25	24	51	570	1.0	4.9673; 4.9700[2]
			1500	2.0	4.9681
15	34	51	1500	1.0	4.9778
10	39	51	1500	2.0	4.9812

[1]Anomalously low value.

[2]Film showing two sets of carbide lines.

A representative group of microstructures from a total of 1224 photomicrographs have been selected and are presented as evidence for the placement of the phase boundaries. Volume-fraction analysis was performed on a number of micrographs and the results are presented in Table IX.

Table IX

ANALYSIS OF U-Pu-C AND Pu-C ALLOYS BY QUANTITATIVE METALLOGRAPHY

Alloy Composition, a/o			Temp	Micrographs	v/o Carbide	w/o Carbide
U	Pu	C	(°C)	Counted	(measured)	(calculated)
U-rich						
82	11	7	400	2	14.7	11.4
			570	2	8.7	6.5
79	14	7	400	2	11.5	9.0
52	41	7	570	2	9.0	6.7
36	57	7	400	2	9.1	6.6
59.5	5.5	35	570	5	58.7	50.1
42	23	35	400	3	66.6	58.8
34.5	30.5	35	570	3	68.2	57.3
28	27	45	570	3	88.5	84.2
Pu-rich						
6	87	7	620	1	11.4	8.9
			635	2	10.2	7.7
5	75	20	628	3	38.6	31.2
5	57	38	620	1	78.5	72.2
			635	2	80.0	74.0
6	52	42	620	5	88.4	84.1
Pu-C						
0	80	20	560	2	46.3	38.0
			580	2	39.1	31.8
			600	2	45.8	37.6
			622	2	42.2	34.6
			643	2	40.9	33.1
0	65	35	595	3	74.1	67.0
0	62.5	37.5	595	2	80.1	74.1
0	61	39	595	3	85.8	81.2
0	59	41	595	1	92.5	89.5
0	57.5	42.5	595	4	99.4	99.1

The spacing of the alloys allowed most boundaries to be bracketed within ±1 a/o. In the few cases where this was not possible, positioning of the boundaries was aided by quantitative metallography.

A. Experimental Results and Interpretation

Isothermal sections at 400, 570, and 635°C were determined, and are shown in Figures 5, 6, and 7. Along with the four invariant ternary reaction planes, also determined, they define the essential phase relationships below the solidus except for certain details in the plutonium corner that are associated with the allotropy of this metal.

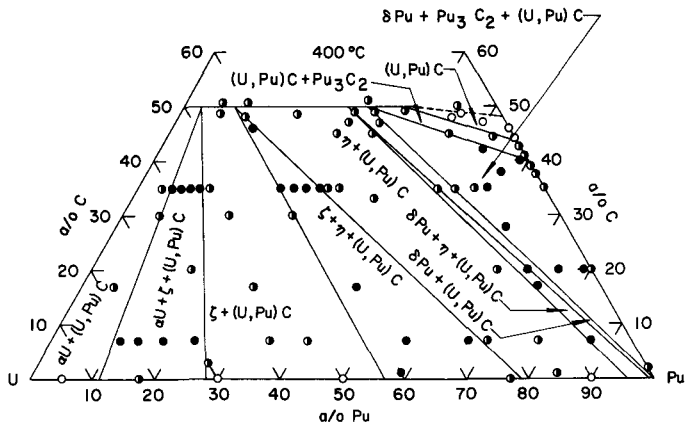

106-6250 Rev.

Figure 5

U-Pu-C Isothermal Section at 400°C*

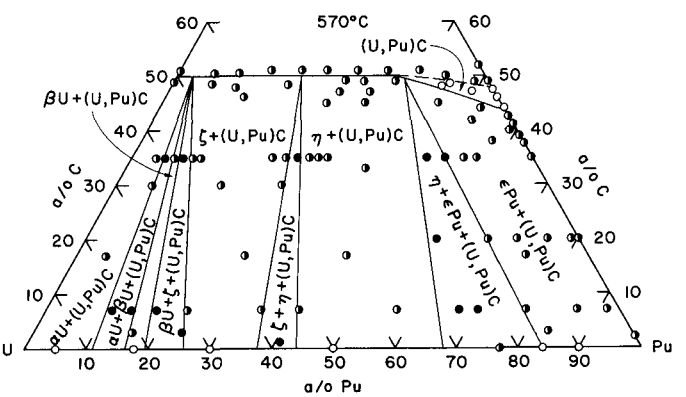

106-6249 Rev.

Figure 6

U-Pu-C Isothermal Section at 570°C

No ambiguity arises in employing the same notations for the ternary phases as appear in the binary diagrams, except in the use of zeta carbide[26] for the Pu_3C_2 phase. To avoid confusion with the zeta phase of the Pu-U system the formula Pu_3C_2 will be used to designate this phase. The Greek-letter designations associated with the allotropies of the elements will be used as prefixes to the chemical symbols. The isomorphous phase extending from pure epsilon plutonium to pure gamma uranium has been designated epsilon Pu in plutonium-rich alloys and gamma U in uranium-rich alloys.

*See Nomenclature for explanation of symbols.

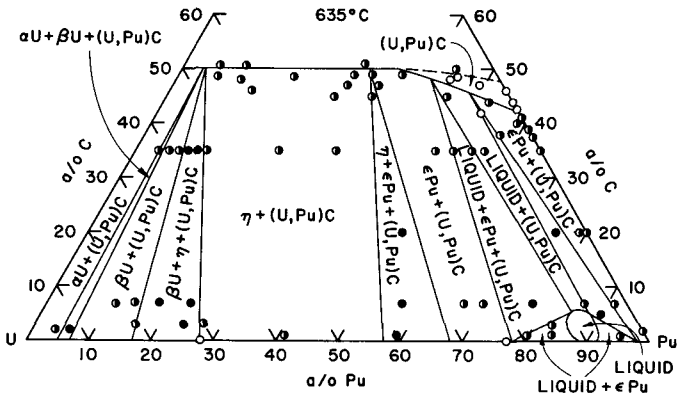

Macro 34175

Figure 7

U-Pu-C Isothermal Section at 635°C

Two general features of the ternary system are apparent in Figures 5, 6, and 7: negligible carbon solubility in the metallic phases, and the absence of ternary phases. The tie-triangle [epsilon Pu/gamma U + liquid + (U,Pu)C] sweeps out a three-cornered, tube-like region as it passes through the ternary system from the U-C to the Pu-C side below the phase space of primary crystallization of (U,Pu)C. Solidification of all ternary alloys begins with the primary crystallization of (U,Pu)C followed by eutectic freezing of the remaining melt, resulting in a two-phase (U,Pu)C gamma U/epsilon Pu alloy immediately after solidification. Except in a small portion of the plutonium-rich corner, which will be discussed later, the primary crystallization of carbide occurs over a temperature range, with growth in the form of dendrites.

For convenience in presentation, the following two-phase fields and their associated three-phase fields will be discussed: [alpha U + (U,Pu)C], [beta U + (U,Pu)C], [gamma U/epsilon Pu + (U,Pu)C], [eta + (U,Pu)C] and [zeta + (U,Pu)C]. Following this will be a discussion of the (U,Pu)C phase field, the solidus and liquidus at the 635°C isothermal section, Pu_3C_2 and its associated phase fields, the ternary four-phase equilibrium reactions, the low-temperature plutonium phases, and the portion of the Pu-C diagram which was investigated.

Except where noted, metallographic identification of phases could be readily made. Nevertheless, diffraction patterns were obtained for at least one specimen in every phase field.

1. The [alpha U + (U,Pu)C] Phase Field

This two-phase field enters the ternary from the U-C side at 668°C and is stable down to room temperature. The alpha-U phase could be easily identified by X-ray diffraction patterns and by its characteristic twinned microstructure, shown in Figure 8. The areas of dark material are the carbide phase.

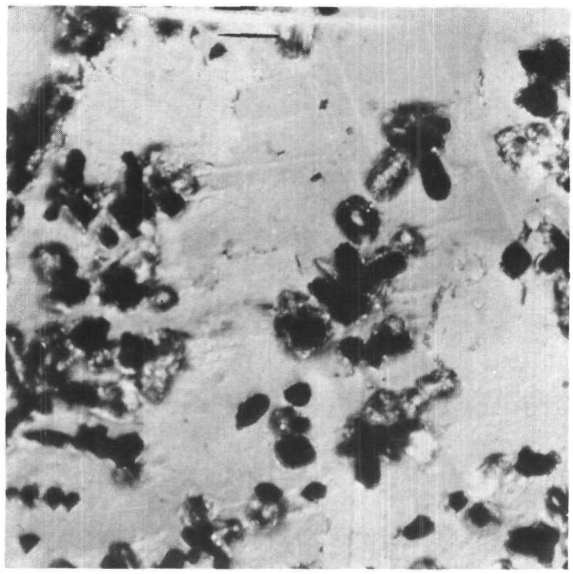

Micro 27776

Figure 8

Photomicrograph of U-5 a/o Pu-17 a/o C Alloy; 400, 4, Q; A, 500, PL; alpha U + (U,Pu)C (b)

Although the plutonium solubility in the alpha-U solid solution varies from 6 a/o plutonium at 635°C to 11 a/o plutonium at 400°C, the monocarbide with which it comes into equilibrium contains less than 4 a/o plutonium regardless of temperature.

2. The [alpha U + beta U + (U,Pu)C] Phase Field

Originating on the U-C diagram at the 668°C horizontal, this three-phase field exists down to 549°C, at which it is one of the reactants in the eutectoidal decomposition of beta U. In ternary space, it lies above the [alpha U + (U, Pu)C] field, its bottom surface being contiguous with the top of the latter. Figure 9 shows the photomicrograph of an alloy, quenched from 570°C, containing beta U and carbide in a matrix of alpha U.

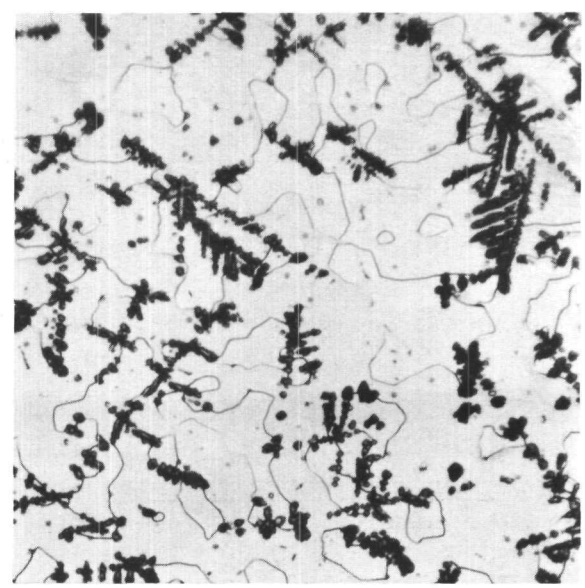

Micro 28047

Figure 9

Photomicrograph of U-11 a/o Pu-7 a/o C Alloy; 570, 5, Q; G, 500, BF; beta U + (U,Pu)C (den) in alpha U matrix

Since the field is narrow at 635°C, only one alloy was located within it. The [alpha U + beta U + (U,Pu)C]/[beta U + (U,Pu)C] boundary was located by X-ray diffraction between the compositions U-4 a/o Pu-35 a/o C and U-5.5 a/o Pu-35 a/o C. The latter alloy showed beta U reflections while the former did not.

3. The [beta U + (U,Pu)C] Phase Field

The field has its origin on the U-C binary diagram at 775°C. Its last remaining tie line vanishes in the eutectoidal decomposition of the beta-U phase at 549°C. The 570°C and 635°C isothermal sections show that only a narrow range of monocarbide compositions come into equilibrium with the beta-U phase.

Grain-boundary etching of beta U, when it was the matrix phase, could not be accomplished. Its retention at elevated temperature was confirmed by X-ray diffraction.

4. The [beta U + eta + (U,Pu)C and the [beta U + zeta + (U,Pu)C] Phase Fields

The [beta U + eta + (U,Pu)C] phase field forms from the eta peritectoid at 712°C and terminates by a class II reaction,* beta U + eta ⇌ zeta + (U,Pu)C, at 594°C (see Figure 63). The [beta U + zeta + (U,Pu)C] phase field results from this reaction and exists down to 549°C, where it is involved in the eutectoidal decomposition of the beta-U phase. The two-phase fields are discussed together because alloys quenched from either phase field yield identical X-ray diffraction patterns and have similar microscopic appearances because the eta phase cannot be retained on quenching.

Figure 10 shows the structure of an alloy that was three-phase [eta + beta U + (U,Pu)C] at 620°C; Figure 11 shows a photomicrograph of the same alloy quenched from the [zeta + beta U + (U,Pu)C] region at 570°C.

5. The [alpha U + zeta + (U,Pu)C] Phase Field

This three-phase field is formed from the eutectoidal decomposition of beta U at 549°C and is stable to room temperature. Figures 12, 13, and 14 show photomicrographs of alloys quenched from this region. In Figure 12, zeta occurs preferentially at the boundaries of veined alpha grains. In Figure 13 zeta occurs within the alpha-phase network. The structures are typical of those used for phase-boundary bracketing. Figure 14 shows an alloy containing about equal amounts of alpha U and zeta.

*A classification of four-phase invariant reactions is given on page 82.

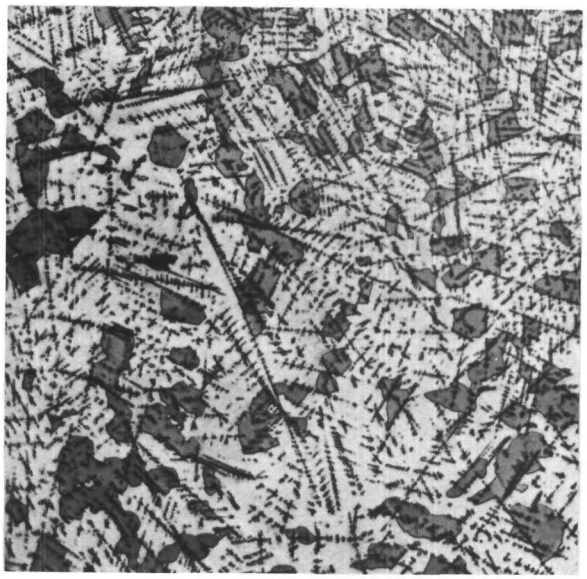

Micro 29608

Figure 10. Photomicrograph of U-18 a/o Pu-7 a/o C Alloy; 620, 11, Q; C, 500, BF; beta U + (U,Pu)C (den) in tr eta matrix

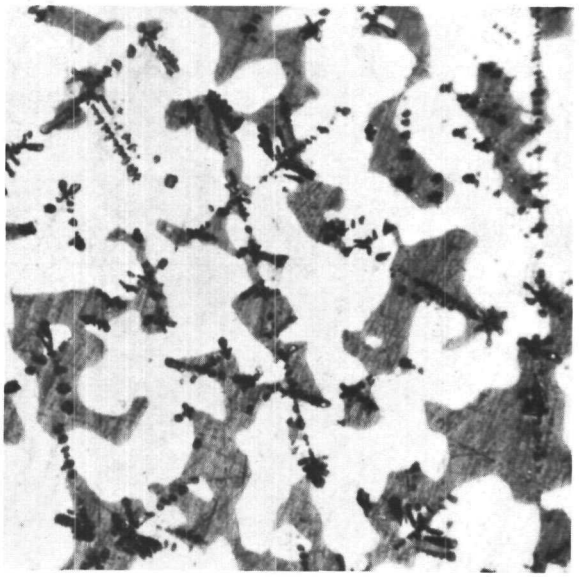

Micro 28044

Figure 11. Photomicrograph of U-18 a/o Pu-7 a/o C Alloy; 570, 5, Q; A, 500, BF; zeta + (U,Pu)C (den) in beta U matrix

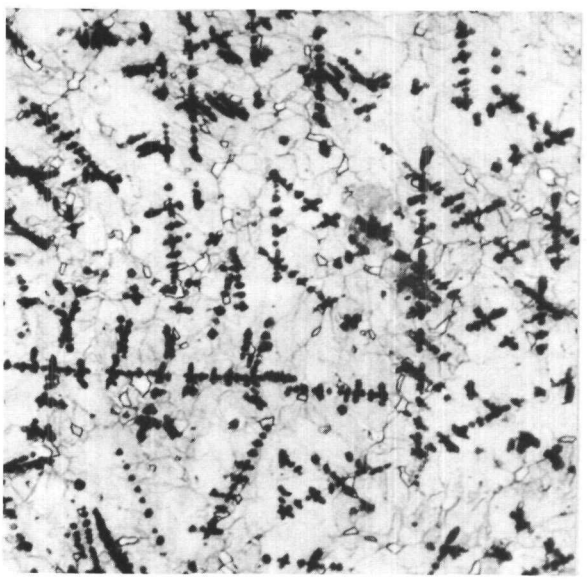

Micro 27813

Figure 12. Photomicrograph of U-11 a/o Pu-7 a/o C Alloy; 400, 5, Q; A, 500, BF; zeta + (U,Pu)C (den) in alpha U matrix

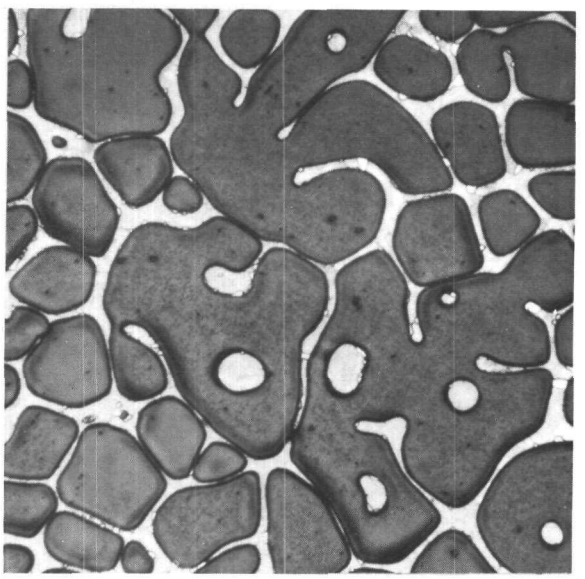

Micro 29641

Figure 13. Photomicrograph of U-5.5 a/o Pu-35 a/o C Alloy; 400, 8, Q; A, 500, BF; zeta (w) + (U,Pu)C (g) in alpha U network

Micro 27815

Figure 14

Photomicrograph of U-18 a/o Pu-7 a/o C Alloy; 400, 5, Q; G, 500, BF; alpha U + (U,Pu)C (den) in zeta matrix

6. The [zeta + (U,Pu)C] and [eta + (U,Pu)C] Phase Fields

The eta phase is stable only at elevated temperatures. It forms peritectoidally at 712°C and decomposes by a class II reaction at 283°C, eta + (U,Pu)C $\rightleftharpoons$ beta Pu + zeta, as shown in Figure 63. The zeta phase forms at 594°C by a class II reaction, beta U + eta $\rightleftharpoons$ zeta + (U,Pu)C.

Although the eta phase decomposes to zeta on quenching and therefore cannot be observed at room temperature, the identity and location of these different two-phase fields in ternary space may be established positively by the following analysis, based on the phase rule. Referring to the 400, 570, and 635°C isothermal sections (see Figures 5, 6, and 7), one may see that the two two-phase fields under consideration must be bounded on one side by the single-phase monocarbide solid solution and on another side, owing to the negligible carbon solubility, by the single-phase areas associated with the U-Pu binary system. On the remaining surfaces there must be the appropriate one- or three-phase fields. Since one-phase fields within ternary phase space are contrary to experimental evidence, it may be concluded that the remaining bounding surfaces are three-phase fields. It follows that the top and bottom surfaces of the [eta + (U,Pu)C] field will be contiguous with the [eta + epsilon Pu + (U,Pu)C] and [eta + zeta + (U,Pu)C] three-phase fields, respectively. Correspondingly, the top surface of the [zeta + (U,Pu)C] field will adjoin the [eta + zeta + (U,Pu)C] field, while the bottom surface will be contiguous with the base of the concentration triangle, on the one hand, and the [alpha U + zeta + (U,Pu)C] field, on the other hand. It remains to establish the extent of these three-phase fields and thereby to locate the intervening two-phase fields. The [alpha U + zeta + (U,Pu)C] phase region has already been established. The remaining three-phase fields will be discussed shortly.

The room temperature diffraction pattern for the zeta phase of composition U-41 a/o Pu-1 a/o C is given in Table X. The indexing of the zeta-phase pattern is in reasonable agreement with the simple cubic structure derived by Ellinger.[12] The lattice parameter as determined from this investigation is 10.659 Å; Ellinger found that the parameter decreased

Table X

X-RAY POWDER DATA FOR ZETA PHASE (U-41 a/o Pu-1 a/o C ALLOY) AT ROOM TEMPERATURE

Line	I[1]	d,Å	$\sin^2\theta$	m[2]	Line	I[1]	d,Å	$\sin^2\theta$	m[2]
1	VW	3.303	0.0545	10	51	W	1.145	0.4536	86
2	W	3.145	0.0601		52	MW	1.125	0.469	89
3	VW	3.033	0.0646	12	53	MW	1.078	0.511	97
4	W	2.827	0.0747	14	54	W	1.063	0.526	100
5	VW	2.722	0.0802		55	W	1.037	0.5531	105
6	MW	2.549	0.0914	17	56	W	1.027	0.5635	107
7	S	2.481	0.0965	18	57	W	1.018	0.5730	109
8	W	2.417	0.1018	19	58	VW	1.010	0.5829	
9	W	2.300	0.1123	21	59	VW	0.9994	0.5950	113
10	MW	2.245	0.1179	22	60	W	0.9951	0.6001	114
11	VW	2.148	0.1288	24	61	VW	0.9906	0.6057	115
12	MW	2.107	0.1338	25	62	W	0.9833	0.6146	117
13	W	2.066	0.1392	26	63	W	0.9786	0.6206	118
14	W	2.029	0.1444	27	64	VW	0.9710	0.6303	120
15	VW	1.958	0.1550	29	65	VW	0.9627	0.6412	122
16	VW	1.933	0.1591	30	66	VW	0.9583	0.6471	123
17	VW	1.874	0.1692	32	67	W	0.9516	0.6592	125
18	VW	1.84	0.176	33	68	W	0.9472	0.6624	126
19	VW	1.81	0.181	34	69	W	0.9365	0.6777	129
20	VW	1.79	0.186	35	70	VW	0.9290	0.6874	131
21	VW	1.761	0.1917	36	71	VW	0.9212	0.6991	133
22	VW	1.738	0.1969	37	72	W	0.9178	0.7043	134
23	VW	1.712	0.2028	38	73	VW	0.9018	0.7295	199
24	VW	1.676	0.2116	40	74	VW	0.8957	0.7895	141
25	MW	1.648	0.2188	41	75	W	0.8831	0.7607	145
26	VW	1.625	0.2250	42 or 43	76	W	0.8801	0.7659	146
27	VW	1.601	0.2320	44	77	W	0.8714	0.7813	149
28	VW	1.573	0.2401	45	78	MW	0.8678	0.7877	150
29	VW	1.56	0.244	46	79	W	0.8602	0.8018	153
30	W	1.526	0.2552	48	80	W	0.8576	0.8067	154
31	W	1.511	0.2602	49	81	VW	0.8497	0.8217	157
32	W	1.496	0.2656	50	82	W	0.8383	0.8442	161
33	W	1.482	0.2706	51	83	W	0.8309	0.8594	164
34	W	1.454	0.2812	53	84	W	0.8263	0.8689	166
35	M	1.441	0.2863	54	85	VW	0.8165	0.8900	170
36	VW	1.416	0.2966		86	W	0.8135	0.8965	171
37	MW	1.403	0.3018	57	87	W	0.8095	0.9053	173
38	VW	1.380	0.3119	59	88	W	0.8091	0.9109	173
39	VW	1.355	0.3237	61	89	VW	0.7979	0.9318	178
40	VW	1.315	0.3439	65	90	W	0.7920	0.9458	181
41	VW	1.305	0.3489	66	91	MW	0.7891	0.9527	182
42	VW	1.285	0.3597	68	92	W	0.7893	0.9571	182
43	MW	1.251	0.3800	72	93	W	0.7856	0.9612	184
44	VW	1.244	0.3838	73	94	VW	0.7854	0.9666	184
45	W	1.225	0.3962	75	95	W	0.7814	0.9716	186
46	W	1.210	0.4060	77	96	W	0.7810	0.9776	186
47	W	1.181	0.4258	81	97	MW	0.7748	0.9882	189
48	W	1.172	0.4323	82	98	MW	0.7749	0.9930	189
49	W	1.164	0.4384	83					
50	VW	1.151	0.4488	85					

[1] Intensity Scale: S = strong; M = medium; W = weak; VW = very weak.

[2] $m(h^2 + k^2 + \ell^2)$ values are not given for lines believed to be due to PuO or Pu_2O_3.

from 10.692 Å at Pu-35 a/o U to 10.651 Å at Pu-70 a/o U. A capillary quenching technique enabled Ellinger to index the complex eta pattern on the basis of a tetragonal unit cell with a_0 = 10.57 Å and c_0 = 10.76 Å for a Pu-25 a/o U alloy quenched from 500°C. In this investigation, an X-ray powder pattern of a U-44 a/o Pu-17 a/o C alloy quenched from the two-phase [eta + (U,Pu)C] region at 570°C showed zeta phase in addition to (U,Pu)C reflections.

On standing at room temperature, zeta shows extensive grain-boundary cracking and over long periods of time in the glovebox atmosphere often disintegrates to a black oxidized powder. Cracking is most pronounced in the region of uranium/plutonium ratio greater than unity. Figure 15 shows a photomicrograph of cast U-27.5 a/o Pu-17 a/o C alloy in the as-polished condition about 45 min after the last polishing step. The carbide particles have been lightly attacked by the atmosphere, while the angular, grain-boundary corrosion of the zeta phase is evident. A photomicrograph of a portion of an alloy of composition U-16 a/o Pu-20 a/o C, quenched from 400°C, is shown in Figure 16. The identification of the matrix is quite easy due to the presence of cracking. The U-78 a/o Pu-7 a/o C alloy (uranium/plutonium ratio, 0.19) quenched from a two-phase [eta + (U,Pu)C] region at 400°C, with structure shown in Figure 17, shows no cracking. The inter- and trans-granular cracking of the zeta phase (transformed eta) in a U-41 a/o Pu-1 a/o C alloy (uranium/plutonium ratio, 1.4) quenched from 570°C is apparent in Figure 18.

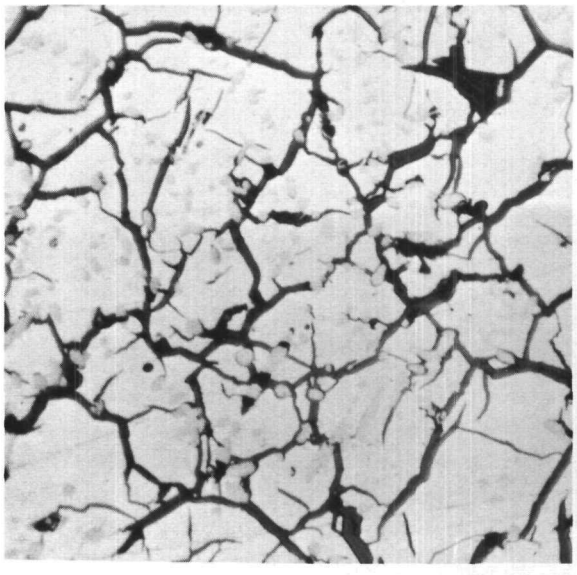

Micro 27326

Figure 15. Photomicrograph of U-27.5 a/o Pu-17 a/o C Alloy; C; E, 500, BF; zeta (w) + (U,Pu)C (g), (barely visible). The dark lines are cracks.

Micro 27339

Figure 16. Photomicrograph of U-16 a/o Pu-20 a/o C Alloy; 400, 4, Q; A, 500, BF; alpha U + (U,Pu)C (b) in zeta (w) matrix

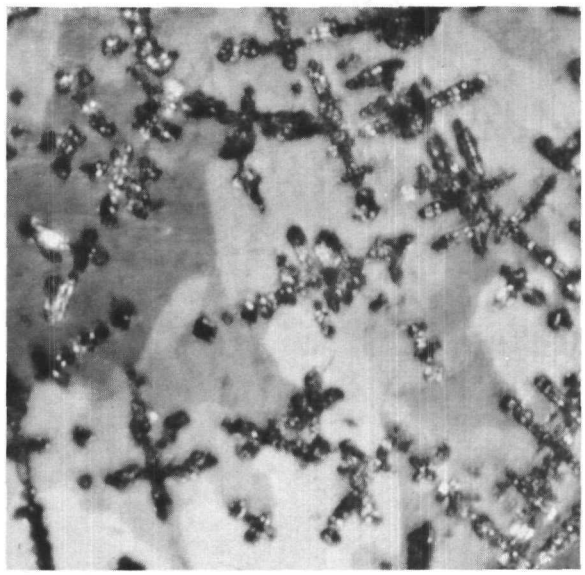

Micro 28024

Figure 17. Photomicrograph of U-78 a/o Pu-7 a/o C Alloy; 400, 4, Q; C, 500, PL; tr eta + (U, Pu)C (den)

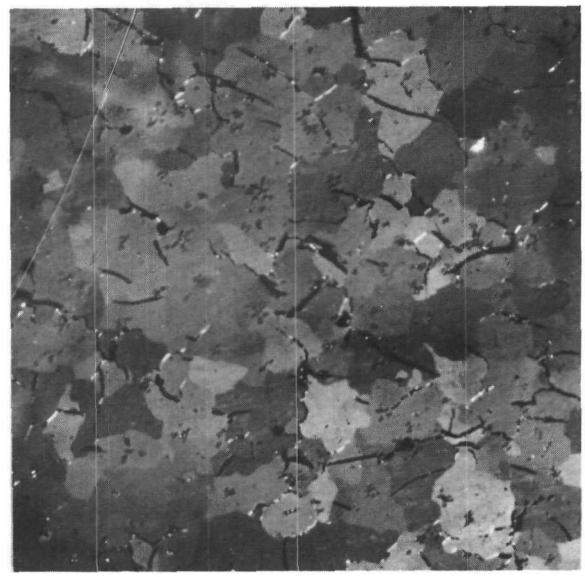

Micro 32719

Figure 18. Photomicrograph of U-41 a/o Pu-1 a/o C Alloy; 570, 4, Q; A, 200, PL; tr eta + (U,Pu)C (very small dendrites). The dark lines are cracks.

7. The [zeta + eta + (U,Pu)C] Phase Field

The class II reaction at 594°C, beta U + eta ⇌ zeta + (U,Pu)C, produces this three-phase field, which terminates at 283°C in the class II four-phase reaction, beta Pu + zeta ⇌ eta + (U,Pu)C. The extent of this three-phase field at 400 and at 570°C has been determined.

The distinguishing of equilibrium zeta from zeta occurring as a transformation product may be illustrated by Figures 19 and 20, where two alloys, both quenched from the [eta + zeta + (U,Pu)C] phase field at 400°C, are shown.

A point of interest in connection with the [zeta + eta + (U,Pu)C] phase field is the large shift in the location of its monocarbide apex on descending from 570 to 400°C. As will be seen, this is associated with the advent of the Pu_3C_2 phase.

8. The Four [eta + Pu + (U,Pu)C] Three-phase Fields

It may be inferred that the gamma, delta, delta prime, and epsilon allotropes of plutonium, each of which enters into a two-phase equilibrium with the eta phase in the Pu-U system (see Figure 1), form three-phase fields in ternary space with the eta and (U,Pu)C phases. With decreasing temperature, the [eta + epsilon Pu + (U,Pu)C] tie-triangle is the first to appear in the ternary diagram, forming from the eta peritectoid at 712°C and being removed by processes involving the Pu_3C_2 phase at about 558°C.

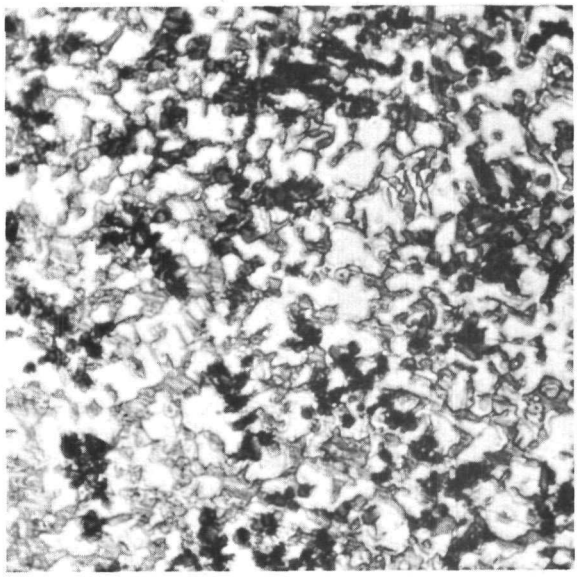

Micro 28022

Figure 19. Photomicrograph of U-57 a/o Pu-7 a/o C Alloy; 400, 4, Q; D, 500, BF; tr eta (g) + zeta (w) + (U,Pu)C (b)

Micro 27825

Figure 20. Photomicrograph of U-67 a/o Pu-7 a/o C Alloy; 400, 4, Q; D, 500, BF; zeta + (U,Pu)C (den) in tr eta matrix

The epsilon phase of plutonium cannot be retained at room temperature. X-ray diffraction has shown that the decomposition product of a U-51 a/o Pu-35 a/o C alloy quenched from the epsilon plutonium field at 570°C is alpha plutonium, whereas that of a U-27 a/o Pu-3 a/o C alloy quenched from the isomorphous gamma uranium field at 800°C is zeta. A U-4 a/o Pu-2 a/o C alloy quenched from the gamma-uranium region at 800°C was found to contain alpha uranium. Thus, the quenching behavior of the epsilon Pu/gamma U phase is seen to vary with composition. The decomposition product of the plutonium-rich phase is readily identified by its martensitic appearance. Figure 21 shows a photomicrograph of a binary alloy quenched from the epsilon plutonium phase field at 620°C after an equilibrating anneal of 13 days.

Micro 29664

Figure 21. Photomicrograph of U-77 a/o Pu Alloy; 620, 13, Q; B, 200, BF; tr epsilon Pu (m)

Figure 22 shows a photomicrograph of an alloy quenched from the three-phase [eta + epsilon Pu + (U,Pu)C] field at the same temperature, 620°C, after an equilibrating anneal of 11 days. The plutonium plates in the latter figure are very much finer than those in the previous

one, although the magnification has been increased $2\frac{1}{2}$ times. Figure 23 shows a photomicrograph of a specimen from the alloy shown in Figure 21, but quenched from 570°C. Eta and epsilon plutonium were the stable phases at the equilibrating temperature. Figure 24 is a micrograph of an alloy containing epsilon plutonium as the matrix phase at 570°C.

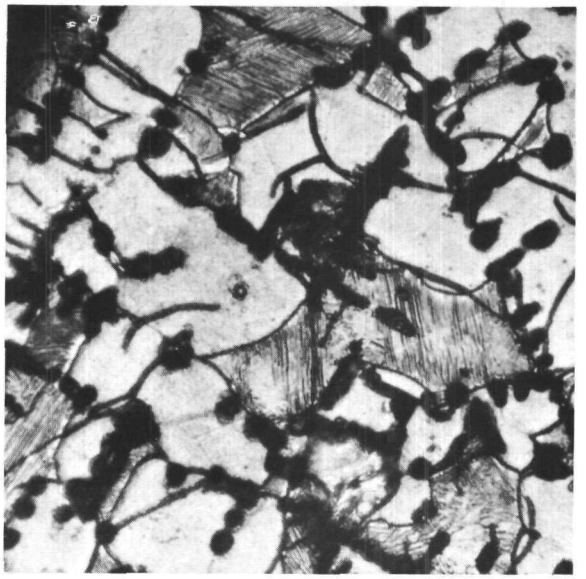

Micro 29605

Figure 22. Photomicrograph of U-57 a/o Pu-7 a/o C Alloy; 620, 11, Q; A, 500, BF; tr epsilon Pu + (U,Pu)C (den) in tr eta matrix

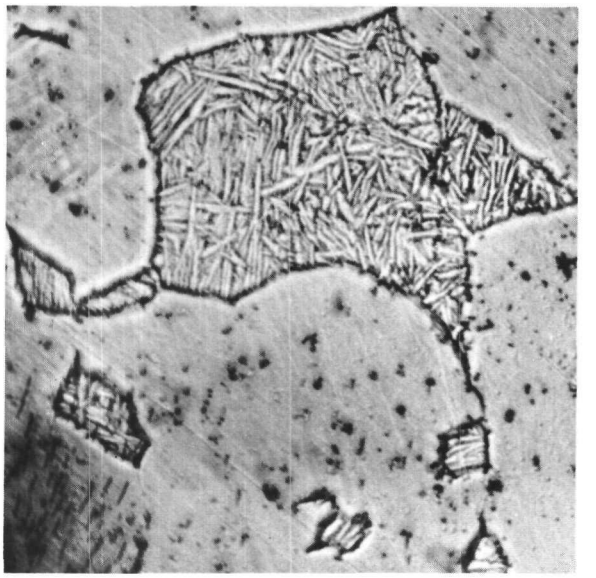

Micro 30013

Figure 23. Photomicrograph of U-77 a/o Pu Alloy; 570, 7, Q; B, 500, BF; tr epsilon Pu (m) in tr eta matrix

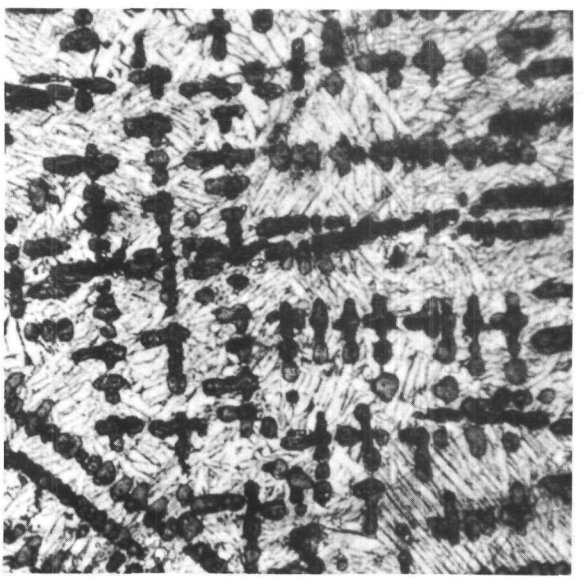

Micro 27331

Figure 24

Photomicrograph of U-73 a/o Pu-17 a/o C Alloy; 570, 10, Q; E, 500, BF; tr epsilon Pu (m) + (U,Pu)C (den)

The microstructures of two alloys quenched from the [eta + delta Pu + (U,Pu)C] field may be seen in Figures 25 and 26. The decomposition products consist of nearly parallel plates. However, other alloys quenched from 400°C had microstructures similar to those of Figures 22 through 24.

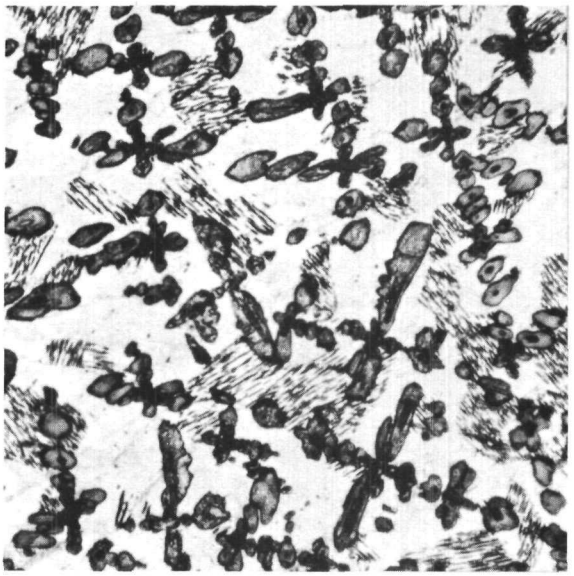

Micro 27324

Figure 25. Photomicrograph of U-73 a/o Pu-17 a/o C Alloy; 400, 4, Q; E, 500, BF; tr delta Pu (m) + (U,Pu)C (den) in tr eta matrix

Micro 32592

Figure 26. Photomicrograph of U-70 a/o Pu-20 a/o C Alloy; 336, 17, Q; E, 500, BF; tr delta Pu (m) + (U,Pu)C (den) in tr eta matrix

Figure 27 has been introduced to show the quenching characteristics of a U-67 a/o Pu-7 a/o C alloy quenched from the two phase [epsilon Pu + (U,Pu)C] phase field at 620°C. The dark regions contained

Micro 28844

Figure 27

Photomicrograph of U-67 a/o Pu-7 a/o C Alloy; 620, 11, Q; A, 500, BF; tr epsilon Pu (mostly m) + (U,Pu)C (b)

the carbide phase prior to etching. A partial transformation to eta has been interrupted by the martensitic transformation.

The remaining [eta + Pu + (U,Pu)C] three-phase fields are discussed in a later section, beginning on page 86, which deals with the low-temperature plutonium phases.

9. The Six [Pu + (U,Pu)C] Phase Fields

The [epsilon Pu + (U,Pu)C] phase field enters the ternary from the U-C binary side at the liquid ⇌ gamma U + UC eutectic horizontal at 1132°C. With decreasing temperature it moves to the plutonium-rich corner, where it is the first of the six [Pu + (U,Pu)C] phase fields to disappear. A representative micrograph has already been shown in Figure 24.

The remaining five phase fields will be discussed later.

10. The (U,Pu)C Phase Field

The (U,Pu)C phase boundaries are based upon evidence obtained from metallographic examination of quenched specimens containing around 50 a/o carbon, quantitative metallographic analysis of alloys containing between 7 and 45 a/o carbon, and X-ray analysis.

Except in alloys containing less than 10 a/o plutonium, the solidification process results in cast microstructures whose carbide phase shows "dendritic ghosts" that may be related to an extension into the ternary system of the peritectic reaction, liquid + Pu_2C_3 ⇌ PuC at 1654°C.[26] In many alloys the inhomogeneity resembles the coring that is sometimes observed in dendritic solid-solution crystals. The range of compositions in which cast microstructures show the effect is indicated in Figure 28. In many of the alloys "coring" could not be removed with the available high-temperature homogenization treatment (12 hr at a maximum temperature of 1500°C). The only portion of the phase boundary that is based principally upon observations of these nonequilibrium structures is the high-carbon side of the (U,Pu)C phase boundary in the region where the deviations from stoichiometry occur, and for this reason the boundary has been indicated by a dashed line on the isothermal section. The low-carbon boundary of the same phase field can be placed with more confidence and is given as a solid line, since an independent determination of its location was made by applying the method of quantitative metallography to the microstructure of alloys containing between 7 and 35 a/o carbon. This technique will be discussed later.

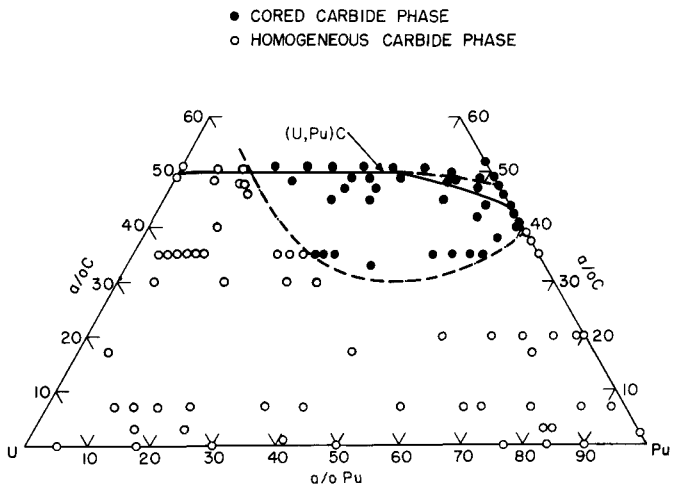

Macro 34173

Figure 28

Concentration Triangle Showing Presence of "Coring" or "Dendritic Ghosts" in Cast Alloys

The (U,Pu)C phase is stoichiometric from 0 to about 35 a/o plutonium, at which point the defect (U,Pu)C structure begins. Here the phase field broadens and also deviates toward a greater metal-to-carbon ratio.

The microstructures of alloys whose carbon concentrations placed them on the low-carbon side of the (U,Pu)C phase field always showed a second phase which could be identified by X-ray diffraction as a binary U-Pu phase or the Pu_3C_2 phase. For example, Figure 29 shows the zeta phase disposed interdendritically in the monocarbide structure of a U-13 a/o Pu-46 a/o C alloy quenched from 570°C. Alloys containing more than 32 a/o uranium and more than 50 a/o carbon were easily identified by the Widmanstätten precipitate of the $(U,Pu)_2C_3$ phase, as shown in Figure 30. The microstructures of many alloys contained a "cored" carbide constituent, as may be seen in the etched appearance of the dendrites shown in the microstructure of the U-24 a/o Pu-51 a/o C alloy (see Figure 31). The occurrence of $(U,Pu)_2C_3$ lines in the diffraction pattern of this alloy suggests that the fine interdendritic constituent is the $(U,Pu)_2C_3$ phase, probably resulting from a Class II ternary reaction, liquid + $(U,Pu)C_2 \rightleftharpoons (U,Pu)_2C_3 + (U,Pu)C$. The dendrites appear to be remnants of primary crystallization. Alloys whose microstructures were similar to that shown in Figure 32 were considered one phase if X-ray diffraction showed only monocarbide reflections; two phase if $(U,Pu)_2C_3$ reflections were also present.

The inhomogeneity in the carbide phase could be successfully removed in plutonium-rich alloys by annealing in a tantalum-tube resistance furnace for 12 hr at 1500°C. The higher-melting uranium-rich alloys, however, were essentially unaffected by this treatment. Figure 33 shows the microstructure of a U-44 a/o Pu-50 a/o alloy after annealing at 1500°C.

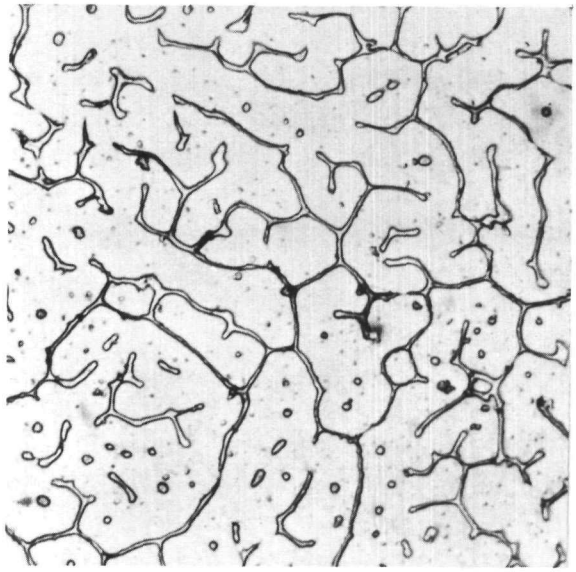

Micro 29945

Figure 29. Photomicrograph of U-13 a/o Pu-46 a/o C Alloy; 570, 11, Q; A, 500, BF; (U,Pu)C (major phase) + interdendritic zeta

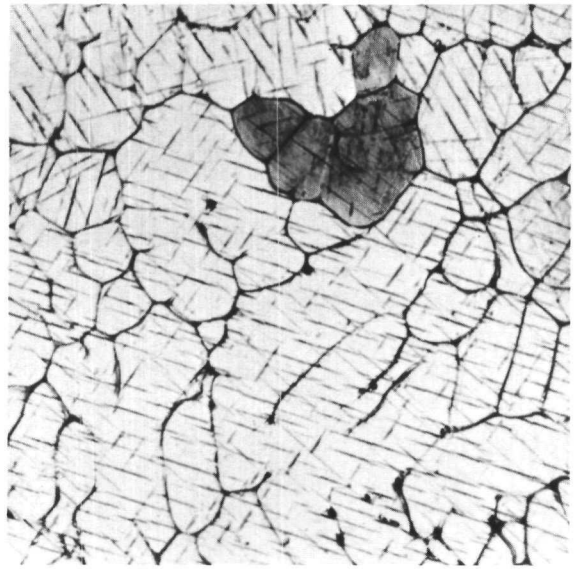

Micro 31683

Figure 30. Photomicrograph of U-6 a/o Pu-50.5 a/o C Alloy; 570, 7, Q; D, 500, BF; (U,Pu)C + $(U,Pu)_2C_3$ (W)

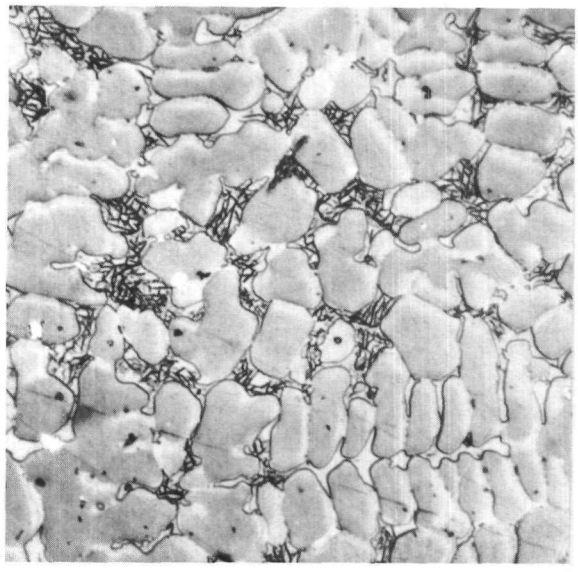

Micro 32574

Figure 31. Photomicrograph of U-24 a/o Pu-51 a/o C Alloy; C; F, 500, BF; cored (U,Pu)C (g-w) + $(U,Pu)_2C_3$ ppt

Micro 31521

Figure 32. Photomicrograph of U-44 a/o Pu-48 a/o C Alloy; 400, 11, Q; E, 200, BF; cored (U,Pu)C

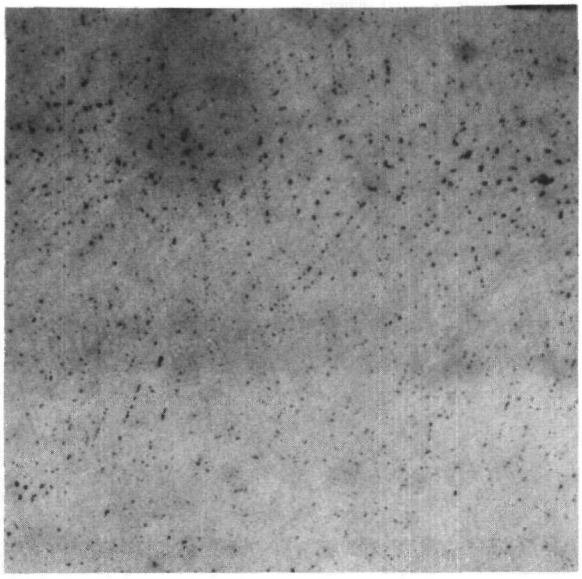

Micro 32652

Figure 33. Photomicrograph of U-44 a/o Pu-50 a/o C Alloy; 1500, 1/2, FC; F, 100, BF; (U,Pu)C + $(U,Pu)_2C_3$ (b)

The dark-etching constituents are probably the remains of $(U,Pu)_2C_3$ dendrites. This microstructure should be compared with that of an alloy which was not annealed at 1500°C, shown in Figure 32. Very faint $(U,Pu)_2C_3$ lines were observed in the diffraction patterns of both alloys.

An independent determination of the low-carbon (U,Pu)C phase boundary was made by quantitative metallography based on microstructural observations of alloys containing between 7 and 35 a/o carbon. The method consisted of a point-counting procedure applied to 4- x 4-in. sections of photomicrograph prints. The procedure is illustrated in Figure 34, in which a point-count grid has been placed upon a photomicrograph of a Pu-41 a/o C alloy. The number of grid points touching the phase to be determined divided by the total number of grid points gives a measure of the fractional area occupied. This quantity can be related to the concentrations of the phases present (see Appendix II). In analogy to the use of the lever rule in a binary system, the weight percent of (U,Pu)C in alloys lying along a given tie-line may be plotted against the carbon concentration in weight percent. The procedure was applied to many alloys and the results are tabulated in Table IX, and presented graphically in Figure 35 and Figure 68. The dimensions of the rectangular blocks indicate the estimated errors. The point-count method is discussed in more detail in Appendix II. The method always yielded a composition for the phase boundary which when converted to atomic percent agreed to within 1.5 a/o carbon with that based upon the metallographic observations of alloys in and near the (U,Pu)C phase field. This suggests that there is a closer approach to equilibrium in

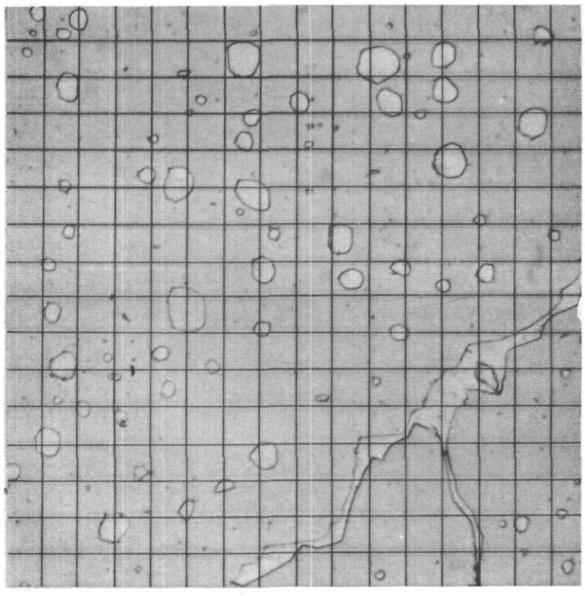

Micro 33288

Figure 34. Photomicrograph of Pu-41 a/o C Alloy; 570, 4, Q; E, 500, BF; tr epsilon Pu (w) in matrix of (U,Pu)C with superimposed point-count grid

many of the alloys than might be inferred from the microscopic appearance of their carbide. Figures 36, 37, and 38 show typical carbide structures in cast alloys.

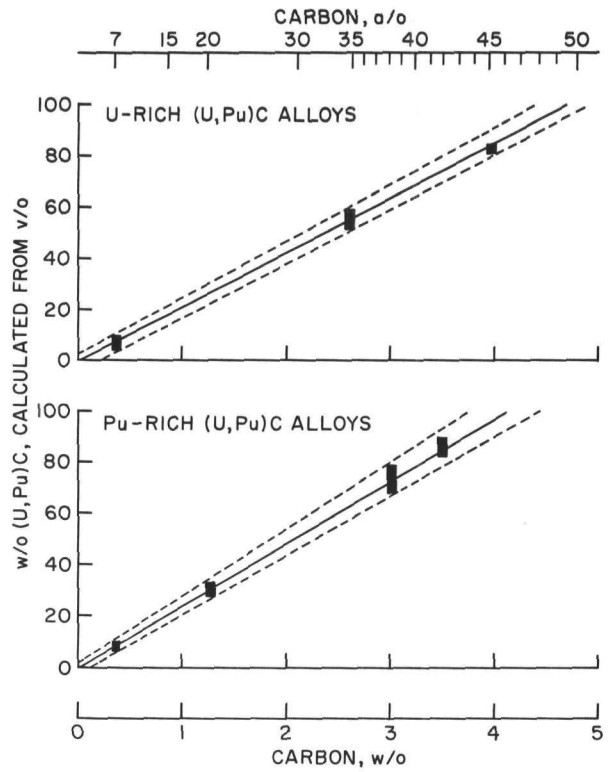

106-6425

Figure 35

Point-count Analysis for (U,Pu)C Alloys

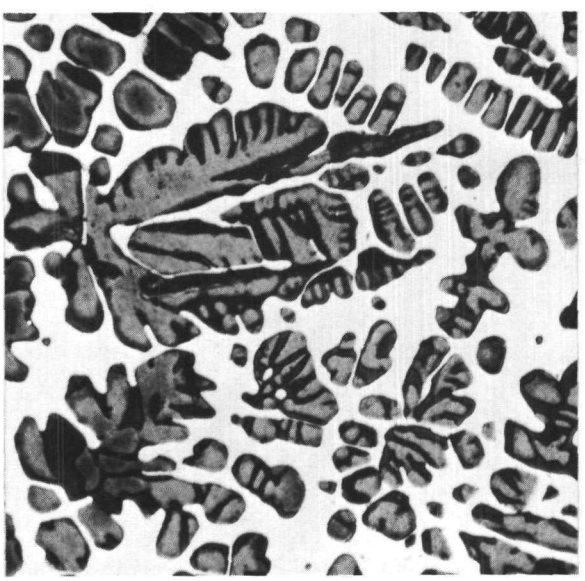

Micro 30581

Figure 36. Photomicrograph of U-30.5 a/o Pu-35 a/o C Alloy; 570, 17, Q; A, 500, BF; tr eta (w) + cored (U,Pu)C

Micro 29674

Figure 37. Photomicrograph of U-56 a/o Pu-35 a/o C Alloy; 620, 13, Q; C, 500, BF; tr epsilon Pu (w) + cored (U,Pu)C

Micro 32695 (a) 100X

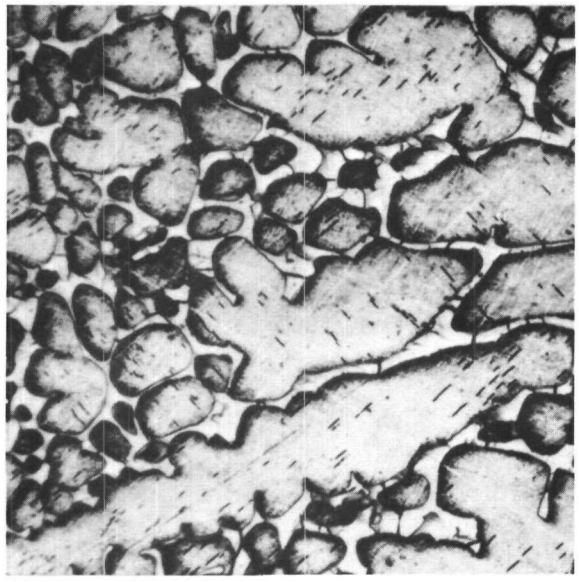

Micro 32697 (b) 500X

Figure 38. Photomicrograph of U-15 a/o Pu-51 a/o C Alloy; C; D, BF; cored (U,Pu)C (den) + $(U,Pu)_2C_3$ (W)

Metallographic observations of cast alloys containing more than 50 a/o carbon showed the following sequential changes in microstructure with increasing plutonium/uranium ratio. Between 0 and 18 a/o plutonium, there is a Widmanstätten rejection of higher carbide (see Figure 30). Between 18 and 37 a/o plutonium, a eutectic-type separation of the higher carbide is observed (see Figure 31). Beyond 37 a/o plutonium there are apparent remnants of $(U,Pu)_2C_3$ dendrites in a (U,Pu)C matrix (see Figure 32).

11. Measurements of Lattice Parameter for the (U,Pu)C Phase

Although it would have been desirable to choose only the diffraction patterns of single-phase alloys for the determination of lattice parameters, the selection was in fact dictated by the quality of the patterns that could be obtained. It was found that the single-phase carbide alloys having low plutonium concentrations always yielded good patterns. On the other hand, at plutonium concentrations of 10 a/o and greater, single-phase alloys gave patterns that had poorly resolved high-angle doublets and sometimes showed two sets of carbide lines having different cell dimensions. (It should be noted that this is the composition region where Figure 28 indicates that "dendritic ghosts" occur.) In such cases better patterns could be obtained from alloys of lower carbon composition, containing up to 10 w/o of a second phase. The various types of diffraction patterns are shown in Figure 39.

The composition of the monocarbide phase in the two-phase alloys was estimated from the isothermal sections. Certain general rules emerged for minimizing the experimental difficulties connected with

diffraction-pattern quality by the selection of alloy compositions: (a) For plutonium concentrations up to 10 a/o, alloys containing 50 ± 1 a/o carbon were selected. (b) At plutonium concentrations between 10 and 37 a/o, use was made of alloys containing between 45 and 48 a/o carbon. (c) Beyond 37 a/o plutonium alloys containing between 38 and 45 a/o carbon were employed. As might be expected, there were a few exceptions to the rules.

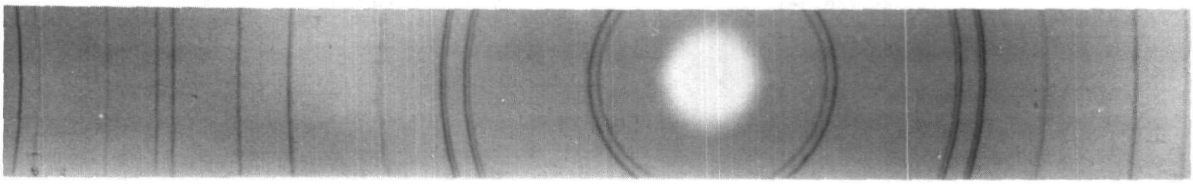

(a) Pu-44 a/o C. Quenched, 570°C, 18 days
(Microstructure showed coring)

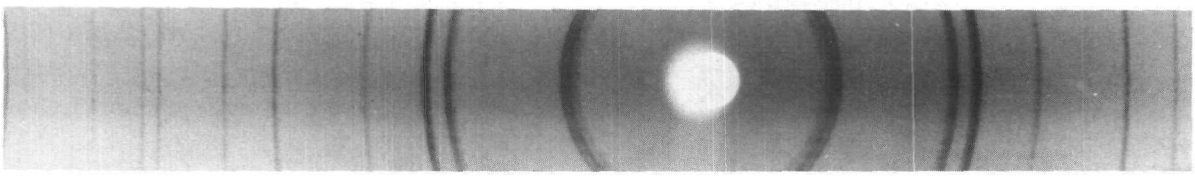

Micro 33350

(b) U-44 a/o Pu-48 a/o C. Quenched, 570°C, 8 days
(Microstructure showed coring)

Figure 39. Powder Diffraction Patterns of Carbides

Figure 40 shows the relationship between lattice parameter and plutonium concentration. Open and filled circles refer to the lattice parameters, measured at room temperature, of alloys quenched from 400

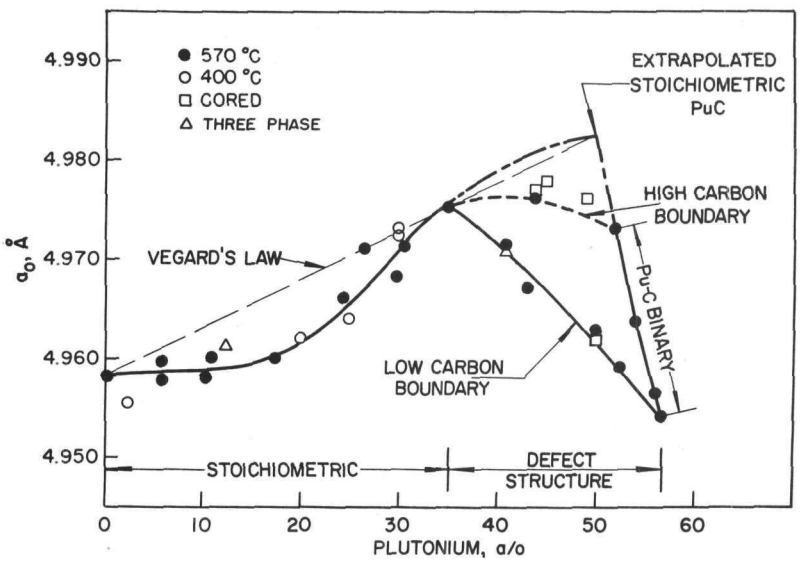

Micro 33636

Figure 40

Lattice Parameter vs. Composition for the (U,Pu)C Phase

and 570°C, respectively. The probable error for a_0 is about $\pm 2 \times 10^{-4}$ Å. The parameters in the composition range from 0 to about 35 a/o plutonium are for monocarbides of ideal stoichiometry. At higher plutonium concentrations the values are for carbides which lie on the high- and low-carbon boundaries of the phase field of the defect structure. The plutonium concentration scale has been extended beyond 50 a/o so that the plot may include data for the defect (U,Pu)C phase and for the binary monocarbide of plutonium, which at the temperatures of interest occurs in the composition range 43 to 48 a/o carbon.

A linear extrapolation of the binary monocarbide data to 50 a/o plutonium yields a lattice parameter for PuC of ideal stoichiometry which is larger than the measured values, and which can be joined by a straight line to the lattice parameter of UC to show that large deviations from Vegard's law characterize the solid solution. The shape of the curve over the region of ideal stoichiometry suggests that the negative deviations which characterize this region might give way to positive deviations at higher plutonium concentrations were it not for the appearance of the defect structure. This hypothetical extension of the stoichiometric curve is shown by the dot-dash line.

The transition from stoichiometry to nonstoichiometry at the approximate composition $U_{0.3}Pu_{0.7}C$ may have its origin in an electron concentration effect proposed by Robbins[29] in his discussion of nonstoichiometry in ternary monocarbides of transition metals. Carbon is regarded as an electron donor, and the maximum bonding energy is assumed to occur when there is an optimum number of bonding electrons in relation to the face-centered cubic coordination of the metal atoms, the number being slightly less than five. When the metal atoms forming the carbide have more than the optimum number of bonding electrons per atom, the favorable ratio of electrons to metal atoms can be attained only if the structure forms with a deficiency of carbon atoms. As applied to the present case in which nonstoichiometry begins close to the Pu-C binary side, Robbins' postulate seems to require that uranium has a valence of four and plutonium a somewhat higher valence. The two elements normally have valences of three through six in their various solutions and compounds. There is need for a systematic study of the effect of valence on the change from stoichiometric carbide to defect carbide in a number of pseudo-binary systems of the monocarbides of the transition metals and the actinide metals.

The triangular data points shown in Figure 40 are the cell dimensions of the carbide phases in two alloys having three-phase structures and lower carbon contents (a U-28 a/o Pu-15 a/o C alloy quenched from 570°C and a U-51 a/o Pu-35 a/o C alloy quenched from 525°C). Most of the diffraction patterns of three-phase alloys contained diffuse high-angle lines and were unsuitable for parameter determinations.

The lattice parameters of a few alloys whose diffraction patterns exhibited two sets of carbide lines are plotted as square data points. Each point represents the weighted average of the parameters derived from both sets of lines, the weighting being based upon relative line intensities. Alloys lying within 1 a/o carbon of the high-carbon (U,Pu)C phase boundary showed only very faint $(U,Pu)_2C_3$ diffraction lines in addition to the (U,Pu)C reflections, and in many instances the patterns which showed two sets of monocarbide lines did not show any $(U,Pu)_2C_3$ lines (see Figure 39).

The point at which the (U,Pu)C phase field begins to deviate from stoichiometry may be estimated from microstructural observations and from the change in curvature of the lattice spacing versus composition curve; 35 ±2 a/o plutonium has been chosen as the point where the defect (U,Pu)C structure forms.

12. The Liquidus and Solidus Boundaries of the 635°C Isothermal Section

The data for determining the plutonium-rich boundaries of the 635°C isothermal section were obtained by metallographic examination of isothermally annealed and quenched alloys. The microscopic appearance of cast microstructures was used as an auxiliary aid. The spacing of the points does not permit bracketing of the phase boundaries as closely here as elsewhere in the ternary diagram; the final result, shown in Figure 41, is an estimate based upon an analysis of the combined data.

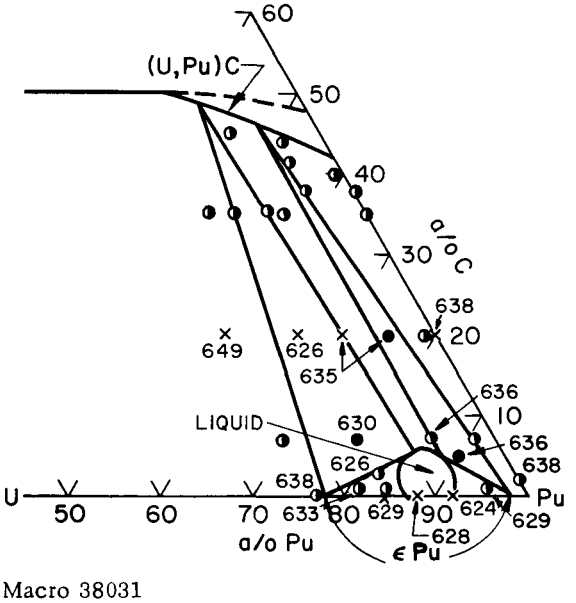

Macro 38031

Figure 41. Datum Points Used to Establish the Plutonium-rich Phase Boundaries at 635°C

Although alloys that contained a liquid phase at the annealing temperature were welded to the tantalum wrap, there was no metallographic evidence of a broad diffusion layer between the tantalum and the molten alloy. It was therefore assumed that contamination resulting from the contact of a molten alloy with its tantalum wrap had no appreciable effect on the phase relations observed.

The [liquid + epsilon Pu + (U,Pu)C] three-phase field that originates on the Pu-C binary system moves very rapidly with temperature, and its position was difficult to determine. The annealing furnaces were regulated with a high-limit controller which prevented the temperature from exceeding 635°C. Even with this precaution, two specimens from the same U-90 a/o Pu-5 a/o alloy

heat treated on different occasions gave different compositions for the two-phase/three-phase boundary. The line was drawn through the average of the two compositions.

Since it is known that all binary phases come into equilibrium with the (U,Pu)C phase and that the gamma-U and epsilon-Pu phases possess unlimited mutual solubility, it may be concluded that immediately below the phase space of primary crystallization of (U,Pu)C, a three-cornered, tube-like [epsilon Pu/gamma U + liquid + (U,Pu)C] phase space extends through the ternary system from the U-C to the Pu-C side. The presence of the minimum in the liquidus-solidus boundary on the U-Pu binary diagram at about 9 a/o plutonium may require the tube to move into ternary space simultaneously from both binary metal-carbon diagrams, uniting in some manner at or near the temperature of the minimum. Another possibility is that the liquid "puddle" created from the U-Pu binary does not extend very far into ternary space and the tube is unaffected by the presence of the minimum, descending continuously from the U-C binary with decreasing temperature, until it exits as a Pu-C eutectic. The two liquid regions must unite somehow near the eutectic temperature. Both constructions were considered in the investigation.

A series of low-carbon plutonium-rich ternary alloys was annealed at 620°C to probe for the solidus. No metallographic evidence of melting was observed, although Ellinger et al.,[12] reported the minimum in the U-Pu system to be at 610°C and 12 a/o U. A preliminary investigation of the U-Pu minimum point was therefore undertaken. Observations of incipient melting in a series of Pu-8, -12 and -15.5 a/o U alloys annealed at temperatures covering in increments of 2°C the range from 600 to 630°C placed the minimum point in the liquidus at Pu-9 a/o U and 624°C.

Some of the alloys involved in the metallographic study and a group of additional alloys (the latter shown on Figure 41 by crosses) were investigated for incipient melting. The temperatures given on Figure 41 are those at which the first signs of melting were detected. These data are taken from Table VI, p. 40.

The results established the existence of a shallow trough or valley in the liquidus surface lying roughly parallel to the [liquid + (U,Pu)C] phase field. At a lower temperature the [liquid + Pu + (U,Pu)C] tie-triangles shown in Figure 41 must fold together to form a tie-line, but there is not sufficient information to decide whether the liquid-phase field vanishes in ternary space or at the U-Pu liquidus minimum point. The fact that no ternary alloy was observed to melt below 624°C supports the latter construction, but the possibility of a ternary liquid-phase field disappearing very close to the U-Pu binary side has not been eliminated.

The plutonium-rich alloys shown in Figures 42, 43, and 44 contain in addition to the typical dendritic carbide, a fine spheroidal of carbide

suggestive of a eutectic-like separation. Figures 43 and 44 show essentially the same structure, but in Figure 44 it may be noted that the etching reagent has corroded the carbide particles while delineating the decomposed plutonium phase. The microstructures of these alloys are consistent with a construction (calling for some isothermal rejection of the carbide phase).

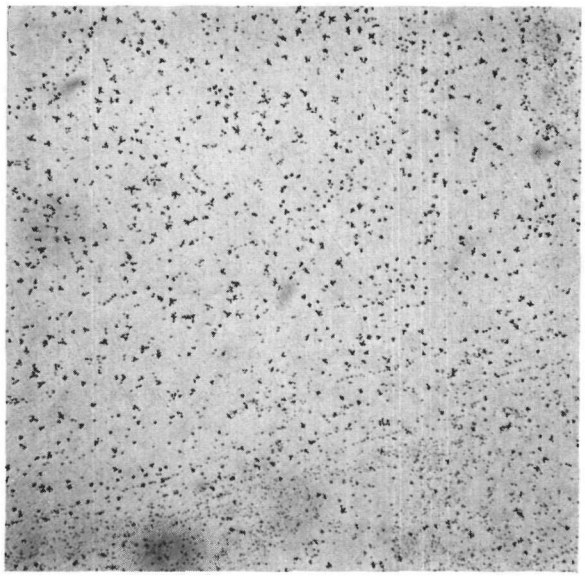

Micro 29696

Figure 42. Photomicrograph of U-95 a/o Pu-1 a/o C Alloy; C; A, 100, BF; tr epsilon Pu + (U,Pu)C (b)

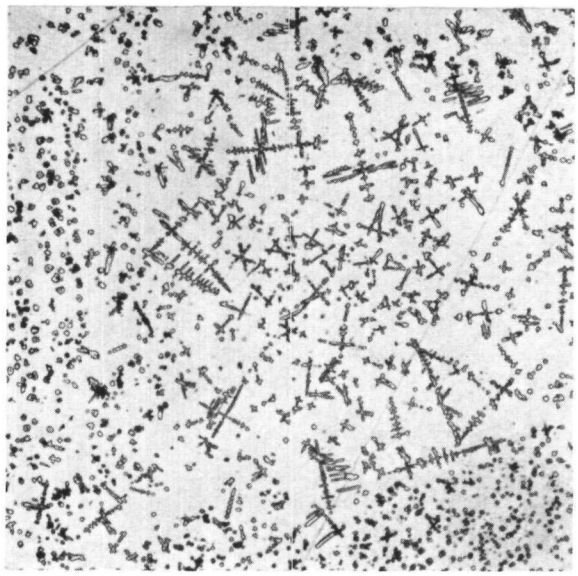

Micro 29673

Figure 43. Photomicrograph of U-87 a/o Pu-7 a/o C Alloy; 570, 5, Q; A, 200 BF; (U,Pu)C in tr epsilon Pu (w) matrix

Micro 29680

Figure 44

Photomicrograph of U-87 a/o Pu-7 a/o C Alloy; 631, 1/48, Q; B, 200, BF; tr epsilon Pu (m) + (U,Pu)C (b)

The photomicrograph shown in Figure 45 is that of a U-90 a/o Pu-5 a/o C alloy quenched from the two-phase liquid plus plutonium region at 635°C. The liquid phase occurred as a grain-boundary network at the annealing temperature, and the carbide was rejected in nondendritic form during resolidification. The appearance of the carbide in Figure 46 indicates that the composition U-75 a/o Pu-20 a/o C is well within one of three-phase fields at 635°C. The liquid apparently nucleated at the carbide dendrite interfaces. The amount of dark-etching carbide is that to be expected in a 20 a/o carbon alloy. Figure 47 shows the transformed liquid phase in a

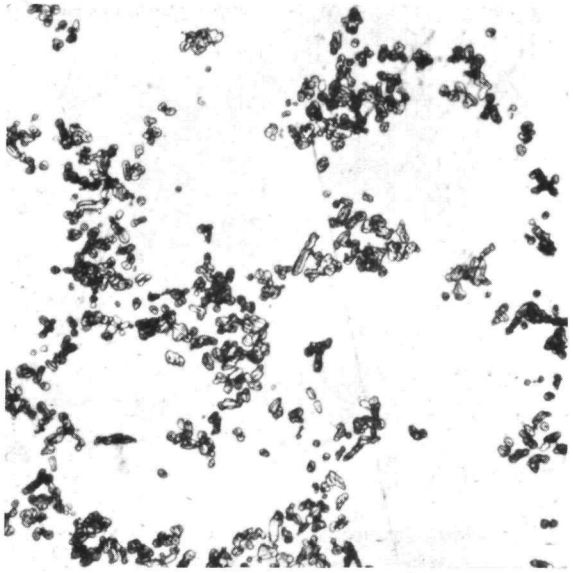

Micro 30609

Figure 45

Photomicrograph of U-90 a/o Pu-5 a/o C Alloy; 635, 7, Q; D, 500, BF; tr epsilon Pu (w) + eutectic (U,Pu)C at grain boundaries

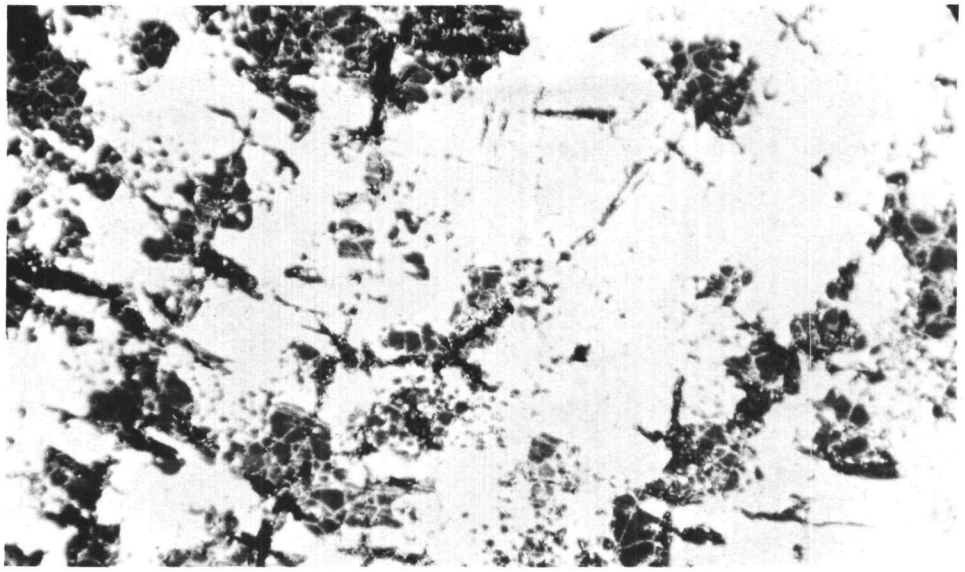

Micro 31645

Figure 46. Photomicrograph of U-75 a/o Pu-20 a/o C Alloy; 635, 6, Q; F, 500, BF; tr epsilon Pu (w) + eutectic (g) and dendritic (U,Pu)C

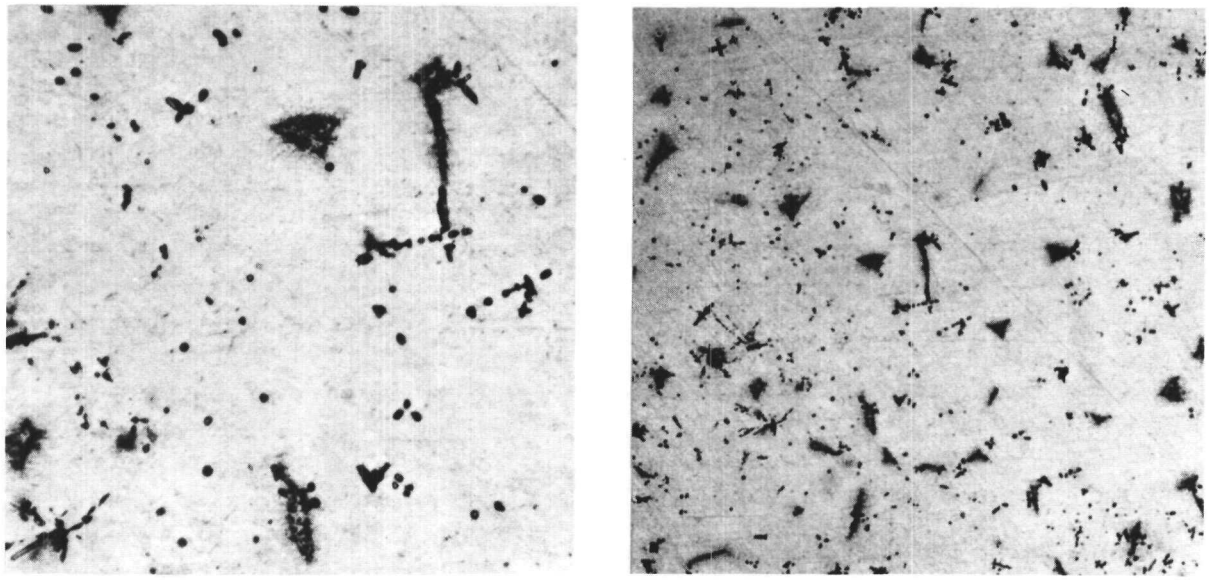

Micro 31668 (a) 500X Micro 31669 (b) 200X

Figure 47. Photomicrograph of U-78 a/o Pu-7 a/o C Alloy; 635, 6, Q; G, BF; tr liquid (g, cusped) + (U,Pu)C (b) remnants in tr epsilon Pu matrix

U-78 a/o Pu-7 a/o C alloy quenched from within the [liquid + epsilon Pu + (U,Pu)C] triangle away from the plutonium corner. The sharp-edged grains were liquid that formed at the epsilon-plutonium grain boundaries at 635°C; the light-etching constituent is transformed epsilon plutonium; the darkest etching constituent is a remnant of the (U,Pu)C phase.

The dark-etching particles shown in the micrograph of the U-95 a/o Pu-1 a/o C alloy in Figure 48 are the carbide particles that have nucleated almost entirely from within a grain-boundary network of liquid.

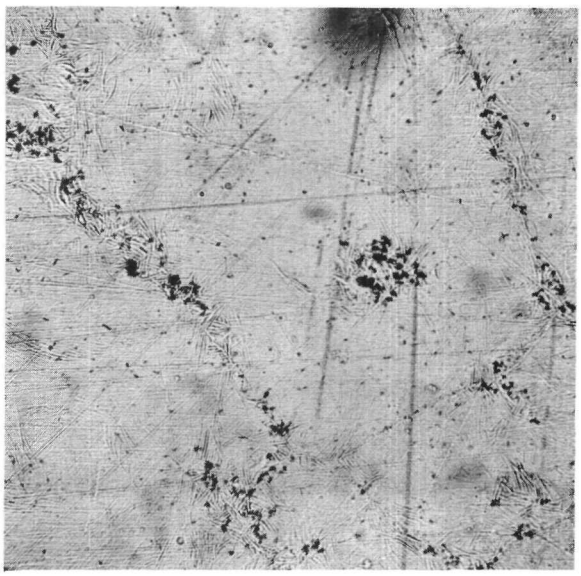

Micro 31533

Figure 48

Photomicrograph of U-95 a/o Pu-1 a/o C Alloy; 635, 7, Q; C, 100, BF; tr epsilon Pu + (U,Pu)C (b) at grain boundaries

The appearance of this 1 a/o carbon alloy is indicative of the very limited solubility of carbon in plutonium.

13. The Compound Pu_3C_2

The investigation of the Pu-C diagram by Mulford et al.,[26] revealed the intermediate phase Pu_3C_2, which has been verified by the present investigation. This compound, the six [Pu + Pu_3C_2 + (U,Pu)C] phase fields, and the [Pu_3C_2 + (U,Pu)C] field are discussed below.

Although the earlier workers experienced difficulties in etching Pu_3C_2, most of the etchants listed on pages 24 and 25 were satisfactory in the nitrogen atmosphere of the glovebox.

It was found that the peritectoid reaction, epsilon Pu + PuC $\rightleftharpoons$ Pu_3C_2, occurs at 558 ± 2°C rather than at 575°C, as reported by Mulford and coworkers. Microstructural evidence will be presented to show that the Pu_3C_2 phase boundary is of negligible width and is located at the stoichiometric composition.

The X-ray diffraction pattern of a Pu-40 a/o C alloy, annealed at 500°C for 14 days and then furnace cooled, is characterized by a mixture of sharp and diffuse lines. The powder data are given in Table XI. The

Table XI

X-RAY POWDER DATA FOR Pu_3C_2 PHASE

Line	I[1]	d,Å	$\sin^2\theta$	Line	I[1]	d,Å	$\sin^2\theta$
1	VW	6.134	0.0157	26	DW	1.103	0.5811
2	VW	5.328	0.0209	27	DVW	0.9891	0.6064
3	VW	3.986	0.0374	28	DVW	0.9766	0.6221
4	VW	2.987	0.0666	29	M	0.9552	0.6502
5	S	2.826	0.0744	30	W	0.9525	0.6539
6	DMW	2.690	0.0822	31	DVW	0.9448	0.6647
7	M	2.577	0.0895	32	DW	0.9268	0.6907
8	S	2.454	0.0986	33	DVW	0.9137	0.7107
9	W	1.939	0.1580	34	MW	0.8783	0.7691
10	W	1.879	0.1683	35	DVW	0.8780	0.7735
11	S	1.746	0.1949	36	DVW	0.8652	0.7925
12	DW	1.713	0.2024	37	DVW	0.8621	0.7982
13	DW	1.695	0.2067	38	DVW	0.8516	0.8181
14	W	1.556	0.2454	39	DVW	0.8516	0.8218
15	S	1.490	0.2678	40	S	0.8402	0.8404
16	DW	1.436	0.2881	41	M	0.8399	0.8451
17	M	1.426	0.2921	42	M	0.8384	0.8645
18	VW	1.358	0.3222	43	MW	0.8279	0.8698
19	VW	1.300	0.3515	44	DW	0.8206	0.8810
20	MW	1.238	0.3876	45	DWM	0.8206	0.8855
21	DW	1.230	0.3928	46	DWM	0.8125	0.8987
22	DW	1.183	0.4249	47	DVW	0.8119	0.9045
23	M	1.137	0.4600	48	M	0.7858	0.9609
24	M	1.108	0.484	49	DW	0.7856	0.9661
25	M	1.013	0.5781				

[1] Intensity Scale: S = strong; M = medium, W = weak; VW = very weak, D = diffuse.

lines could not be indexed on the basis of a cubic structure, and efforts to index them as tetragonal or orthorhombic were also unsuccessful. The close correspondence of the strong lines with those of the PuC phase seems to indicate that the structure is related to the NaCl type.

The density of a sample of Pu_3C_2 weighing 1.7 gm was obtained by a liquid-displacement method with carbon tetrachloride as the liquid; three determinations were made with the same sample. On the basis of the average value and an estimate of the random error associated with the method, the density of the phase is 14.6 ± 0.02 gm/cm^3.

Although it might be expected that peritectoid rimming would be observed in the formation of Pu_3C_2, metallographic observation shows that Pu_3C_2 nucleates as plate-shaped particles at preferred sites on the carbide-plutonium interface, and that the plates grow into the plutonium phase. Figure 49, a photomicrograph of a Pu-20 a/o C alloy annealed at 400°C for 11 days, shows the incomplete transformation of PuC (dark) and delta Pu (white matrix which transformed to alpha on quenching) to Pu_3C_2 (blades). The microstructure of a specimen from the same alloy annealed at the same temperature for 34 days is shown in Figure 50. The presence of some untransformed monocarbide shows that equilibrium has still not been reached.

Micro 28757

Figure 49. Photomicrograph of Pu-20 a/o C Alloy; 400, 11, Q; A, 500, BF; Pu_3C_2 blades + tr delta Pu (w) + PuC (den)

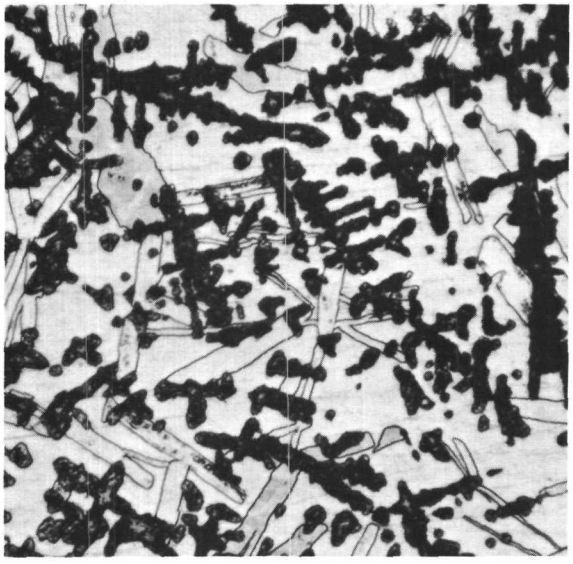

Micro 29610

Figure 50. Photomicrograph of Pu-20 a/o C Alloy; 400, 34, Q; B, 500, BF; Pu_3C_2 blades + tr delta Pu (w) + PuC (den)

Crystallographic factors are probably responsible for the morphology of Pu_3C_2. Nabarro[27] has demonstrated that the strain-energy factor favors the formation of plate-shaped precipitates in crystalline solids; this factor is particularly important at low temperatures, at which the lattice

of the matrix is more rigid. The relative ease of lattice diffusion and grain-boundary diffusion at low temperature may also influence the mode of the reaction. If peritectoid rimming occurs, the reaction can proceed only by bulk diffusion of plutonium or carbon through the Pu_3C_2 lattice, and this diffusion will probably be the rate-controlling step. On the other hand, if the product is formed as narrow platelets originating at the interface, the reactants remain in continuous contact. Furthermore, carbon atoms, which are insoluble in the plutonium phase, can be continuously supplied for the reaction by grain-boundary diffusion along the surfaces of the plates. As carbon is consumed in the formation of the new phase, the monocarbide dendrites decrease in size and eventually disappear. The experimental observation of this effect is shown in Figures 49, 50, 51, and 52.

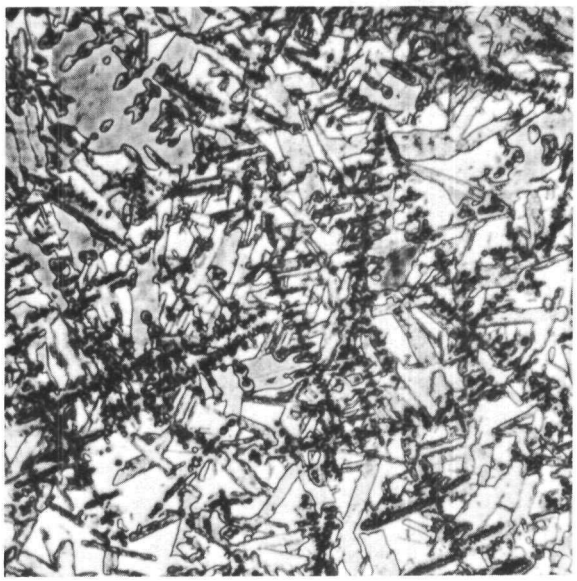

Micro 28829

Figure 51. Photomicrograph of Pu-20 a/o C Alloy; 300, 21, Q; AP, 500, BF; Pu_3C_2 blades + tr gamma Pu (w) + PuC (den)

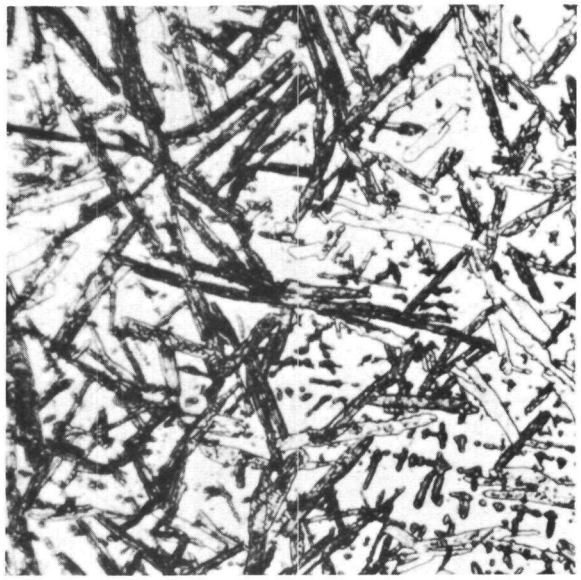

Micro 32534

Figure 52. Photomicrograph of U-79 a/o Pu-20 a/o C Alloy; 440, 14, Q; AP, 500, BF; Pu_3C_2 blades + tr delta Pu (w) + PuC (den)

In a survey of the binary diagrams in Hansen[14] only one reference was found to a peritectoid reaction that proceeded in a somewhat similar manner. While studying the Ni-Mo diagram, F. H. Ellinger found the Ni + NiMo $\rightleftharpoons$ Ni_3Mo reaction at 890°C proceeded with the formation of banded grains.[13]

Precipitation of Pu_3C_2 within the monocarbide grains was only observed in alloys which are hyperstoichiometric with respect to Pu_3C_2. For example, Figure 53 shows the Widmanstatten rejection of Pu_3C_2 within the monocarbide in a Pu-42.5 a/o C alloy annealed at 500°C.

In an experiment designed to bracket the Pu_3C_2 boundaries in the Pu-C system, a series of alloys containing 39, 41, and 42.5 a/o carbon

were heat treated at a temperature of about 530°C for 17 days. (Because of a thermocouple malfunction the exact temperature is unknown.) The coarse blades of Pu_3C_2 shown in Figures 54 and 55 indicate that equilibrium conditions were closely approached. On the basis of the relative amounts of Pu_3C_2 and PuC present in the microstructures shown in Figures 54, 55, and 56, the Pu_3C_2 phase boundary was placed at 40 a/o carbon, and the [Pu_3C_2 + PuC]/PuC boundary between 43 and 44 a/o carbon. It will be shown that the latter boundary is placed at 43.5 a/o carbon by the X-ray results.

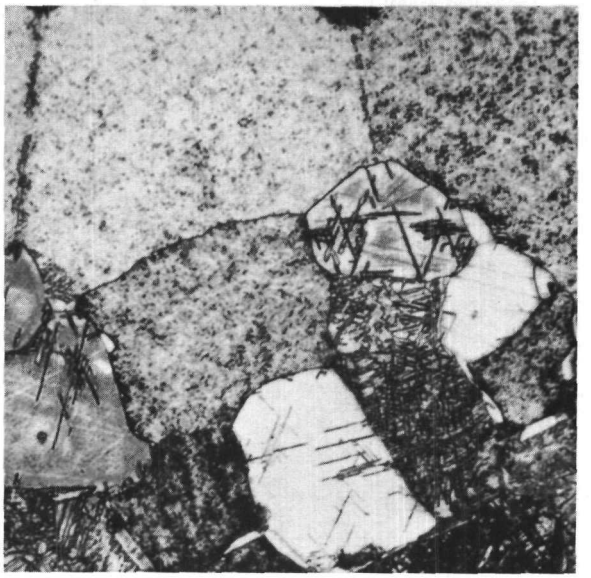

Micro 32686 (a)

Micro 32685 (b)

Figure 53. Photomicrograph of Pu-42.5 a/o C Alloy; 500, 14, FC; D, 500, BF; Pu_3C_2 (W) + PuC

Figure 54

Photomicrograph of Pu-39 a/o C Alloy; 530, 17, Q; E, 500, BF; Pu_3C_2 blades

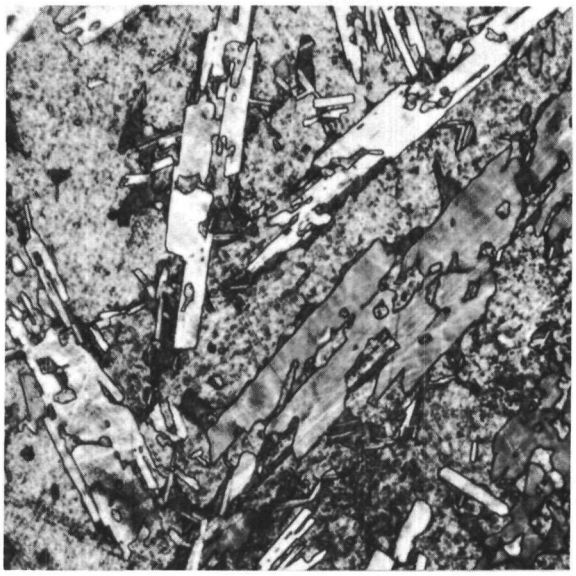

Micro 30551 (a) 500X

Micro 30016 (b) 200X

Figure 55. Photomicrograph of Pu-41 a/o C Alloy; 530, 17, Q; E, BF; Pu_3C_2 blades + PuC

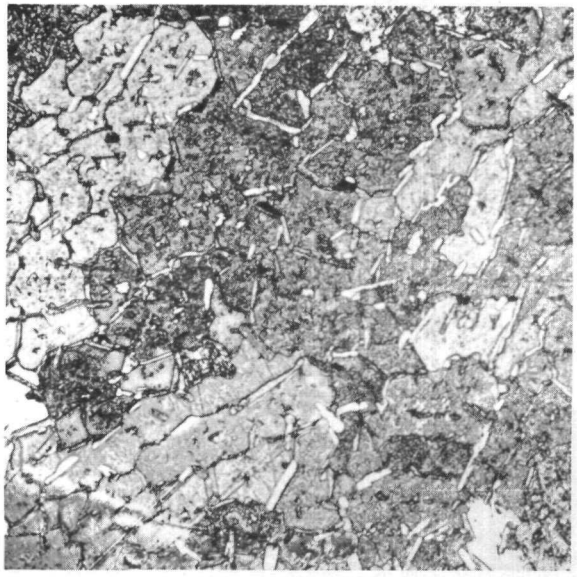

Micro 28758 (a) 200X

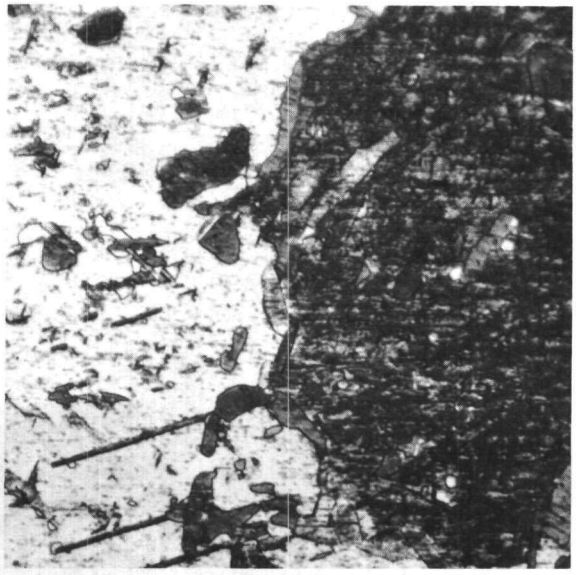

Micro 28769 (b) 500X

Figure 56. Photomicrograph of Pu-42.5 a/o C Alloy; 530, 17, Q; A, BF; Pu_3C_2 blades + PuC

A careful study of photomicrographs of binary and ternary alloys (138 micrographs of 46 different specimens) has yielded some information concerning the morphological relations. There are usually only three or four directions in which the new phase grows when nucleating at the carbide-plutonium interface (see especially Figure 57), and usually no more than four directions when secondary branches grow from the existing Pu_3C_2 plates (see Figure 62c).

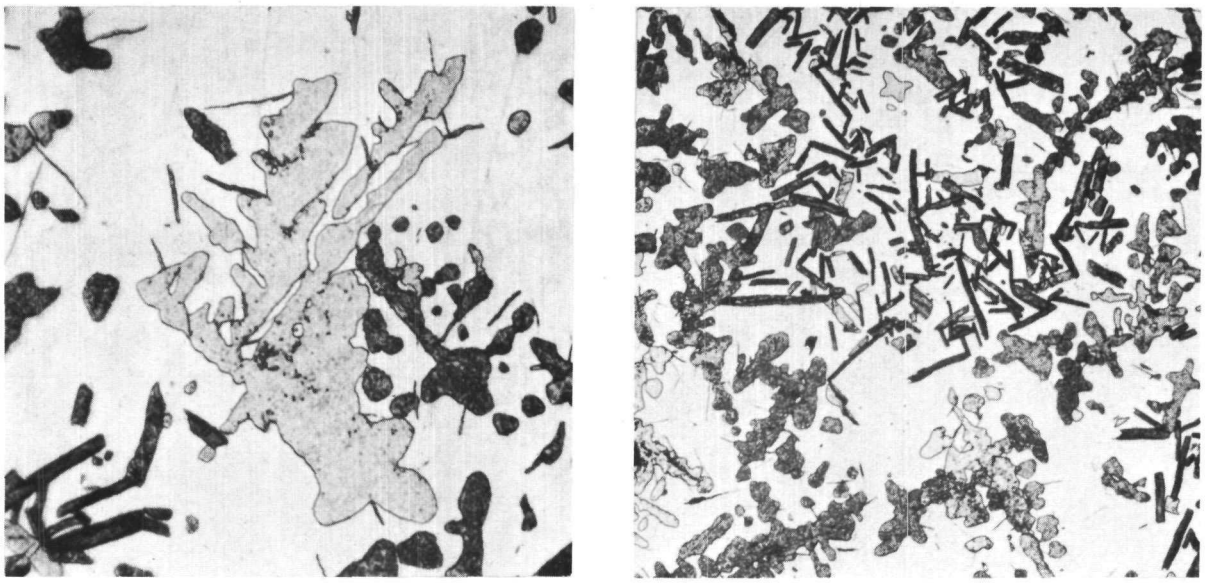

Micro 29611 (a) 500X Micro 29613 (b)

Figure 57. Photomicrograph of Pu-20 a/o C Alloy; 545, 28, Q; AP, BF; Pu_3C_2 blades + tr epsilon Pu (w) + PuC (den)

14. The [Pu + Pu_3C_2 + (U,Pu)C] Phase Fields

Although no trouble was expected in fixing the extent of these phase fields at temperatures above 500°C, it was believed that prohibitively long anneals might be required to obtain equilibrium microstructures at 400°C (see Figures 51 and 52, in which 11- and 34-day anneals are compared). However, the sluggishness that characterizes the formation of Pu_3C_2 in Pu-C alloys is not observed in the ternary alloys. The proportions of phases shown in Figure 58 for a U-75 a/o Pu-20 a/o C alloy annealed

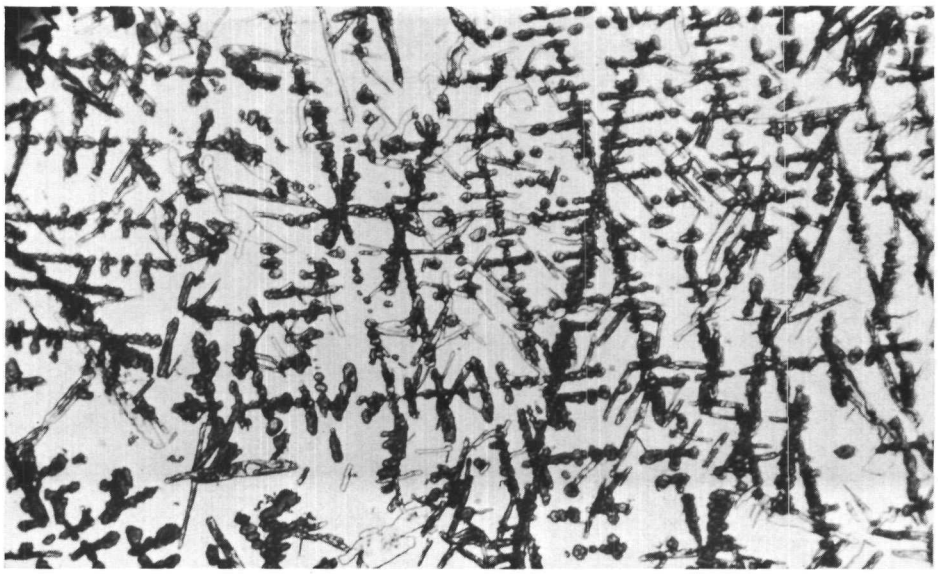

Micro 28782

Figure 58. Photomicrograph of U-75 a/o Pu-20 a/o C Alloy; 400, 8, Q; AP, 500, BF; Pu_3C_2 blades + tr delta Pu (w) + PuC (den)

for 8 days at 400°C were unchanged after a 34-day anneal at the same temperature. The uranium addition may increase the rate of diffusion of carbon or may serve as a source of strain energy which is expended in nucleation and growth. Two photomicrographs of completely transformed U-79 a/o Pu-20 a/o C alloys are shown in Figures 59 and 60.

Micro 32613

Figure 59. Photomicrograph of U-79 a/o Pu-20 a/o C Alloy; 470, 11, Q; E, 500, BF; Pu_3C_2 blades in tr delta prime matrix

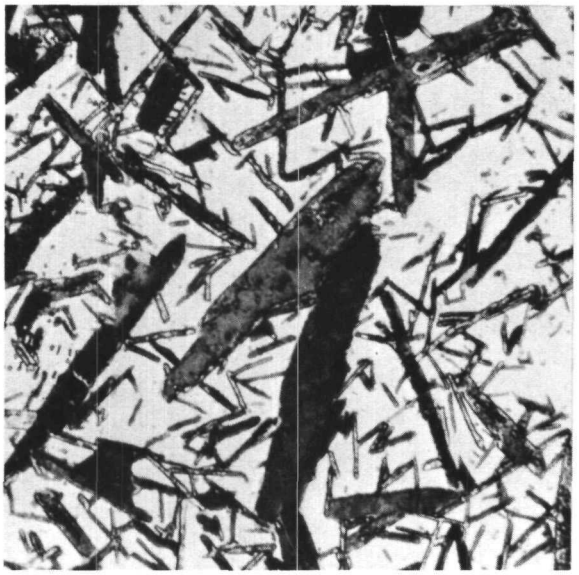

Micro 32537

Figure 60. Photomicrograph of U-79 a/o Pu-20 a/o C Alloy; 500, 7, Q; AP, 500, BF; Pu_3C_2 blades + tr epsilon Pu(w) + trace (U,Pu)C (den remnants)

Figure 61 shows a U-57 a/o Pu-38 a/o C alloy annealed at 400°C for 8 days, and prepared for metallographic examination with two different

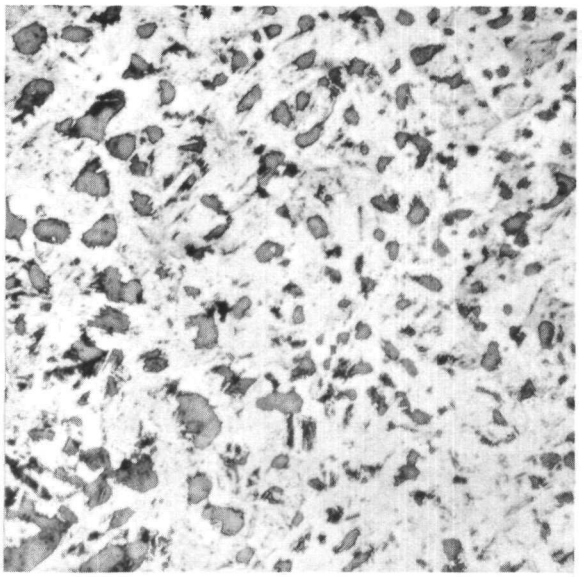

Micro 28806 (a) "G" etch

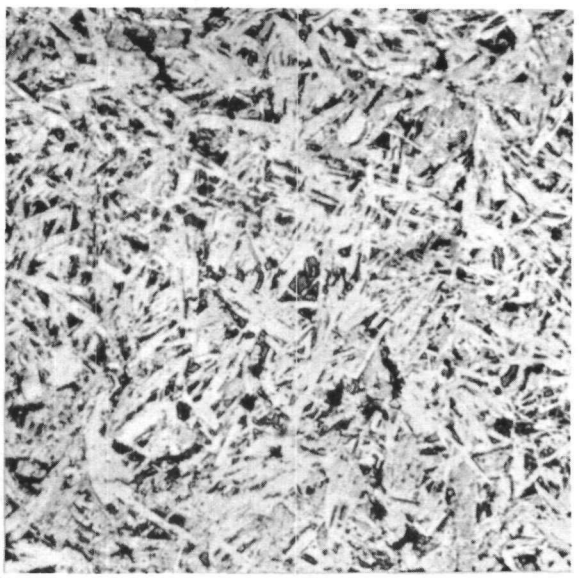

Micro 28808 (b) "B" etch

Figure 61. Photomicrograph of U-57 a/o Pu-38 a/o C Alloy; 400, 8, Q; 500, BF; Pu_3C_2 blades + (U,Pu)C (g)

etching reagents. Figure 61a distinguishes the residual monocarbide phase whereas Figure 61b shows the blades of Pu_3C_2 more clearly. The small amount of plutonium expected in this alloy is not visible; however, faint alpha-plutonium lines were observed on the powder diffraction pattern.

Two micrographs of a portion of an incompletely transformed U-79 a/o Pu-20 a/o C alloy quenched from 311°C after 22 days is shown in Figure 62. Unusually large blades of the new phase have developed. Apparently in this case, a reduction in free energy could more easily be attained by a continued growth on existing crystals. Figure 62b shows

Micro 32625 (a)

Micro 32626 (b)

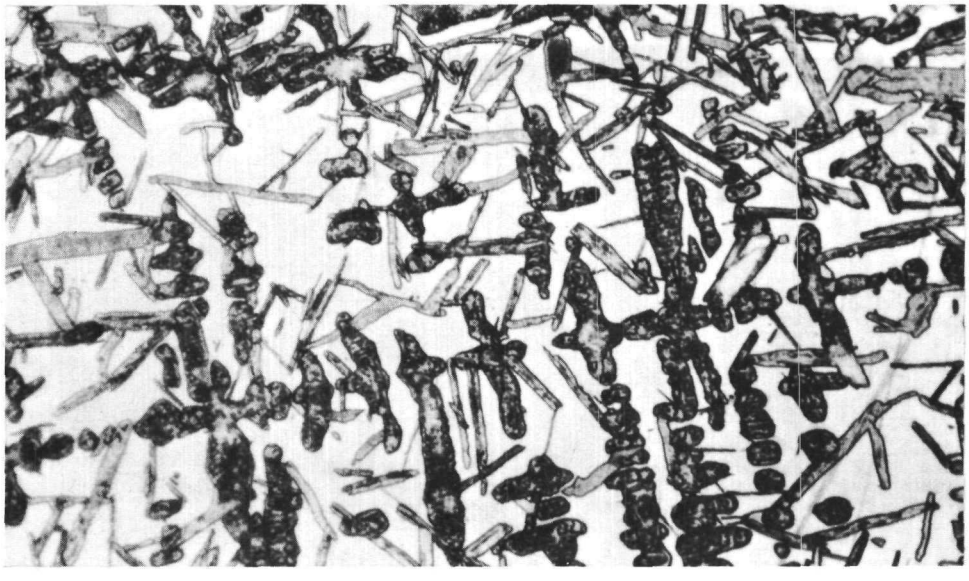

Micro 32627 (c)

Figure 62. Photomicrograph of U-79 a/o Pu-20 a/o C Alloy; 311, 22, Q; AP, 500, BF; Pu_3C_2 blades + tr gamma Pu (w) + PuC (den)

a micrograph at 500X of the largest Pu_3C_2 blades. Figure 62c has been introduced to show the different directions of growth of the Pu_3C_2 phase.

15. The [Pu_3C_2 + (U,Pu)C] Phase Field

This phase field is created when the [epsilon Pu + Pu_3C_2 + (U,Pu)C] peritectoid tie-triangle enters the binary at 558°C. It remains essentially unchanged in the interval to room temperature.

Establishing the boundaries of the adjacent three-phase field and the single-phase monocarbide solid solution fixed the boundaries of this phase field.

16. Four-phase Equilibrium Reactions

To obtain a more comprehensive view of the ternary equilibrium than is given by the isothermal sections, four invariant, ternary-reaction planes were determined. Three of these involved uranium-rich phases and defined all of the invariant four-phase equilibrium reactions for uranium-rich alloys from room temperature to the solidus. In the vicinity of the plutonium corner the allotropy of plutonium introduces a considerable number of four-phase reactions which occur over a narrow band of temperatures and compositions.

The classification of the four-phase invariant reactions is, according to the notation of Rhines:[28]

Class I	$\alpha \rightleftharpoons \beta + \gamma + \delta$;
Class II	$\alpha + \beta \rightleftharpoons \gamma + \delta$;
Class III	$\alpha + \beta + \gamma \rightleftharpoons \delta$.

The overall pattern is outlined in Figure 63. The equations in boxes represent the three-phase and four-phase reactions. Surrounding each four-phase box are shown groupings of three phases, each of which corresponds to a tie-triangle participating in the four-phase reaction. The origin or termination of a three-phase triangle on one of the binary systems is indicated by an arrow. An arrow is also used to connect a three-phase triangle with the next four-phase reaction in which it is involved. The binary U-C reaction temperatures are from the work of Blumenthal.[3] The remaining temperatures are the results of this investigation.

The reaction temperatures were established by metallographic observations of the changes produced by annealing four series of alloys containing 0, 1, or 3 a/o carbon and having an approximately constant uranium/plutonium ratio. The anneals bracketed the various reaction

temperatures. In almost every instance, all of the alloys of a series were annealed at the same time in the same furnace. The results are summarized in Table XII and commented upon below.

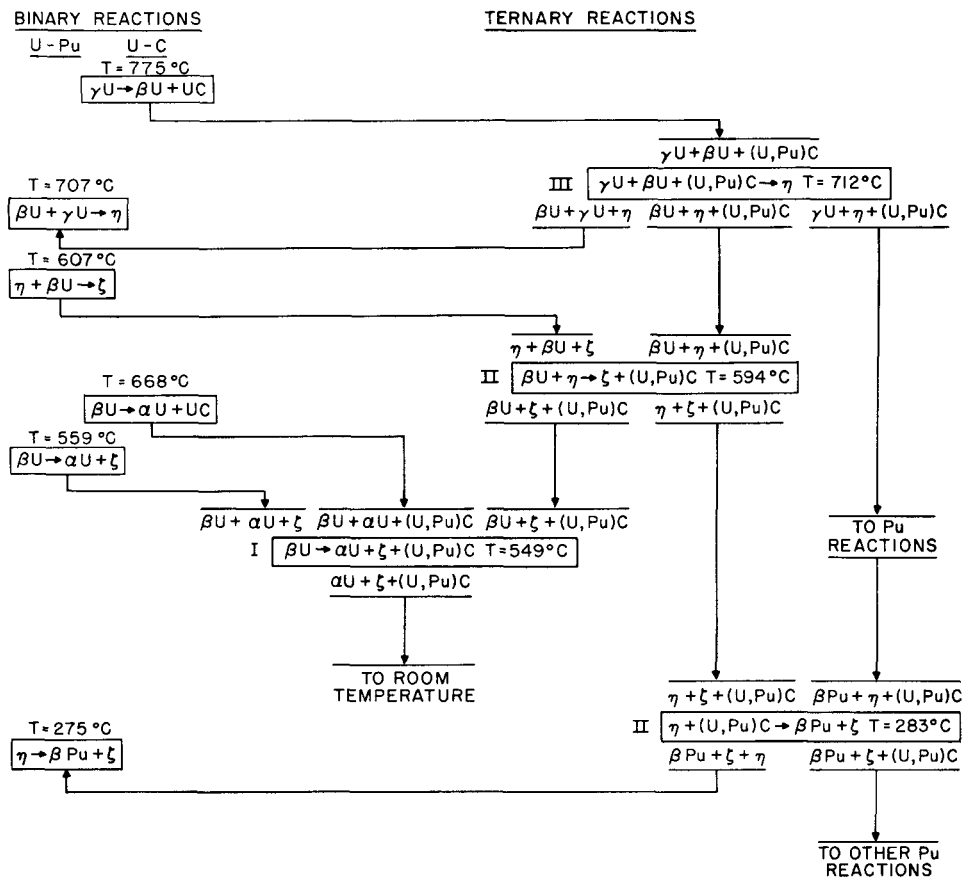

106-6440

Figure 63. Outline of Ternary Four-phase Equilibrium Reactions

Figure 64 shows partial isothermal sections, in the order of decreasing temperature, illustrating each of the four-phase reactions. The figure has been drawn out of scale and the carbon solubility in the U-Pu phases has been exaggerated so that all of the participating tie-triangles can be included. The placement of the alloys is indicated by circles. For clarity, only the one-phase fields have been labeled. The center isothermal section in each sequence has been drawn just above the ternary reaction plane.

Class I: Beta U $\rightleftharpoons$ Alpha U + Zeta + (U,Pu)C; T = 559 ± 4°C

The average value of the [beta U $\rightleftharpoons$ alpha U + zeta] binary-reaction temperature, 559 ± 4°C was substantially in agreement with the earlier value of 560°C,[12] so it was believed that no further information would be gained by annealing another series of alloys in the temperature range between 553 and 562°C.

Table XII

OBSERVATIONS ESTABLISHING EQUILIBRIUM REACTIONS

Alloy Composition, a/o			Annealing Temperature, °C	Observation[1]	Conclusion
U	Pu	C			
			Class I: Beta U ⇌ Alpha U + Zeta + (U,Pu)C		
82	18	0	553	alpha U + zeta	Only class I reaction possible
82	17	1	553	beta U + trace zeta	
81	16	3	553	beta U + trace zeta	
82	18	0	545	alpha U + zeta	Class I reaction between 545-553°C
82	17	1	545	alpha U + zeta	
81	16	3	545	alpha U + zeta	
82	18	0	562	beta U + trace zeta	Beta U ⇌ alpha U + zeta binary reaction between 553-562°C
82	17	1	562	beta U + trace zeta	
81	16	3	562	beta U + trace zeta	
			Class II: Beta U + Eta ⇌ Zeta + (U,Pu)C		
72	28	0	598	zeta	Only class II reaction possible
71	28	1	598	beta U + tr eta	
70	27	3	598	beta U + tr eta	
70	23	7	590	zeta	Class II reaction between 590-598°C
72	28	0	604	zeta	Beta U + eta ⇌ zeta binary reaction between 604-610°C
71	28	1	604	beta U + tr eta	
70	27	3	604	beta U + tr eta	
72	28	0	610	beta U + tr eta	
71	28	1	610	beta U + tr eta	
70	27	3	610	beta U + tr eta	
			Class II: Eta + (U,Pu)C ⇌ Beta Pu + Zeta		
23	77	0	278	zeta + tr eta	Only class II reaction possible
15	78	7	278	beta Pu + zeta	
15	85	0	288	zeta + tr eta	Class II reaction between 278-288°C
14.5	84.5	1	288	zeta + tr eta	
14	83	3	288	zeta + tr eta	
15	85	0	272	zeta + beta Pu	Eta ⇌ beta Pu + zeta binary reaction between 272-278°C
14.5	84.5	1	272	zeta + beta Pu	
14	83	3	272	zeta + beta Pu	
			Class III: Beta U + Gamma U + (U,Pu)C ⇌ Eta		
75	25	0	710	beta U + gamma U	Only class III reaction possible
74.5	24.5	1	710	beta U + tr eta	
73	24	3	710	beta U + tr eta	
75	25	0	714	beta U + gamma U	Class III reaction between 710-714°C
74.5	24.5	1	714	beta U + gamma U	
73	24	3	714	beta U + gamma U	
75	25	0	704	tr eta	Beta U + gamma U ⇌ eta binary reaction between 704-710°C
74.5	24.5	1	704	tr eta	
73	24	3	704	tr eta	

[1] (U,Pu)C appeared in all ternary alloys; tr = transformed.

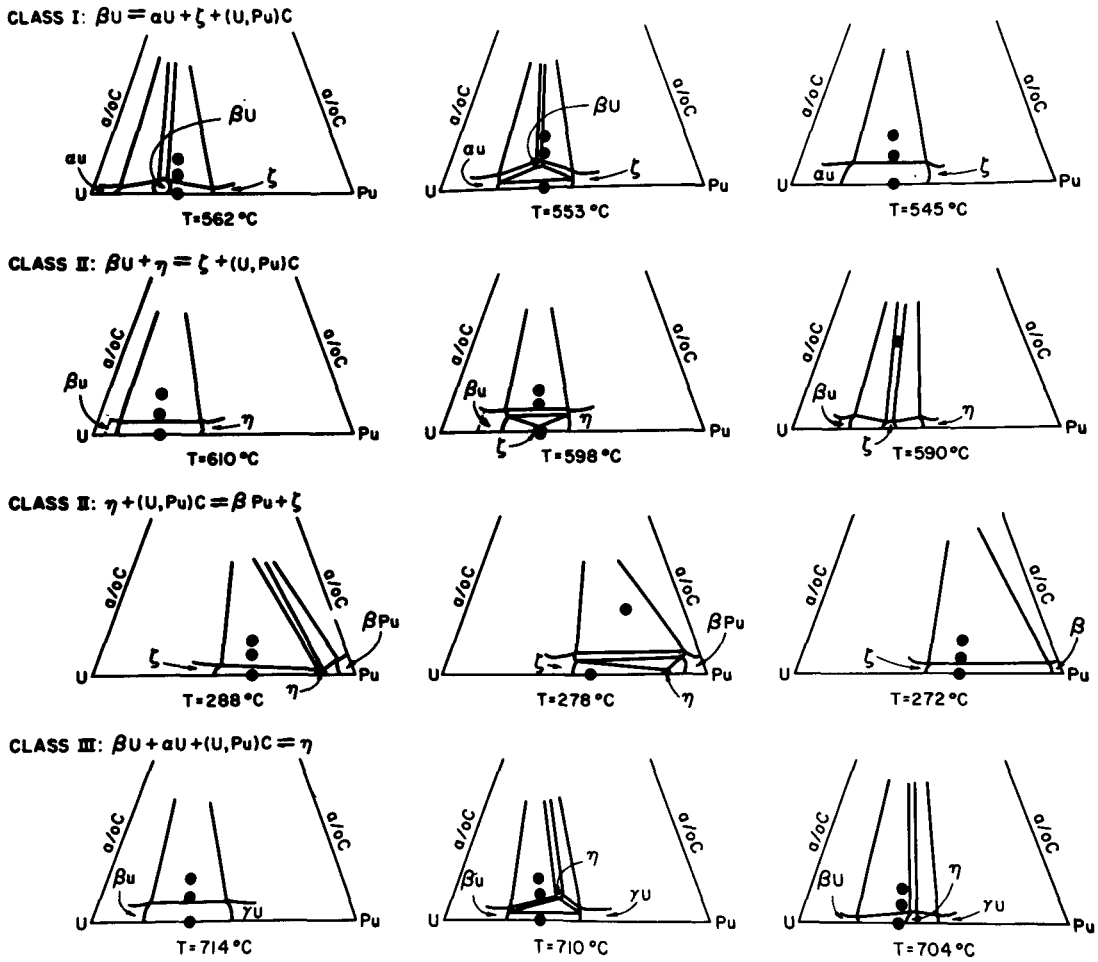

Micro 38106

Figure 64. Isothermal Sections Illustrating Four-phase Reaction Mechanisms

Class II: Beta U + Eta ⇌ Zeta + (U,Pu)C; T = 594 ± 4°C

This reaction must occur at a lower temperature than the reaction of the U-Pu binary system, beta U + eta ⇌ zeta. In the present study the latter reaction was placed at 607 ± 3°C (see p. 91).

Class II: Eta + (U,Pu)C ⇌ Beta Pu + Zeta; T = 283 ± 5°C

The powder pattern of the U-78 a/o Pu-7 a/o C alloy quenched from 278°C showed the presence of alpha plutonium, zeta, and (U,Pu)C. No metallography was performed, but it is presumed that the alpha plutonium resulted from the decomposition of beta plutonium. Only zeta reflections (zeta + transformed eta) were obtained for the U-77 a/o Pu alloy quenched from 278°C.

The diffraction patterns of the series of alloys quenched from 272°C contained many broad and diffuse lines. Partly for this reason, and partly because many of the alpha-Pu, beta-Pu, and zeta-phase reflections

coincide, it was difficult to recognize the partial retention of beta plutonium. The specimens were not examined metallographically. Ellinger et al., placed the binary U-Pu reaction, eta ⇌ beta Pu + zeta, at 278°C,[12] a temperature which is in agreement with the present results to within error.

Class III: Beta U + Gamma U + (U,Pu)C ⇌ Eta; T = 712 ± 2°C

Ellinger et al.,[12] reported 705°C as the temperature of the binary U-Pu reaction, beta U + gamma U ⇌ eta.

17. The Low-temperature Plutonium Phases

The allotropy of plutonium introduces a number of four-phase reactions that occur over a narrow range of temperature and composition. Reaction rates are so rapid that the different plutonium allotropes cannot be retained at room temperature by quenching. In view of the fact that equipment was not available to observe these polymorphic changes, four-phase reactions involving more than one plutonium allotrope could not be studied.

Some information about the plutonium corner was obtained by annealing a series of ten alloys at temperatures within the ranges of stability of the various plutonium allotropes. The phases present were identified on the basis of their microstructural appearance; X-ray diffraction patterns were not obtained. The structure of the plutonium phase that was stable at the annealing temperature has been inferred from the Pu-U binary phase diagram, Figure 1. The results indicate that the plutonium-rich corner of the isothermal section at 400°C is representative of sections from 558°C to room temperature, except for the changes associated with the movements of the one-phase/two-phase boundaries on the binary Pu-U diagram.

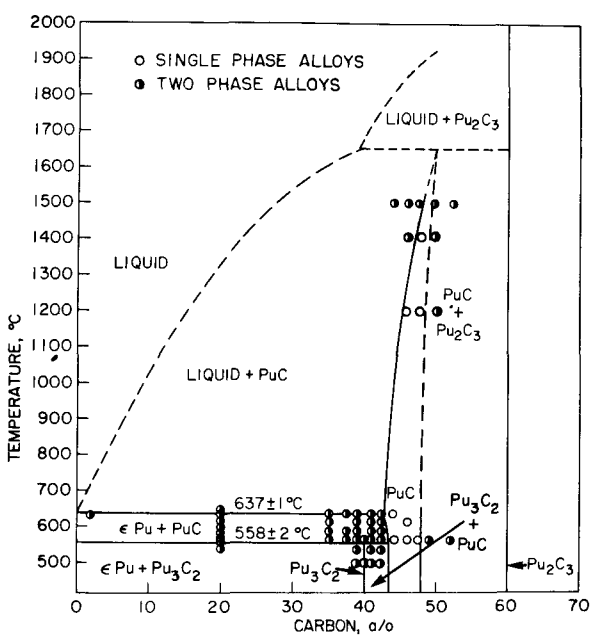

Macro 34930

Figure 65. Pu-C Phase Diagram

18. Pu-C Diagram

The partial Pu-C phase diagram shown in Figure 65, derived from the present study, is based principally on metallographic evidence, although the temperature-invariant boundary, liquid/[epsilon Pu + PuC], was determined by incipient

melting, and a portion of the boundary of the PuC phase was established from the composition dependence of the lattice parameter of the monocarbide phase. The data points refer only to the metallographic results. The principal contribution of the present work is the placing of the boundaries of the monocarbide phase. The temperature of the eutectic, 637°C, differs only slightly from the temperature reported by Mulford et al.,[26] 630 ± 2°C, who used thermal analyses. There is a somewhat larger disagreement in the temperature of the peritectoid formation of Pu_3C_2: 558°C in the present work and 575°C in the earlier version.

Figures 66 and 67, showing the microstructures of a Pu-46 a/o C alloy before and after annealing at 1400°C, are illustrative of a cored carbide phase and a homogeneous carbide phase. Figure 67 also shows that at 1400°C a liquid phase existed at the grain boundaries. The absence of the liquid phase in the Pu-47.5 a/o C alloy (not illustrated) provided the evidence for placing the [liquid + PuC/PuC] phase boundary at 1400°C as shown on Figure 65.

Micro 29684

Figure 66. Photomicrograph of Pu-46 a/o C Alloy; 570, 17, Q; B, 200, BF; cored PuC

The location of the low-carbon PuC phase boundary was determined by quantitative metallographic analysis (see Appendix, Part II). Figure 68 gives the results for alloys quenched from 595°C. The weight percent of PuC derived from the quantitative metallography is plotted against the concentration of carbon in weight percent, and the straight line obtained is extrapolated to 100 w/o PuC to give the carbon concentration at the one-phase/two-phase boundary, 3.68 w/o [43.5 a/o].

Micro 34906

Figure 67. Photomicrograph of Pu-46 a/o C Alloy; 1400, 1/24, FC; AP, 350, BF; tr liquid at PuC grain boundaries

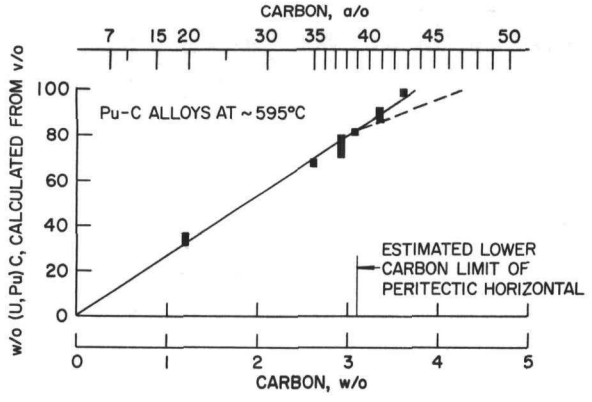

106-6437

Figure 68

Point-count Analysis for Pu-C Alloys

The room-temperature lattice constant of the carbide in one- and two-phase alloys in the as-cast condition and as quenched from various annealing temperatures is plotted vs carbon concentration in Figure 69. The patterns contained sharp lines with well-resolved doublets. The

probable error of the parameter determinations is about 2×10^{-4} Å; the uncertainty in chemical composition is of the order of 0.5 a/o carbon. The parameters are essentially invariant with carbon concentration in the composition ranges of the (epsilon Pu + PuC) and (PuC + Pu_2C_3) phase fields and follow a smooth curve within the monocarbide region. These data support the occurrence of the (epsilon Pu + PuC)/PuC boundary at 43.5 a/o carbon in the temperature range from 570 to 595°C. The evidence from X-ray results for placing the boundary at a slightly lower carbon concentration in the temperature range from 620 to 635°C is not strong because the data show considerable scatter, but it is supported by metallographic observations and by quantitative metallographic analysis. The PuC/(PuC + Pu_2C_3) boundary at 570°C can be placed at 48 a/o carbon on the basis of the X-ray results, but data are not available for other temperatures.

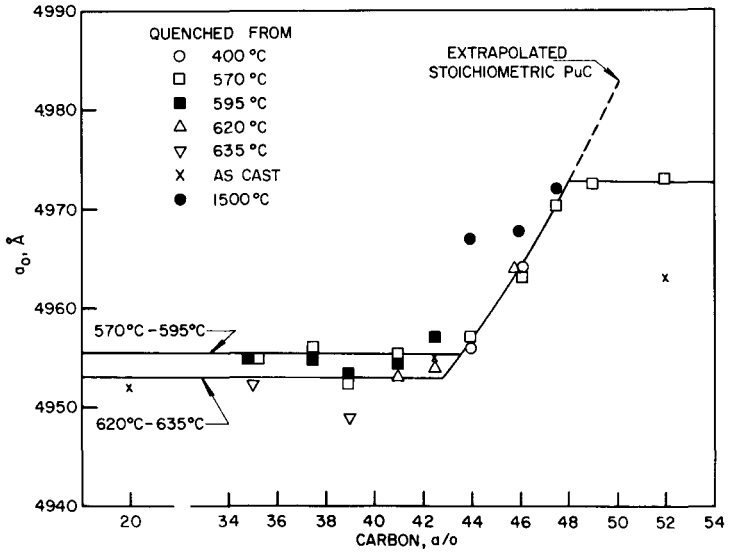

Macro 33637

Figure 69. Lattice Parameter vs Composition Curve for the PuC Phase

The PuC/(PuC + Pu_2C_3) phase boundary at elevated temperatures could not be satisfactorily delineated because of metallographic difficulties. Metallographic study of Pu-C alloys becomes more difficult with increasing carbon content, a condition that is caused by the increasingly rapid contamination of the surface of the specimens by impurities in the nitrogen atmosphere of the glovebox. In this investigation small amounts of the Pu_2C_3 phase could not be detected. Larger amounts, as illustrated by the micrograph of Figure 70, could readily be distinguished from the PuC phase.

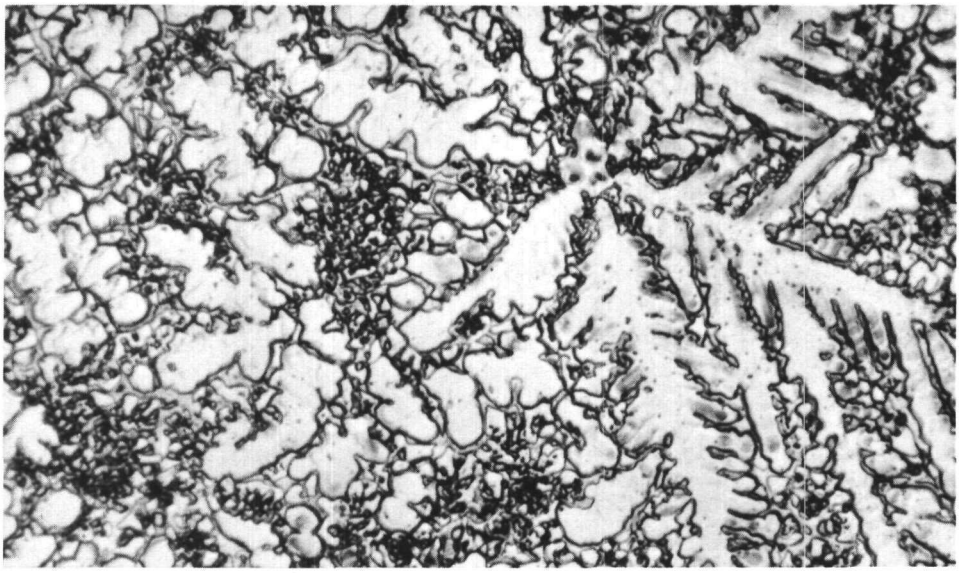

Micro 32705

Figure 70. Photomicrograph of Pu-52 a/o C Alloy; C, G, 500, BF; Pu_2C_3 den in matrix of PuC

B. Discussion of Results

The significant factors affecting the accuracy of the phase diagram determined in this investigation were the purity of the alloys, the number of alloys, the uncertainties in the chemical compositions of the alloys, the attainment of equilibrium structures, and the accuracy with which the annealing temperatures were measured.

The use of high-purity materials and of a protective atmosphere during processing resulted in minimum contamination. This was verified by chemical analyses and by the absence of appreciable concentrations of microscopic inclusions in binary and ternary alloys.

Because of the very limited carbon solubility in the binary phases and the absence of ternary phases, the phase boundaries at 400 and 570°C could be bracketed by two series of alloys, one at 7 a/o carbon, the other at 35 a/o carbon. Along the constant-carbon lines the spacing of alloys was at approximately 1 a/o intervals.

By means of a comparison of the intended compositions with the results of chemical analyses, the uncertainty in the stated concentration of any component in any alloy was estimated to be ± 1 a/o.

The attainment of equilibrium can best be discussed by dividing the phase diagram into two sections: low-carbon alloys containing less than 35 a/o carbon, and high-carbon alloys containing more than 35 a/o carbon. For the low-carbon alloys the criterion for determining that equilibrium

existed or was closely approached was to compare the structures of the same alloy after 4- and 34-day anneals. In every alloy for which this test was made there was no change in the microstructure with increasing time, so it was assumed that the phases were in equilibrium after the shorter annealing period. High-carbon alloys were found to contain inhomogeneous cast microstructures which in many cases could not be removed with the available high-temperature annealing facility. The only phase boundary whose location is dependent upon observations on inhomogeneous alloys is that of the (U,Pu)C phase field in the region where the deviations from stoichiometry occur. This boundary is considered tentative, being shown as a dashed line.

It is believed that the compositional uncertainties in the locations of the phase boundaries can be summarized as follows:

(a) boundaries involving solid phases except the monocarbide phase field: ±1 a/o;

(b) the monocarbide phase field: ±1.5 a/o except higher in the region of the defect structure;

(c) boundaries involving the liquid phase: ±2 a/o.

Temperatures were maintained constant to within ±3°C; in most cases the control was better than this. (One exception to this generalization, involving a thermocouple malfunction, was mentioned on p. 77.) For the solid ⇌ liquid reactions, the temperatures were maintained to within ±1°C of the desired value. When features were determined by bracketing within a temperature interval, the temperature reported is the midpoint of the interval.

C. Comparison with Other Results

Figure 71, showing the low-carbon portion of the 400, 570, and 635°C isothermal sections, designates by filled circles on the U-Pu axis the locations of the phase boundaries on the Los Alamos diagram. Significant differences from the present results occur only at two points. On the 400°C isotherm there is a discrepancy of 5 a/o in the position of the zeta/(eta + zeta) boundary. Figure 1 indicates that this boundary is a tentative one on the Los Alamos diagram. At 635°C the liquidus boundaries differ appreciably. This conflict is consistent with the fact that in the present work the liquidus minimum was found at 624°C, a temperature 14°C higher than that previously reported.

The temperature of the [beta U + eta ⇌ zeta] binary reaction horizontal, 607 ± 3°C, is 17°C higher than the Los Alamos value, 590°C. Mardon et al.,[24] report 595°C, while the Russian value is about 600°C.[4] It is not clear what factors are responsible for this temperature spread.

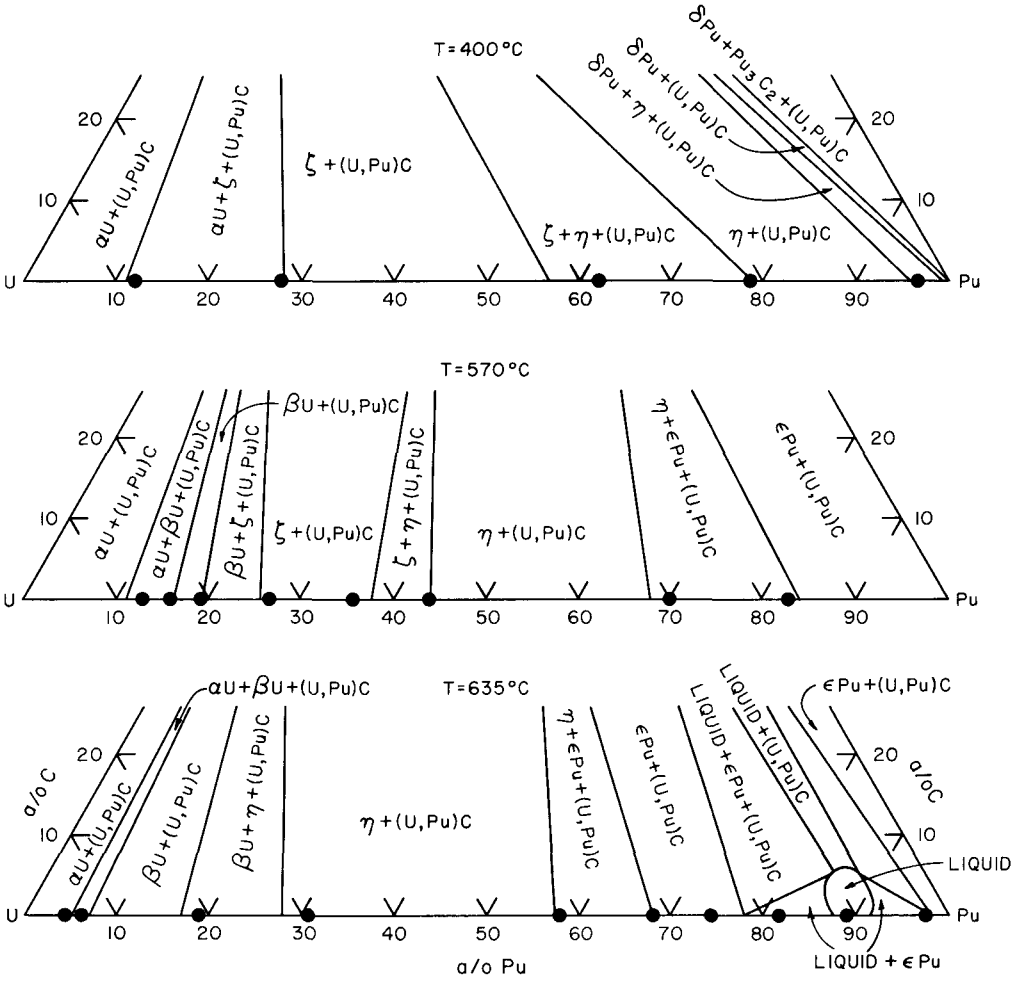

106-6435

Figure 71. Isothermal Sections Showing Comparison with Los Alamos U-Pu Phase Boundaries. Filled Circles on Pu-U Axis Denote Phase Boundaries on on Los Alamos Diagram

The minor discrepancies between the Pu-C diagram of Mulford et al., and the results of this investigation have already been discussed.

V. SUMMARY

The 400, 570, and 635°C isothermal sections of the U-Pu-C system in the composition range from 0 to 50 a/o carbon were investigated by metallographic, X-ray diffraction, and melting-range techniques with arc-melted alloys prepared from uranium of 99.96 w/o purity, plutonium of 99.95 w/o purity, and spectroscopic-grade carbon. Particular care was taken during processing to prevent contamination of the alloys.

The ternary system is characterized by negligible solid solubility of carbon in the binary phases, by the complete series of solid solutions formed between UC and PuC, and by the fact that all the binary phases come into equilibrium with (U,Pu)C. All phase boundaries other than those of the monocarbide phase represent the sides of a three-phase tie-triangles that has one side essentially coincident with either the U-Pu or the Pu-C binary side and an opposite apex touching the phase boundary of (U,Pu)C.

The metal-carbon stoichiometry of the monocarbide is influenced by the uranium/plutonium ratio. Over the range of temperature employed, the (U,Pu)C phase is stoichiometric as regards its carbon content in the composition range from 0 to 35 a/o plutonium. With a further increase in plutonium content it deviates from ideal stoichiometry toward greater metal-to-carbon ratios to form a defect (U,Pu)C phase. Plutonium expands the unit cell of the monocarbide over the composition range in which it retains its stoichiometric character. In the region of the defect structure the lattice parameter decreases with increasing plutonium content, the extent of the decrease being dependent upon the carbon content.

Corroborating the essential features of the Los Alamos version of the U-Pu and Pu-C binary phase diagrams, the investigation showed the following three-phase reactions:

beta U + gamma U $\rightleftharpoons$ eta	at 707 ± 3°C
beta U + eta $\rightleftharpoons$ zeta	at 607 ± 3°C
beta U $\rightleftharpoons$ alpha U + zeta	at 559 ± 4°C
eta $\rightleftharpoons$ beta Pu + zeta	at 275 ± 3°C
epsilon Pu + PuC $\rightleftharpoons$ Pu_3C_2	at 558 ± 2°C
liquid $\rightleftharpoons$ epsilon Pu + PuC	at 637 ± 1°C

The minimum point on the liquidus of the U-Pu binary diagram has been placed at 9 a/o uranium and 624 ± 2°C, in contrast with the value of 610°C and 12 a/o uranium reported by Ellinger et al.[12] The liquid phase first appears in the ternary at this temperature and was found to extend to about 5 a/o carbon at 635°C.

The following four-phase ternary equilibrium reactions and temperatures were found in the U-Pu-C system:

beta U + gamma U + (U,Pu)C $\rightleftharpoons$ eta	at 712 ± 2°C
beta U + eta $\rightleftharpoons$ zeta + (U,Pu)C	at 594 ± 4°C
beta U $\rightleftharpoons$ alpha U + zeta + (U,Pu)C	at 559 + 4°C
eta + (U,Pu)C $\rightleftharpoons$ beta Pu + zeta	at 283 ± 5°C

Metallographic observations have revealed a unique characteristic of the epsilon Pu + PuC $\rightleftharpoons$ Pu_3C_2 peritectoid reaction, namely, the preference of the Pu_3C_2 phase to grow as platelets rather than as an interfacial envelope surrounding the PuC reactant.

VI. ACKNOWLEDGMENTS

The authors wish to cite the valuable help of many members of the staff of the Argonne National Laboratory. R. W. Bane, B. D. Holt, and E. A. Huff, Chemistry Division, performed the chemical analyses. Members of the Applied Mathematics Division provided the analytical determinations of the lattice parameters. L. R. Kelman and the members of the Applied Physical Metallurgy Group rendered assistance in glovebox operations. W. J. Stuparitz, H. W. Knott, and A. P. Baudino provided services in connection with optical and X-ray metallography and photography. J. H. Handwerk and O. L. Kruger gave their cooperation in the use of melting and high-temperature annealing facilities.

One of the authors (S. R.) acknowledges the support of the Argonne National Laboratory in the form of a Resident Student Associateship.

VII. REFERENCES

1. Austin, A. E., Carbon Positions in Uranium Carbides, Acta Cryst., 12, 159 (1959).

2. Blumenthal, B., Constitution of Low Carbon U-C Alloys, J. Nucl. Mat., 2, 206-207 (1960).

3. Blumenthal, B., The Transformation Temperatures of High Purity Uranium Alloys, J. Nucl. Mat., 2, 29 (1960).

4. Bochvar, A. A., Konobeevsky, S. T., Kuitaitsev, V. I., Menshikova, I. S., and Chebotarev, N. T., Interaction of Plutonium and Other Metals in Connection with Their Arrangement in Mendelev's Periodic Table, Proc. of Second United Nations International Conference on the Peaceful Uses of Atomic Energy, Geneva, Switzerland, 6, 184 (1958).

5. Boettcher, A., and Schneider, G., Some Properties of Uranium Monocarbide, ibid., 6, 561 (1958).

6. Burdick, M. D., Parker, H. S., Roth, R. S., and McGandy, E. L., An X-ray Study of the System UC-UC_2-Be_2C, J. Research Bur. Standards, 54, 217 (1955).

7. Chikalla, T. D., 12th High Temperature Fuels Committee Meeting Preliminary Report, Hanford Atomic Power Laboratory (May 11, 1961).

8. Chiotti, P., Klepfer, H. H., and White, R. W., Lattice Parameters of Uranium from 25 to 1132°C, Trans. ASM, 51, 772-786 (1959).

9. Coffinberry, A. S., and Miner, W. N., The Metal Plutonium, The University of Chicago Press, Chicago (1961).

10. Cottrell, A. H., Theoretical Structural Metallurgy, St. Martin's Press, New York (1959).

11. Ibid, pp. 107 and 119.

12. Ellinger, F. H., Elliot, R. O., and Cramer, E. M., The Plutonium-Uranium System, J. Nucl. Mat., 3, 241 (1959).

13. Ellinger, F. H., The Ni-Mo-System, Trans. ASM, 30, 607-638 (1942).

14. Hansen, M., Constitution of Binary Alloys, McGraw-Hill Book Co., New York (1958).

15. Hilliard, J. E., and Cahn, J. W., An Evaluation of Procedures in Quantitative Metallography for Volume-Fraction Analysis, Trans. AIME, 221, 344-352 (1961).

16. Holt, B. D., Determination of Micro Quantities of Hydrogen-Combustion Manometric Method, Anal. Chem., 28, 1153 (1956).

17. Hume-Rothery, W., Christian, J. W., and Pearson, W. B., Metallurgical Equilibrium Diagrams, Unwin Brothers, London (1952).

18. Imalah, K., and Cramer, E. M., The Metallographic Preparation of Plutonium and Its Alloys at Los Alamos, Los Alamos Internal Report (February 18, 1958).

19. Kelman, L. R., in Glove Boxes and Shielded Cells, Academic Press, New York (1958).

20. Kruger, O. L., Phase Studies on Arc-melted Pu-C Alloys near the Monocarbide Composition, J. Am. Cer. Soc., 46, 80 (1963).

21. Litz, L. M., Garrett, A. B., and Croxton, F. C., Preparation and Structure of the Carbides of Uranium, J. Am. Chem. Soc., 70, 1718 (1948).

22. Mallett, M. W., Gerds, A. F., and Vaughan, D. A., Uranium Sesquicarbide, J. Electrochem. Soc., 98, 505 (1951).

23. Mallett, M. W., Gerds, A. F., and Nelson, H. R., The Uranium-Carbon System, Trans. Electrochem. Soc., 99, 197-204 (1954).

24. Mardon, P. G., Evans, J. P., Hodkin, D. J., North, J. M., and Pearce, J. H., The Constitution and Fabrication of Uranium-Molybdenum-Plutonium Fuels, in Plutonium 1960, Cleaver-Hume Press, London (1961).

25. Mueller, M. H., and Heaton, L., Determination of Lattice Parameters with the Aid of a Computer, ANL-6176 (1961).

26. Mulford, R. N., Ellinger, F. H., Hendrix, G. S., and Albrecht, E. D., in Plutonium 1960, Cleaver-Hume Press, London (1961).

27. Nabarro, F. R. N., The Influence of Elastic Strain on the Shape of Particles Segregating in an Alloy, Proc. Phys. Soc., 52, 90 (1940).

28. Rhines, F. N., Phase Diagrams in Metallurgy, McGraw-Hill Book Co., New York (1956).

29. Robbins, D. A., in The Physical Chemistry of Metallic Solutions and Intermetallic Compounds, Vol. II, Chemical Publishing Co., New York (1960).

30. Rough, F. A., and Bauer, A. A., BMI-1300 (1958).

31. Rundle, R. E., Baenziger, N. C., Wilson, A. S., and McDonald, R. A., The Structure of the Carbides, Nitrides and Oxides of Uranium, J. Am. Chem. Soc., 70, 99 (1948).

32. Russell, L. J., United Kingdom, AERE; Chikalla, T. D., General Electric, Hanford, Washington; Pascard, R., Centre d'Etudes Nucleaires de Fontenay-aux-Roses, France.

33. Smiley, W. G., Determination of Oxygen in Metals without High Vacuum by Capillary Trap Method, Anal. Chem., 27, 1098 (1955).

34. Smith, M. C., Principles of Physical Metallurgy, Harper, New York (1956).

35. United States Atomic Energy Commission Report TID-7614, Proceedings of the Symposium on Uranium Carbides as Reactor Fuel Materials (1961).

36. United States Atomic Energy Commission Report TID-8505, Report on Civilian Reactor Fuel Elements (1959).

37. Waldron, M. B., and Coffinberry, A. S., in Metallurgy and Fuels, Pergamon Press, London (1956).

38. Wilkinson, W. D., Extractive and Physical Metallurgy of Plutonium and Its Alloys, Interscience Publishers, New York (1960).

39. Williams, J., Various Remarks on the Formation of Uranium Monoxide, Revue de Metallurgie, 53, 189-204 (1956).

40. Williams, J. and Sambell, R. A. J., The Uranium Monocarbide-Uranium Mononitride System, J. Less-Common Metals, 1, 217 (1959).

41. Williams, J., Sambell, R. A. J., and Wilkinson, D., The Variation of Unit-cell Edge of Uranium Monocarbide in Arc Melted Uranium-Carbon Alloys, J. Less-Common Metals, 2, 354 (1960).

APPENDIX

PART I

CHEMICAL ANALYSIS PROCEDURES

Chemical analyses were performed by the Chemistry Division of the Argonne National Laboratory.

Carbon Analysis

Carbon was determined by a modification of the standard combustion technique. The weighed sample was dropped into a vertical quartz combustion tube onto a bed of copper oxide at 950°C, held in a quartz liner (of 2.54-cm diameter and 11.4-cm long). One hundred-fifty cubic centimeters of purified oxygen gas per minute were passed through the bed, and the CO_2 produced was collected in absorption tubes of Ascarite (KOH in asbestos). The Ascarite was weighed before and after the run, the CO_2 absorbed being a measure of the carbon content. The reported accuracy of the determination is ±2 percent.

Uranium and Plutonium Analyses

Plutonium carbides dissolve readily in hydrochloric acid. However, those ternary alloys that approach 50 a/o uranium dissolve with difficulty even in a HCl-HNO_3 solution, and it is necessary to volatilize the carbonaceous residue with perchloric acid in the presence of nitric acid.

Plutonium (+6) is titrated with iron (+2); the end point is detected amperometrically with a rotating platinum-mercurous sulfate electrode system. The sample is converted to sulfate by fuming and oxidized to (+6) with argentic oxide. Excess oxidant is eliminated by heating. The rotating platinum electrode is operated at 0.6 V versus a saturated mercurous sulfate electrode. Sample size can vary from 5 to 20 mg. The coefficient of variation is about 0.05 percent, with an accuracy of 0.2 percent at the 95 percent confidence level. Uranium does not interfere.

For the uranium analyses, plutonium must be removed. This separation is accomplished by reducing the plutonium to the (+3) state with $NH_2OH \cdot HCl$ and transferring the solution in 6 M HCl + $NH_2CH \cdot HCl$ to a Dowex 1 x 10 anion exchange column. This column is then washed with 6 M HCl + 0.2 M $NH_2OH \cdot HCl$ to remove the last traces of plutonium and americium. The uranium is finally eluted with 0.03 M HCl, and the sample is converted to sulfate and reduced on a lead column in a hydrochloric acid solution. The uranium (+4) is oxidized with ceric sulfate and the excess is backtitrated with ferrous ammonium sulfate, using ferroin as an indicator.

The reported accuracy of the determinations varied between $\pm\frac{1}{2}$ and ±1 percent.

Oxygen Analysis

The samples for oxygen analysis were transferred by means of a vinyl pouch from the glovebox train to the analytical line. In many cases it was found that specimens which had remained in the pouch overnight prior to introduction into the analytical line had oxidized completely to a fine powder, presumably because oxygen and nitrogen had diffused from the laboratory atmosphere into the pouch. It is thought that the relatively high oxygen values reported in Table III were caused by contamination from this source, especially since no undue amounts of inclusions were observed in metallographic specimens of binary alloys of uranium and plutonium.

Oxygen was determined by a combustion method.[33] The sample was dropped into molten platinum contained in a graphite crucible. Any oxygen in the sample reacted to form CO, which was swept out by a stream of argon at atmospheric pressure. A modified form of Schultze's reagent (silica gel impregnated with iodine pentoxide) oxidized the CO to CO_2, which was condensed in a capillary trap and measured with a capillary manometer. The apparatus was sensitive to 0.3 μg oxygen in 0.25-gm samples.

Spectroscopic Analyses

Analyses for tungsten, copper, and other elements were obtained by conventional spectroscopic methods, after plutonium was removed by anion exchange. The results are believed to be accurate to within a factor of two.

PART II

VOLUME-FRACTION ANALYSIS

A calculation made by Hilliard and Cahn,[15] based upon the standard deviations to be expected in the measurements of volume fractions by areal, lineal, and point-count analyses, showed that the most efficient method of analysis was a point-count scheme with a coarse, two-dimensional grid. They defined a coarse grid as one in which the magnification relative to the grid spacing is such that in the ideal case each structural feature does not occupy more than one grid corner.

In the present work, the volume-fraction analysis made use of a point-count method on photomicrographic images, 10.16 cm x 10.16 cm in size. The photomicrographs were taken at either 100, 250, or 500X; contact prints were made on glossy, single-weight, Kodak Azo paper. A grid having about 4 lines per cm (exactly 10 lines per inch) was used to count fine-grain constituents, while a coarser grid having about 0.8 line per cm (exactly 2 lines per inch) was employed for coarse-grained structures. The grids were applied randomly.

In determining the relative areas occupied by the two constituents, there are two important requirements for obtaining high precision. One is to obtain reproducible counts for a given micrograph, and the other is to take enough pictures so that the specimen can be adequately represented.

In a study of the reproducibility factor, each of a representative set of four photomicrographs of the same U-70 a/o Pu-20 a/o C specimen (quenched from an anneal at 336°C for 17 days) was counted five times. The results for the carbide phase are given in Table XIII. As might be expected, the standard deviation is considerably lower when the total number of points counted is higher. For this reason, at least 2000 points were counted when the method was applied. The reproducibility from one photomicrograph to another can be assessed by comparing the mean values of $N_p \times 100/N$ for micrographs A through D. The fact that the values do not differ by more than about two parts in forty indicates that the specimen is structurally homogeneous and that a larger number of different section is not necessary. For most structures counted, only two or three micrographs were available.

By assuming that 13.6 gm/cm^3 is the average density of the carbide phase and 19.0 gm/cm^3 is the average density of the metallic phases existing at room temperature (see Table I), the following relationship may be obtained between w/o and v/o for the (U, Pu)C phase:

$$w/o = \frac{0.716}{\frac{1}{v/o} - 0.284}.$$

The above equation was used to obtain Figures 35 and 68.

Table XIII

REPRODUCIBILITY OF POINT-COUNT RESULTS

(Data are for one U-70 a/o Pu-20 a/o C specimen)

Micrograph	Grid Orientation	Total Grid Points (N)	Grid Points Counted (N_p)	$\frac{N_p \times 100}{N}$	Mean $\frac{N_p \times 100}{N}$	Std Dev
A	1	441	159	36.1		
	2	289	109	37.7		
	3	441	172	39.0		
	4	441	178	40.3		
	5	289	111	38 4		
					38.3	1.5
B	1	441	158	35.8		
	2	289	103	35 7		
	3	289	110	38.1		
	4	441	155	35.1		
	5	441	168	38.0		
					36.5	1.4
C	1	81	29	35 8		
	2	79	31	39.2		
	3	81	27	33.3		
	4	79	30	38.0		
	5	81	33	40 7		
					37 4	2.9
D	1	81	35	43.2		
	2	79	31	39.2		
	3	79	28	35.5		
	4	81	28	34.6		
	5	79	32	40 4		
					38.6	3.6

PART III

DETERMINATION OF LATTICE PARAMETERS

Pertinent data for the X-ray film shown in Figure 39a is given in Table XIV. The line positions were measured with a vernier film scale (the smallest division being 0.05 mm) and a G.E. Fluoroline illuminator. Broad lines were positioned by estimating the center of the line. Theta values were calculated from the line measurements, and the corresponding d-spacings were obtained from the Bragg equation. The intensities were measured with a calibrated film scale.

Table XIV

X-RAY POWDER PATTERN OF A Pu-44 a/o C ALLOY

Line	d, Å	$Sin^2\theta$	I	hkl
1	2.831	0.0741	8	111
2	2.461	0.0981	8	200
3	1.743	0.1956	8	220
4	1.487	0.2687	12	311
5	1.465	0.2769	6	222
6	1.235	0.3894	6	400
7	1.135	0.4616	8	331
8	1.104	0.4873	8	420
9(1)	1.010	0.5810	8	422
10(2)	1.010	0.5845	6	422
11(1)	0.9525	0.6539	12	511,333
12(2)	0.9523	0.6574	8	511,333
13(1)	0.8755	0.7740	8	440
14(2)	0.8752	0.7783	6	440
15(1)	0.8371	0.8466	20	531
16(2)	0.8369	0.8514	12	531
17(1)	0.8254	0.8708	16	600,442
18(2)	0.8252	0.8555	12	600,442
19(1)	0.7832	0.9671	24	620
20(2)	0.7832	0.9720	16	620

(1)Refers to CuKα_1 (1.54050 Å)
(2)Refers to CuKα_2 (1.54434 Å)

The lattice parameters were obtained by a least-squares analysis programmed for the IBM 704 computer.(25) As many as three separate correction terms for eccentricity, absorption, divergence, etc., may be used in a single computation. The method also allows for a weighting factor and a refraction correction. A total of 70 parameters were programmed into the computer.

The different solutions obtained with the same data but with different systematic correction terms were found to yield essentially the same lattice parameter. The only parameter which differs significantly from the others of the same set is that in which no systematic correction term was used. The corrections and solutions are listed in Table XV.

Table XV

LATTICE PARAMETERS CALCULATED BY THE USE OF VARIOUS CORRECTION FUNCTIONS

Alloy Composition, a/o			Temp	Lattice Parameter, Å				
U	Pu	C	(°C)	(1)	(2)	(3)	(4)	(5)
55.5	27.5	17	400	4.9564	4.9612	4.9614	4.9610	4.9612
0	80	20	C[a]	4.9500	4.9521	4.9522	4.9520	4.9521
61	4	35	400	4.9534	4.9547	4.9547	4.9546	4.9546
5	57	38	400[b]	4.9705	4.9724	4.9719	4.9724	4.9719
5	57	38	400[c]	4.9687	2.9739	3.9733	4.9737	4.9731
0	61	39	570	4.9499	4.9532	4.9531	4.9530	4.9529
0	59	41	570	4.9530	4.9550	4.9548	4.9549	4.9548
0	59	41	620	4.9512	4.9526	4.9526	4.9526	4.9526
6	52	42	400	4.9666	4.9680	4.9686	4.9678	4.9684
6	52	42	570	4.9606	4.9629	4.9632	4.9627	4.9630
6	52	42	620	4.9605	4.9619	4.9621	4.9618	4.9620
0	57.5	42.5	C[a]	4.9474	4.9552	4.9534	4.9549	4.9532
0	57.5	42.5	620	4.9527	4.9540	4.9543	4.9538	4.9542
0	56	44	570	4.9558	4.9567	4.9567	4.9567	4.9567
28	27	45	400	4.9606	4.9622	4.9624	4.9620	4.9623
28	27	45	570	4.9665	4.9663	4.9665	4.9663	4.9665
22	33	45	400	4.9609	4.9623	4.9625	4.9621	4.9624
22	33	45	570	4.9639	4.9677	4.9675	4.9675	4.9675
41	13	46	400	4.9537	4.9546	4.9545	4.9545	4.9545
41	13	46	570	4.9556	4.9586	4.9590	4.9583	4.9588
0	54	46	400	4.9628	4.9636	4.9638	4.9635	4.9638
0	54	46	570	4.9620	4.9642	4.9644	4.9640	4.9643
0	54	46	620	4.9633	4.9642	4.9639	4.9642	4.9639
51	0	49	570	4.9562	4.9578	4.9573	4.9577	4.9573

[a] As cast
[b] 8-day anneal
[c] 34-day anneal

Correction Functions

	Systematic	Weighting
(1):	None	None
(2):	$\sin^2 2\theta$	None
(3):	$\sin^2 2\theta$	$\sin^2 2\theta$
(4):	$\sin^2 2\theta(1/\sin\theta + 1/\theta)$	None
(5):	$\sin^2 2\theta(1/\sin\theta + 1/\theta)$	$\sin^2 2\theta$

Figure 72 shows for each reflection of a representative film the difference between the computed $\sin^2\theta$ and the observed $\sin^2\theta$, v, plotted againt θ. It can be seen that the variation of v with θ which occurs when no systematic correction function is applied is replaced by a smaller, random change in v when a correction function is used. All solutions involving a systematic correction are almost equally suitable.

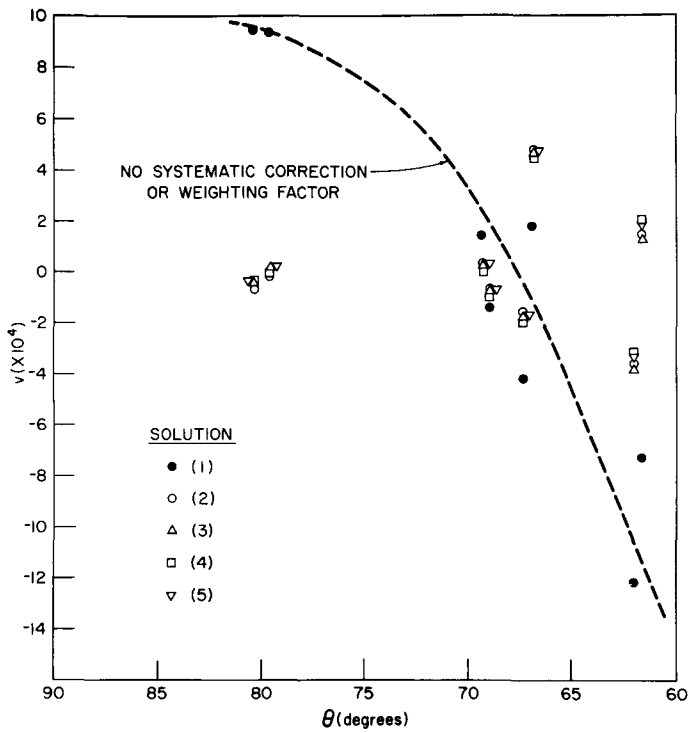

Figure 72

Plot of v vs. θ for PuC Pattern

Micro 36098

After an initial exploratory study the remaining parameters were programmed with the Cohen's least-square analysis of the Nelson and Riley extrapolation (function [4] in Table XV) and without a weighting factor.